Copyright

by

Bryan Earl Heller

2003

Fatigue Response of Pretensioned Concrete Beams

by

Bryan Earl Heller, B.S.C.E.

Thesis

Presented to the Faculty of the Graduate School of

The University of Texas at Austin

in Partial Fulfillment
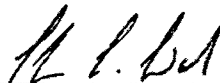
of the Requirements

for the Degree of

Masters of Science in Engineering

The University of Texas at Austin

August 2003

Fatigue Response of Pretensioned Concrete Beams

Approved by
Supervising Committee:

_____
Dr. Sharon L. Wood, Supervisor

_____
Dr. Michael E. Kreger

Dedication

To my beautiful wife and children, whose love and support motivate my life's

endeavors.

Acknowledgements

Abstract

Fatigue Response of Pretensioned Concrete Beams

Bryan Earl Heller, M.S.E.

The University of Texas at Austin, 2003

Supervisors: Sharon L. Wood and Michael E. Kreger

The objective of this thesis is to discuss the suitability of using a extreme fiber concrete tensile stress of $12\sqrt{f_c'}$ calculated using uncracked section analysis as a limit state criterion for evaluating prestressed concrete highway bridges as a part of required serviceability inspections. This thesis reviews strand fatigue test results as well as fatigue test results of prestressed beams from past experiments. Test results of four new prestressed beam fatigue tests are reported and analyzed. Finally, a recommendation is made that beam fatigue analysis should be based on the stress range of the prestressing strands, unless the calculated extreme fiber concrete tensile stress is limited to less than $3\sqrt{f_c'}$ based on uncracked section analysis.

Table of Contents

List of Tables

List of Figures

xiii

CHAPTER 1

Introduction

1.1 GENERAL

Structural engineering design is the application of knowledge in the physical sciences to produce structures for the improvement of the lives of those who use those structures. The precision of the design process has always been tempered by available time to produce the design, the allotted funding for a project, and the generally accepted theories and design methods at any point in history. Frequently, design methods are conservatively simplified to reduce the time and expense of using more detailed models.

All structural designs are based upon assumed loads. These design loads usually are determined using conservative values from design guides or by conducting research on the loading of similar existing structures. Over the course of decades, however, the actual load requirements of a structure may increase beyond what was initially assumed. Because the original design was based on conservative assumptions, engineers may then reanalyze the existing structure using refined methods, thereby showing an increase in the nominal strength of that structure.

As larger, heavier trucks have been introduced over the past decades, this problem is particularly true of highway bridges. A very large percentage of existing highway bridges use pretensioned, prestressed concrete beams. This thesis discusses fatigue testing on pretensioned, prestressed, high-strength concrete beams and associated prestressing strand. These tests were done as a part of the Texas Department of Transportation (TXDOT) Project 0-1895,

1

hereafter called TXDOT Project 1895 in this thesis. The beam and associated strand tests are only a part of the scope of this project. The full project scope and discussion of findings are discussed by Hagenberger (2003). For the convenience of the reader, a brief discussion of the background of the project follows.

1.2 BRIEF DESCRIPTION OF TXDOT PROJECT 1895

TXDOT bridge engineers have standard methods and scheduling frequencies for conducting serviceability inspections on highway bridges in Texas. The frequency of these serviceability checks is based on a criterion that evaluates the ability of the prestressed concrete beam to resisting cracking. In the background information of the project description from TXDOT engineers, it is stated that in the past an allowable tensile stress limit of $7.5\sqrt{f_c'}$ in the bottom face was used to check for cracking of pretensioned concrete beams. Many bridges that were designed 30 to 40 years ago using H15 loading now fail this criterion when the HS20 design vehicle is used. As a result, the required frequency of the serviceability inspections decreases from once every two years to once a year.

Because the inspected bridges exhibited no visible deterioration, the criterion was judged by TXDOT bridge engineers to be too restrictive, and the stress limit was increased to $12\sqrt{f_c'}$. This higher tensile limit was based on ACI 318-95, Section 18.4.2, for beams with small long-term deflections. This section, however, was intended for application in buildings and building loads where fatigue is generally not the controlling design state. Thus, TXDOT bridge engineers requested that the use of the higher tensile limit of $12\sqrt{f_c'}$ be evaluated for application in highway bridges with many cycles of repeated design load.

2

1.3 PURPOSE OF TESTS

As a part of this project, several existing bridges were evaluated. Construction material reports were obtained from the project records, and measured material properties were used to recalculate the structural capacity of the bridge girders. Additionally, for one bridge, concrete core samples were taken and also used to evaluate the structural capacity of that bridge. This bridge, known as the Chandler Creek Bridge (Hagenberger 2003), which crosses Chandler Creek on the northbound frontage road of Interstate 35 in Round Rock, Texas, will be identified as the "prototype" highway bridge throughout this thesis. A complete discussion on the analyses of these bridges is found in Hagenberger (2003).

1.3.1 Beam Fatigue Tests

Six test beams were constructed and tested as a part of the TXDOT 1895 project. The test beams were constructed with the intent of modeling material properties in the test beams to match those in the prototype bridge girders. The beams would then be fatigue tested with response carefully monitored and recorded. The intent of these tests was to demonstrate how the existing prototype bridge would respond to cyclic loading at three levels of index stress: the calculated tensile stress at the bottom face. The levels of index stress investigated were $6\sqrt{f_c'}$, $7.5\sqrt{f_c'}$, and $12\sqrt{f_c'}$ which were calculated using uncracked section analysis of the prototype bridge. Best estimates of actual bridge material properties were used in the analyses. Detailed discussion of these analyses is available in Hagenberger (2003).

3

1.3.2 Strand Fatigue Tests

Samples of the prestressing strand that was used in the construction of the test beams were thoroughly tested to verify the material characteristics of the strand. As will be discussed in Section 1.5, the prestressing strand is the most probable location of fatigue failure in a prestressed concrete beam. Because of this, it was desirable to establish that the strand being used was characteristic of strand used in typical highway bridges, and, thereby, that the beam test results are valid.

1.4 EFFECT OF CYCLE FREQUENCY AND TEMPERATURE ON FATIGUE

One of the obvious differences between the loading of the test beams and the prototype girders is the loading cycle frequency. It is not practical to load test individual beams in a laboratory over a 50-year period, or even over a 5-year period. While a very busy highway bridge girder may experience design service loads 200 times in a day, a test beam may be loaded at rates of 100 to 500 cycles per minute. Without some background understanding of the mechanics of fatigue, one may feel uncomfortable comparing laboratory results with the actual fatigue performance of an in-service bridge. Additionally, one may be uncomfortable with the varying environmental conditions, especially temperature, of the different laboratories where fatigue testing has been conducted.

Materials engineers (Brooks and Choudhury 2002, Polák 1991, Bílý 1993, Klesnil and Lukáš 1992) have determined that fatigue cracking usually begins at locations of surface irregularities or other microstructural features. On a macroscopic scale, the loads being applied to a structural element may be well below that required to produce plastic deformation. However, microscopically in the region of these irregularities, local microscopic stresses exceed the yield

4

strength of the material and the material at the end of the irregularity deforms plastically until the local stress is lowered back into the elastic range.

Figure 1-1 Simplified Fatigue Crack Growth Mechanism

Figure 1-1 illustrates how fatigue crack propagation occurs (Brooks and Choudhury 2002). The figure shows two complete loading cycles. While the simplified figure is not to scale, it illustrates the mechanism. Five phases are shown in each cycle. The last phase (e) of the first cycle is the same as the first phase (a) of the second cycle. In phase (a), the crack is closed or under minimum load. In phase (b), tension is applied. If sufficient tension is applied, the end of the crack will experience local plastic deformation, propagating the crack length a small amount (phase (c)). When the tension is relieved, the crack begins to close

5

(phase (d)), and finally, the crack returns to its original width (phase (e)). In the next cycle, the same phases occur, extending the crack still further. Eventually, the remaining supporting material is inadequate to transmit the applied load, and a fracture occurs, usually catastrophically with little plastic deformation.

Time is not a factor in the sequence just described. The crack growth rate is simply a function of how many times the end of the crack has undergone plastic deformation. Crack growth rate is, however, dependent on how much relative tension and compression (the stress range) the element experiences, because this determines how much plastic deformation the end of the crack experiences during each cycle. If the stress range is larger, the end of the crack experiences greater amounts of plastic deformation, and the fatigue crack propagates in fewer cycles.

According to Brooks and Choudhury (2002), loading frequency usually does not affect crack growth rate. Others have stated that frequency and load hold time are not factors except at elevated temperatures (above 300 °C or 570 °F). In very high temperature environments exposed to an oxidizing environment such as air, the fatigue process becomes one of corrosion fatigue. Thus, in these types of environments, the lower the frequency and the longer the load hold time, the faster fatigue occurs (Polák 1991, Bílý 1993, Klesnil and Lukáš 1992). Because normal highway bridges and laboratory beam specimens typically do not experience these temperature ranges, the fatigue crack growth rates should be independent of cycle load frequency and the comparatively small temperature differences.

1.5 LITERATURE REVIEW

The research described in this section focuses primarily on the influence of stress range on the fatigue performance of prestressing strand. This is primarily because researchers and designers almost never produce structures in

which the fatigue strength of concrete governs the design. The stresses induced in the concrete by the required design fatigue loads are generally small compared with the fatigue strength of the concrete (Shahawi and Batchelor 1996). ACI Committee 215 (1997) states that the fatigue strength of concrete is approximately 55 percent of the static strength, whether in compression, tension, or flexure. Because concrete does not have an endurance limit, this fatigue strength is based on enduring 10,000,000 cycles.

In design of prestressed concrete bridge girders, the AASHTO Standard Specifications for Highway Bridges (2002) do not provide specific fatigue requirements. Only the traditional inferred limit that the concrete extreme fiber tensile stress not exceed $6\sqrt{f_c'}$ is provided. In severe corrosive exposure conditions, such as coastal areas, AASHTO lowers this limit to $3\sqrt{f_c'}$.

In the current interim AASHTO LRFD Bridge Design Specifications (2003) additional requirements related to fatigue loading are given. If the extreme concrete fiber tensile stress exceeds $3\sqrt{f_c'}$ under a prescribed service load state, then the stress range in the prestressing strands shall not exceed 18.0 ksi for straight, prestressed, bonded tendons that are not susceptible to fretting caused by tendons rubbing on hold-downs or deviations. Neither the Standard nor the LRFD Specifications limit concrete stresses under fatigue loads.

In the fatigue design of beams with prestressed reinforcement, ACI Committee 215 (1997) does not include limits for concrete in fatigue, but does recommend that prestressing strand with a minimum stress less than $0.6f_{pu}$ be limited to a stress range of less than $0.06f_{pu}$ based on cracked section analysis if the concrete extreme fiber tensile stress exceeds a nominal stress of $3\sqrt{f_c'}$,

calculated using an uncracked section analysis. For Grade 270 strand, this corresponds to a stress range of 16.2 ksi.

Because of the emphasis on the prestressing strand, the remainder of this section will focus first on research regarding fatigue performance of prestressing strand, and then on research regarding fatigue performance of pretensioned, prestressed concrete beams.

1.5.1 Previous Research on Prestressing Strand Fatigue

A comprehensive study of the fatigue characteristics of prestressing strand was completed by Paulson, et al. (1983). This work reported on a literary review of over 700 individual specimen tests, as well as 67 strand fatigue tests conducted for that project. The research included data from nearly all published sources on the subject at that time, and is used as a baseline document for the TXDOT Project 1895.

Paulson, et al. (1983) ran various regression models on the data, and recommended a model representing the expected (or mean) number of cycles a prestressing strand should experience before failure when subjected to cyclic loading at a given constant stress range. The model for mean fatigue strength was given as

$$\log N = 11.45 - 3.50 \log S_r \qquad\qquad (1\text{-}1)$$

where N is the number of load cycles at failure, and

S_r is the stress range, in ksi.

Paulson, et al. (1983) went further to recommend a design model based upon a one-sided tolerance limit where it was 95 percent probable that 97.5 percent of the distribution would be above the limit. The design model is given in Equation (1-2).

$$\log N = 11.0 - 3.50 \log S_r \qquad\qquad (1\text{-}2)$$

Both models and the associated data are plotted in Figure 1-2.
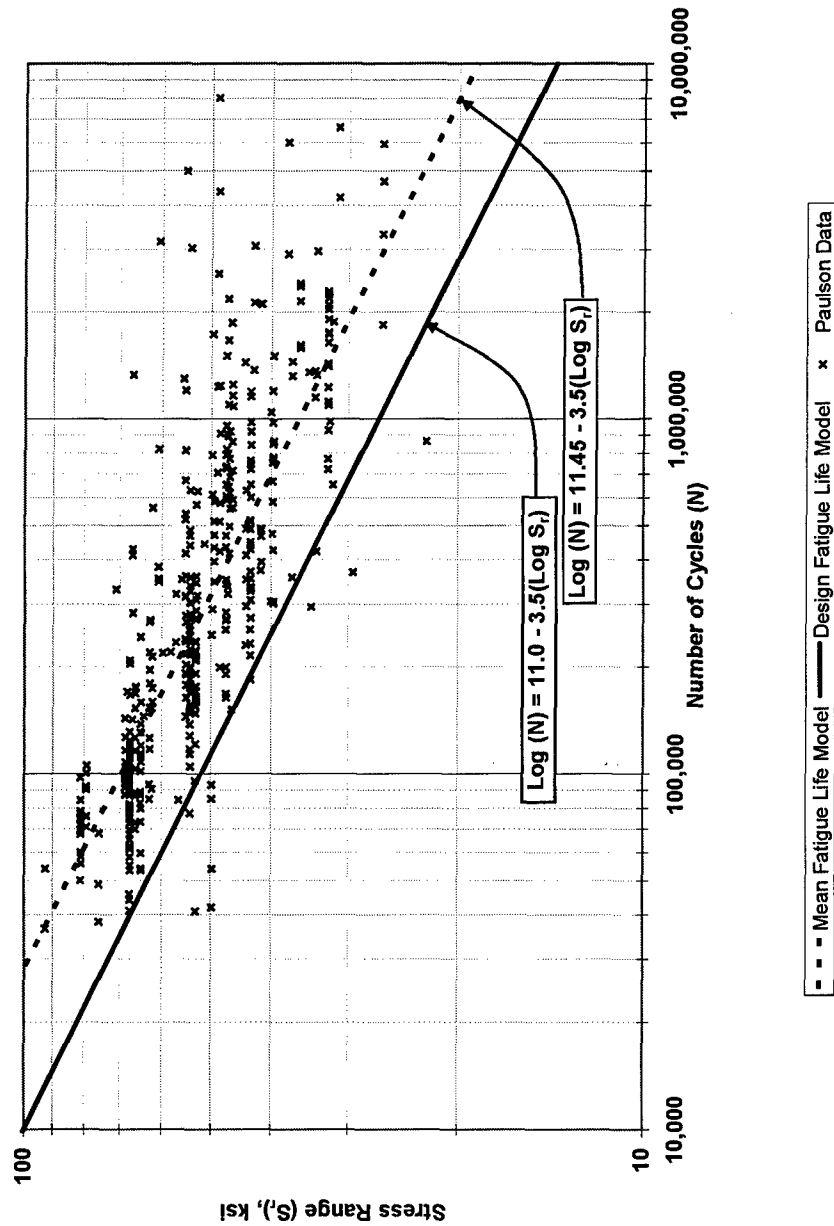
Figure 1-2 Strand Fatigue Life Models Developed by Paulson

9

Additional research was conducted as part of TXDOT Project 1895 in an effort to obtain additional, more recent strand fatigue data. There have been several studies on the fatigue of bundled cables such as those found in post-tensioned structures and cable-stayed bridges. Additionally, there are numerous papers written on new composite types of materials. Unfortunately, there were no published works that provided any new laboratory test data for single prestressing strand.

In 1992, VSL Corporation provided test data to the University of Texas at Austin that were gathered from industry sources. This industry information included data on approximately 800 strand tests. The great majority of those tests were not carried out to failure, but were stopped once various thresholds were exceeded, thus demonstrating that the specimens exceeded a given, required standard. The data from the tests in which the strand failed in fatigue are added to the data from Paulson et al. (1983) in Figure 1-3. Data from the industry tests are summarized in Appendix A. Although the test procedures for this data are unknown, this figure is provided to demonstrate that the data from VSL agree with the models developed by Paulson et al. (1983).

Although the VSL Corporation's compilation of industry tests provides additional information, it does not substantially differ from the information already provided by Paulson et al. (1983). Additionally, the validity of the industry data cannot be confirmed. Therefore, tests conducted as a part of TXDOT Project 1895 will be compared against the data collected by Paulson et al. (1983) representing tests performed in the 1960s through the early 1980s.

10

The chart shows:
- Y-axis (left): Stress Range (S$_r$), ksi, ranging from 10 to 100
- X-axis (bottom): Number of Cycles (N), ranging from 10,000 to 10,000,000

Equation boxes on chart:
- Log (N) = 11.0 - 3.5(Log S$_r$)
- Log (N) = 11.45 - 3.5(Log S$_r$)

Legend:
- – – Mean Fatigue Life Model
- —— Design Fatigue Life Model
- × Paulson Data
- O VSL Industry Data
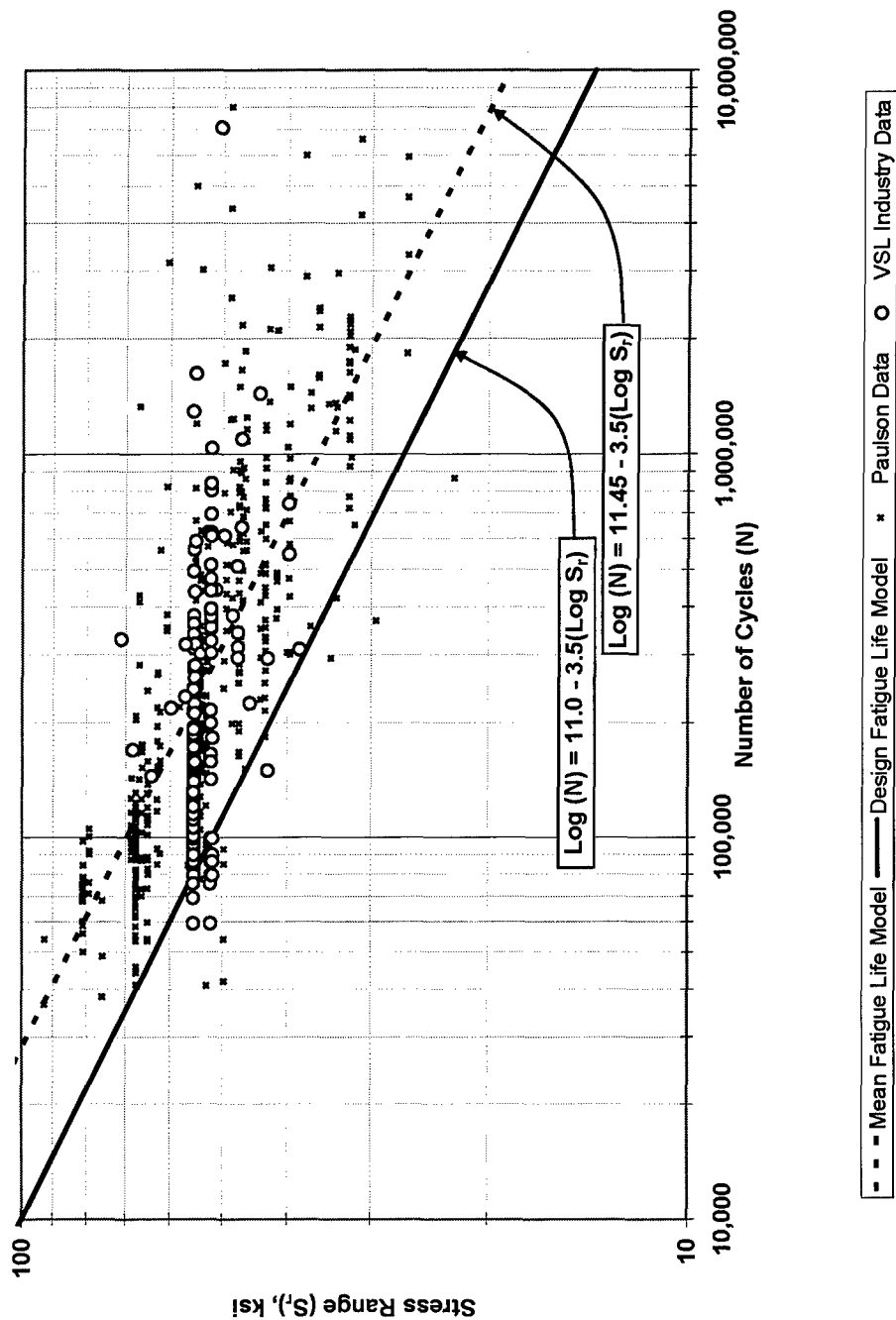
Figure 1-3 Comparison of Industry Strand Data and Model by Paulson

11

1.5.2 Previous Research on Pretensioned Concrete Beams

In close association to the work by Paulson, et al. (1983), Overman (1984) conducted fatigue testing on 11 full-scale, prestressed concrete beams. Of these 11 beams, 7 had straight strands, and 4 had a combination of straight strands and draped strands. One of the beams with draped strands was loaded such that the maximum calculated tensile fiber stress for an uncracked section was $3.5\sqrt{f_c'}$. This resulted in a very low strand stress range (7.5 ksi), and after 5.9 million cycles, the test was discontinued when the beam showed no signs of deterioration. An exhaustive literary review was also conducted as a part of that project and data from 47 prestressed concrete beam tests were reported from tests in the 1950s through the late 1970s. Figure 1-4 provides a plot of the data from Overman (1984) compared with the data and models developed by Paulson, et al. (1983).
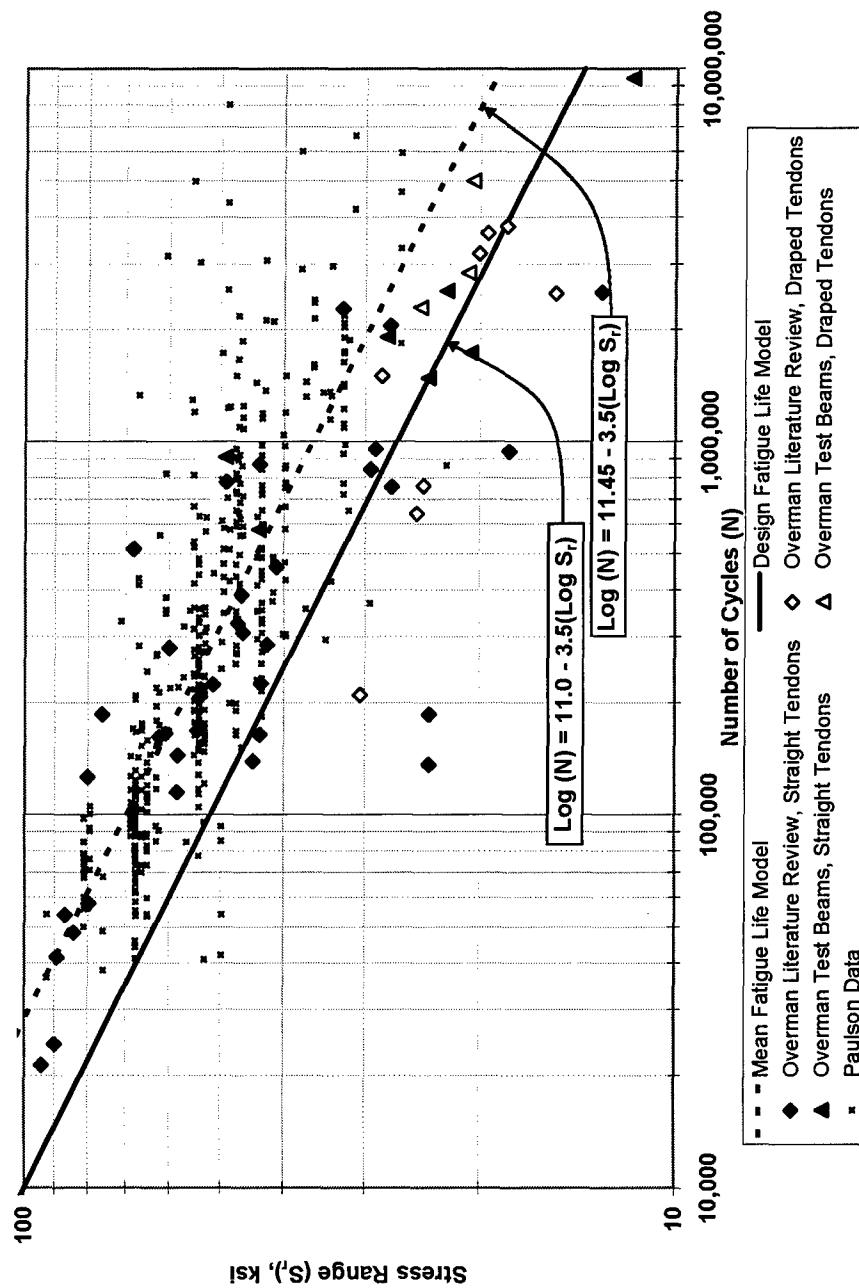
Figure 1-4 Comparison of Beam Data Compiled by Overman and Strand Data Compiled by Paulson

13

Over the past two decades, a limited number of fatigue tests of prestressed beams have been conducted which are directly comparable with the previous results. Most researchers were not attempting to establish the simple fatigue life of prestressed concrete beams, rather they were determining how a particular aspect of the response changed when the beam was subjected to cyclic loading. Because of this, many of the beams were not tested to failure and strand stresses were not provided in the results. Therefore, comparison with the earlier data is not possible.

Others have conducted tests on actual bridge girders that have been taken out of service (Rao and Frantz, 1996). While their analyses of the strand stress ranges are given, the loading history of these beams is obviously unknown, preventing comparison with other beam fatigue tests.

In other investigations, the influence of variable amplitude testing on partially prestressed beams was studied. The random amplitude fatigue testing aimed at being more realistic in its modeling of actual traffic patterns (Naaman and Founas, 1991). In these tests, a distribution of stress ranges was modeled, and then the stress ranges were applied in "blocks" of a given number of cycles at individual stress ranges. The order of the stress ranges was randomly chosen. Because the stress ranges were applied in blocks, instead of a random order, the loading history affected the results. Naaman and Founas (1991) claimed that the results of their tests showed that random testing was not only more realistic, but was more damaging than constant amplitude loading.

Despite the peculiarities of the random amplitude testing, Naaman and Founas (1991) did provide valuable insight into a lack of correlation between the concrete extreme fiber tensile stress and fatigue life. They stated that they could find no rational correlation between the two, reporting that a beam with a calculated nominal tensile stress ranging between $30\sqrt{f_c'}$ and $69\sqrt{f_c'}$ did not fail

14

in fatigue after 2,000,000 cycles, while another beam with a calculated nominal tensile stress ranging between $11\sqrt{f_c'}$ and $32\sqrt{f_c'}$ failed after 1,900,000 cycles. All of their beams had calculated maximum concrete extreme fiber tensile stresses of at least $32\sqrt{f_c'}$, well above any criteria listed in any code publications. However, over half of their test beams had fatigue lives in excess of 2,000,000 cycles.

Still others conducted tests on partially prestressed beams (Shahawi and Batchelor, 1986, Harajli and Naaman, 1985). A few fully-prestressed concrete beams were tested in these studies. Harajli and Naaman (1985) also reported inconsistencies between the calculated maximum concrete extreme fiber stress and the observed fatigue life of prestressed concrete beams. A beam with a calculated extreme fiber stress of $24\sqrt{f_c'}$ had a fatigue life of about 2,000,000 cycles, while another beam with a calculated extreme fiber stress of only $9\sqrt{f_c'}$ had a fatigue life of only about 1,000,000 cycles. It should be noted, however, that for a given stress range, the measured fatigue life of strand can vary by two orders of magnitude. Comparisons of individual tests may not be valid. Fatigue life and stress range data for the three fully-prestressed concrete beams tested by Harajli and Naaman (1985) are summarized in Appendix A.

Wollmann et al. (1996) conducted research on fretting fatigue of post-tensioned concrete beams. While the data from this research are not directly comparable with pretensioned beams, they also noted that the U.S. traditional practice of indirectly addressing strand fatigue by limiting nominal concrete tensile stresses in prestressed beams was not appropriate in all designs. They stated that while the approach can be effective, it lacks accuracy and can be unconservative in some cracked structures.

15

Russell and Burns (1993) conducted fatigue tests on three full-size prestressed beams constructed with high-strength concrete. Unfortunately, they did not test the beams to failure, so there are no comparable data from these tests.

Roller et al. (1995) conducted a fatigue test on a 70-ft long, full-scale, high-strength concrete bulb tee section, but not to failure. The strand stress range was only about 9.5 ksi, and the beam performed very well to 5,000,000 cycles, when testing was terminated.

Muller and Dux (1994) conducted fatigue tests on 31 prestressed concrete beams. Some of their tests were conducted with constant amplitude cyclic loads, while others were subjected to varying load amplitudes. In this case, the varying loads were not random, but increased in amplitude with time. Beams would be tested at low stress ranges for a set number of cycles, then the stress range would be increased for a set number of cycles, and so forth. Most of their beams had draped strand configurations, using metal hold downs. They noted that all failures in beams with draped strands occurred on the inclined side of the hold down devices. Seven beams with straight strands and 13 beams with draped strands were tested with constant amplitude cyclic loads, and the stress ranges and fatigue life results for those 20 beams are summarized in Appendix A.

Figure 1-5 provides a comparison of all available constant-amplitude fatigue data from prestressed concrete beams with the in-air strand test data and associated models reported by Paulson et al. (1983). One can notice that there is reasonably good correlation between the in-air data and the data from beams with straight tendons, while the beams with draped tendons generally experienced reduced fatigue resistance.

16
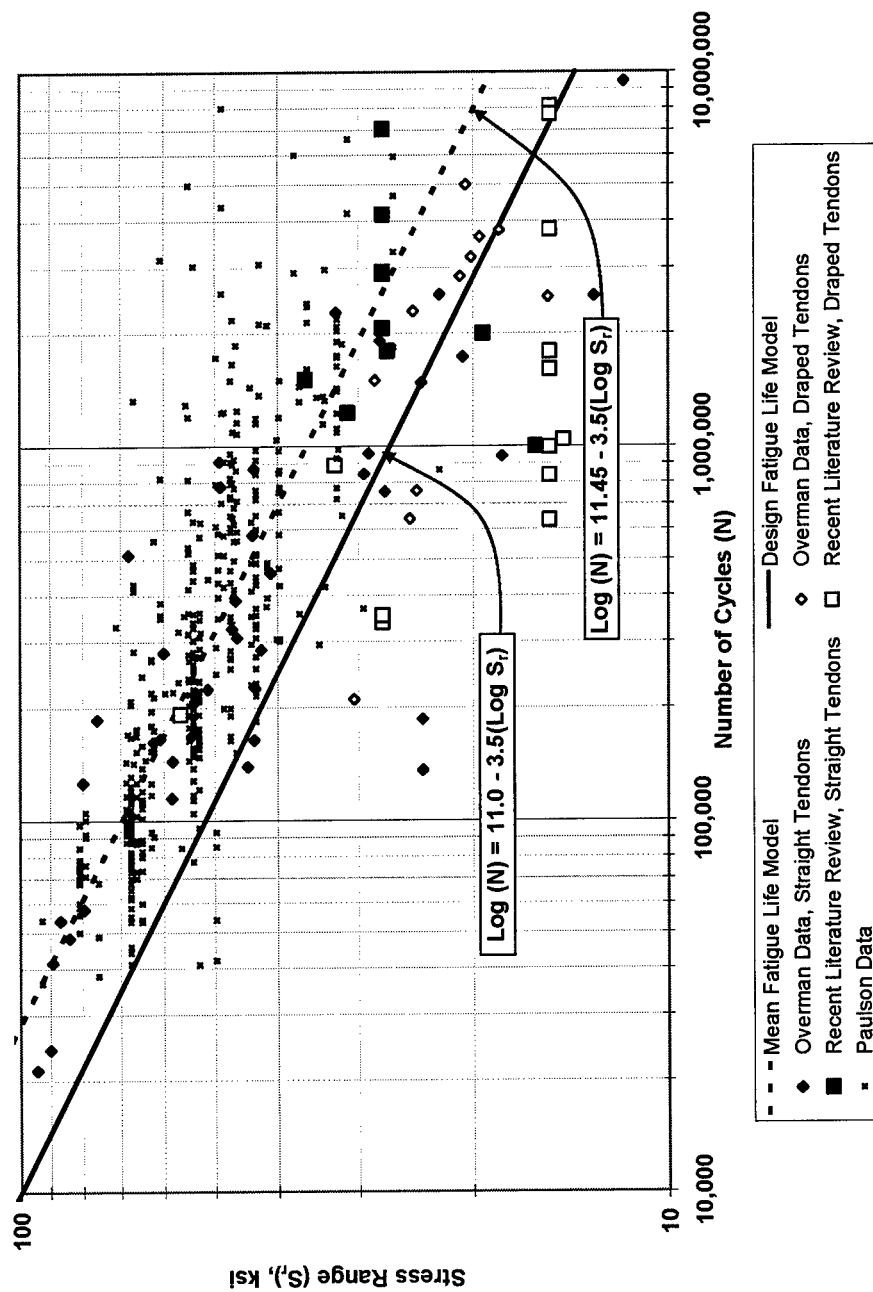
Figure 1-5 Comparison of Beam Data From Constant-Amplitude Fatigue Tests and Strand Data Compiled by Paulson

17

1.6 EXPECTED RESULTS BASED ON PREVIOUS TESTING

As stated in Section 1.3.1, six beams were designed and constructed as a part of TXDOT Project 1895. Loading levels in the tests were based on strand stresses in the prototype bridge girder with index extreme fiber stress levels of $6\sqrt{f_c'}$, $7.5\sqrt{f_c'}$, and $12\sqrt{f_c'}$ using uncracked section analysis. Two beams were to be tested at each index stress level. Results of the fatigue tests run on four of the six beams will be presented in this thesis. Two of these beams were tested based upon the $7.5\sqrt{f_c'}$ index stress level and two were tested based on the $12\sqrt{f_c'}$ index stress level. Based on the analyses by Hagenberger (2003), these two index stress levels will result in stress ranges of approximately 22 ksi and 42 ksi, respectively, in the test beams.

Based on the plot in Figure 1-5, it is hypothesized that the fatigue life of the beams with an index stress of $7.5\sqrt{f_c'}$ should be between 2,000,000 and 9,000,000 cycles, while the fatigue life of the beams with an index stress of $12\sqrt{f_c'}$ should be between 200,000 and 1,000,000 cycles

1.7 DESCRIPTION OF FOLLOWING CHAPTERS

This thesis contains six chapters and three appendices. Chapter 2 discusses the details of the strand testing and verifies that the strand conforms to applicable industry standards. Chapter 3 provides a discussion of the beam test setup and general procedures used to test all of the beams. Chapter 4 presents the data measured during the fatigue tests of each beam. Chapter 5 evaluates the response of the beams and compares the measured response with the expected results. Finally, Chapter 6 presents conclusions and recommendations for further research.

18

The appendices provide details to support the information presented in the chapters. Appendix A provides data assembled during the literature review process. Appendix B gives a detailed report about strand test grips developed for the in-air tests of prestressing strand. Appendix C describes an extensometer that was designed and constructed to determine modulus of elasticity of prestressing strand.

CHAPTER 2

Strand Fatigue Tests

2.1 PURPOSE OF IN-AIR FATIGUE TESTS

As discussed in Chapter 1, in nearly all properly designed prestressed concrete beams failing in fatigue, strand fatigue is overwhelmingly the dominant failure mode. Concrete compression stress fatigue is almost never a concern. Knowing this, characterizing the strand used in the beam testing was deemed essential. Abnormal failure of the beam because of abnormal characteristics of the prestressing strand had to be ruled out.

2.2 STRAND PROPERTIES

The strand used in the beam specimens was typical seven-wire, ½-in. diameter, Grade 270 low-relaxation strand. As such, the strand should meet the requirements for prestressing steel specified by ASTM A 416, namely:

Minimum Tensile Strength	270 ksi
Minimum Yield Stress*	245 ksi
Minimum Elongation at Rupture	3.5 %
Minimum Gage Length	24-in.

* Yield stress taken as the stress at an elongation of 1.0 %.

Because the beams were to be tested in fatigue, verification of normal strand fatigue characteristics was also critical. Additional elastic characteristics were also verified because strain gages were used to monitor the performance of the strands in the beams. Because the strain gages are attached to the individual

wires oriented along the local axis of the wire, which is at a set pitch or angle from the axis of the strand, the strain gages do not indicate the average strain experienced along the axis of the strand. Consequently, the modulus of elasticity of the strand when using the strains from the gages will appear higher than expected. In order to correlate the "apparent modulus" from the gage data to the axial strand modulus of elasticity, modulus of elasticity tests were also performed.

2.3   TESTS PERFORMED

There were physically four separate tests performed on various strand samples. All strand tests were performed on an MTS 220-kip capacity load frame, model 311.31 using MTS TestStar software, version 4.0C. In all tests, the specimen length is the distance between the inside faces of the grips, not the cut length of the strand, which was longer to incorporate the length of the grips.

2.3.1   Apparent Modulus of Elasticity

The first test performed on the strand was what will be named the "apparent modulus of elasticity." As previously mentioned, data from this tests were used to correlate the measured strain from the strain gages with the longitudinal strain in the strand.

Twelve four-ft specimens were prepared with strain gages attached to the outside wires of the strands. The twelve specimens were taken from strands that extended beyond the ends of the beams, and had undergone the same loading history as the strands in the beams. The number of specimens was driven by the number of beams (6) and the number of strands per beam (2). The strain gages were attached to the exterior face of individual wires, along the local longitudinal axis of the wire. Four strain gages were attached to four wires of the first specimen, to determine if significant difference in strain should be expected among the strain gages, depending on their circumferential location on the strand.

21

Because prestressing strand is transported and stored on large reels, residual curvature remains when the strand is removed from the reel and released from tension. However, the strains measured on the first specimen did not indicate significant differences in strain. Consequently, on the other eleven specimens, only two strain gages were attached. Strain gages were attached approximately at the mid-point of all specimens.

All specimens were loaded into the testing machine using the threaded aluminum grips described in Appendix B. A parallel jig was used to place the strand in the machine's grip heads to ensure parallel, aligned placement of each specimen, which was then verified plumb and straight with a level.

Load and strain data were recorded by use of an automatic data acquisition program. Manual data were taken at 2 kip increments to ensure that the computer generated data were accurate. Each strand was loaded two times from 0 to 24 kips and then unloaded.

Graphs of load versus gage strain were plotted, and then the slope of the data from each graph was determined using standard linear regression functions in Microsoft Excel. The slopes were averaged for each gage to determine its apparent modulus of elasticity. All of the gages were then averaged to determine an average apparent modulus of elasticity of 31,200 ksi with a standard deviation of 330 ksi. The values are summarized in Table 2-1.

The strands were numbered 1 through 6 as they sat in the prestressing bed. Because two beams were constructed end to end, strands 1 and 2 went through beams 1 and 2, strands 3 and 4 went through beams 3 and 4, etc. For labeling purposes, the strand specimen labeled "1" was taken from the static end of strand 1, and the strand specimen labeled "1L" was taken from the jacking end of strand 1, which had a longer exposed length between the end of the beam and the gripping wedges.

22

Table 2-1 Apparent Modulus of Elasticity Test Results

Strand	Gage	Apparent Modulus of Elasticity (ksi)
1	1	31327
	2	31228
	3	31098
	4	30877
1L	1	30895
	2	31231
2	1	31270
	2	31418
2L	1	31738
	2	30388
3	1	30764
	2	31278
3L	1	30834
	2	31106
4	1	31309
	2	31584
4L	1	31248
	2	31345
5	1	31117
	2	31040
5L	1	31357
	2	30709
6	1	31155
	2	31437
6L	1	31778
	2	31616
Average Apparent Modulus		31198
Standard Deviation		330

2.3.2 Strength of Strand

While the tensile strength of the strands was inconsequential to the fatigue tests of the beams, this property was measured to verify that the strand satisfied all the requirements of ASTM A 416. The specimens used for this test were taken

23

from the same reel of strand immediately after the lengths of strand used to construct the beams. Grips were threaded aluminum, as described in Appendix B. Grip head hydraulic pressure was increased to prevent significant grip slip at the high tensile loads.

Strain for these tests was measured using machine head displacement. While head displacement would not have been satisfactory for modulus tests, for the purposes of verifying ultimate strength, it was considered sufficiently accurate.

Strand Specimen T2
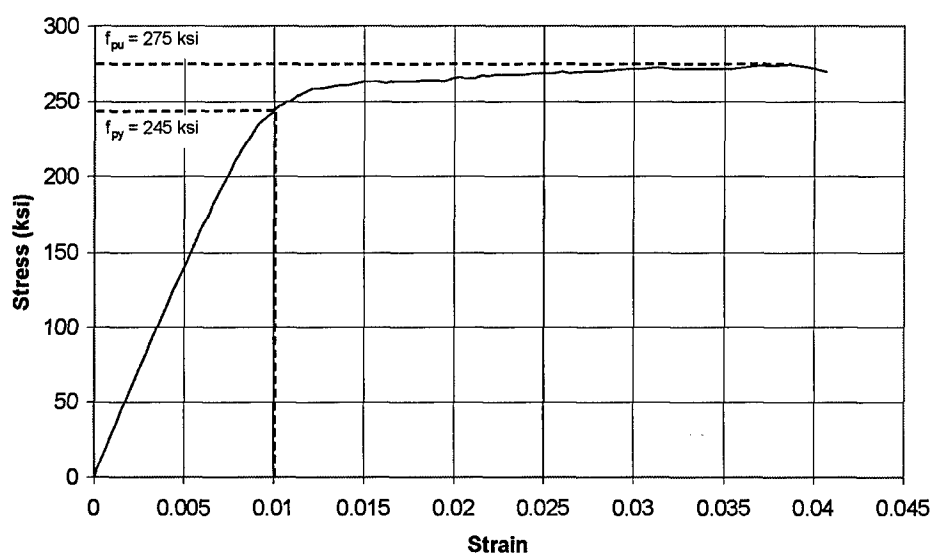
Figure 2-1 Representative Results From Strength Tests

Figure 2-1 shows a plot of the representative test to failure. As can be seen on the plot, the yield stress was 245 ksi and the tensile strength was 275 ksi.

24

2.3.3 Strand Modulus of Elasticity

It is obvious that the apparent modulus of elasticity (based on strain gage readings) is higher than would be expected for typical strand. This increased value is caused by the pitch angle of the wires in the strand and the complex interactions among the wires. While the apparent modulus is useful for determining stress changes in the beam strands based on strain gage readings, it does not verify that the strand modulus of elasticity is typical of normal strand. A specific test for stand modulus of elasticity was conducted for this verification.

For this test, a strand specimen was chosen from the twelve previously tested for apparent modulus of elasticity. The strand was chosen because it displayed approximately average apparent modulus, and was thus considered representative of the twelve for comparison purposes between strand modulus of elasticity and apparent modulus of elasticity.

The strand was fitted with an extensometer which had a gage length of 24 inches. The strand used the threaded aluminum grips described in Appendix B.

Four tests were run on the test specimen. Data were collected by automatic data acquisition, with manual records taken for verification. Slopes of the stress/strain data were then determined from each of the tests using the linear regression functions of Microsoft Excel. The resulting modulus of elasticity value for each test is reported in Table 2-2. The four modulus values were then averaged to render an average strand modulus of elasticity value of 29,400 ksi with a standard deviation of 83 ksi.

Table 2-2 Strand Modulus of Elasticity Tests

	Modulus of Elasticity (ksi)		
	LVDT 1	LVDT 2	LVDT Average
Test 1	29673	28853	29259
Test 2	29757	29130	29441
Test 3	29742	29092	29414
Test 4	29740	29097	29416
Average	29728	29043	29382
Average Modulus of Elasticity			29382
Standard Deviation			83

2.3.4 Strand Fatigue

Certainly one of the characteristics of the strand that needed to be verified was the strand performance under fatigue loads. The purpose of these tests was not necessarily to try to correlate in-air tests to beam tests, rather it was, like all the other strand tests, meant to verify that the strand used in the beam is representative of strand satisfying ASTM A 416. The fatigue testing was considerably more in depth than the other tests described in this section. The test setup and results are discussed in greater detail in Sections 2.4 and 2.5.

2.4 FATIGUE TEST SETUP AND PROCEDURE

2.4.1 Strand Specimen Length

In accordance with ASTM A 931 (2002), the length of test specimen shall not be less than 3-ft for specimens up to 1-in. in diameter. Four feet was used as the specimen length simply because it matched the length of the constant moment region in the test set up for the beams. Fatigue cracks begin at locations of flaws and other deformations along the strand, which act as stress raisers (Collins and Mitchell, 1997). Intuitively, the worse the stress raiser, the sooner fatigue cracks

form. Thus, a length effect can be observed. The longer the length of strand that is tested, the more likely a significant stress raiser will be found in that strand, and thus the shorter the fatigue life will be.

2.4.2 Equipment

All fatigue tests were performed in an MTS 220-kip capacity load frame, model 311.31, using MTS TestStar software, version 4.0C. Hydraulic pump pressure was set between 2200 and 3000 psi, which depended on test machine tuning requirements balanced against the ability to cool the hydraulic pump. Loading frequency was set based on the ability of the loading frame to respond to the command signal. The higher the stress range required, the more hydraulic fluid has to be pumped, the lower the frequency has to be. Figure 2-2 shows the test machine with the control station at the Ferguson Structural Engineering Laboratory.

Figure 2-2 MTS Machine and Control Station

2.4.3   Gripping Methods

The test machine gripping heads squeeze down on the specimen perpendicular to the specimen longitudinal axis, necessitating the use of a block shaped grip. The initial grip design was an aluminum block which had been drilled and threaded longitudinally, then cut in half to place the specimen between the halves. The threading was intended to allow the aluminum to squeeze into the interstitial area between wires in the strand, increasing the surface area of the

strand, not just contacting the outside faces of the wires. All tests run with this grip resulted in fatigue failures at the face of the grip.

An alternative grip was eventually developed. Lamb and Frank (1985) reported that in their strand tests, "None of the tests performed with the pre-deformed copper wedges produced failures within the anchorage region." With this in mind, copper wire was wound between the wires along the strand and the insides of the aluminum block gripping surfaces were machined smooth. Figure 2-3 shows a successful grip after use. The design has some distinct advantages over other methods. It is relatively inexpensive, because the aluminum block can be used repeatedly; only the copper wire need be replaced. It is also reasonably quick to use, especially compared to systems where epoxies or other substances must be hardened around the strand.
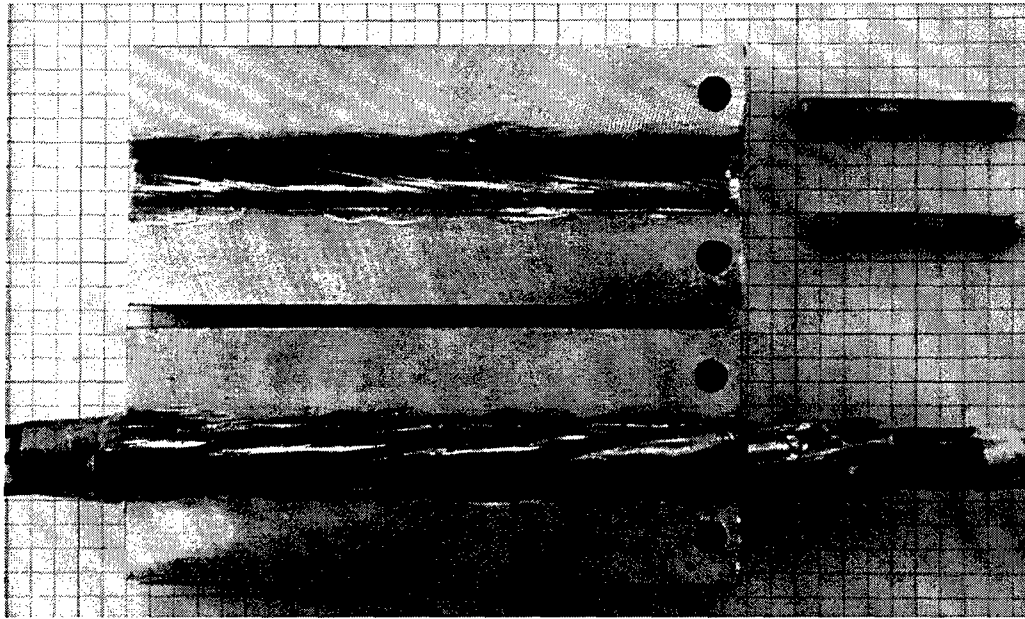
Figure 2-3 Picture of Successfully Used Grip

The grip is also relatively easy to make accurately. No threading is used, which makes it possible to machine the circular groove for the strand with a round cutting tool, rather than drilling a long slender hole and risking drill bit wobble. The details of the grips used and gripping procedure are available in Appendix B.

2.4.4 Installation Procedures

The most important principle in placing the specimen in the test apparatus is to keep the specimen concentric in the machine on both ends, keeping the specimen straight along the axis of the machine, in order to prevent bending stresses in the strand at the grip faces. To accomplish this, the machine head faces were verified in line and plumb using a high quality level. Because the faces were in line, a parallel jig was made for quick installation of the aluminum grips inside the head. Figure 2-4 shows an installed grip.

30
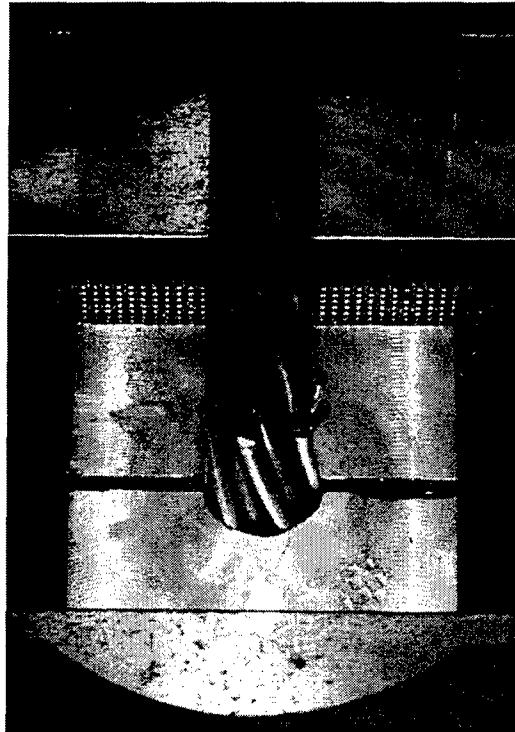
Figure 2-4 Installed Grip Ready for Testing

For successful fatigue testing, grip pressure is of great importance. The grip needs to be barely tight enough not to slip, but not so tight that the grip produces stress raisers that cause fatigue. Leaving a gap between the two halves of the grip allows for adjusting the grip pressure on the strand.

2.4.5 Test Procedure

Fatigue testing is straight forward with the machine used. With the control software, one must simply enter in the mean tension and the amplitude of the load range desired, along with the frequency and the desired wave shape. The program then controls the machine. The first important factor for the operator is to ensure that the machine is properly tuned (gain settings properly adjusted).

Tuning the machine is best done with a spare specimen. Reducing the error between the command generated signal and the system response is key.

Once the machine error is minimized, the error detection control levels can be adjusted just outside of the normal operating error signal, which stops the test when a wire breaks and the machine response varies momentarily from the input signal. The tests were run in load-control mode to control the stress ranges closely. When the error detection levels were properly set, the machine stopped at the first wire failure, accurately showing the number of cycles to failure.

2.5   FATIGUE TEST RESULTS

The initial intent of the tests was to conduct in-air tests at the same mean stress and stress range that would be experienced in the beams. However, the strands did not fail except when tested at the high stress range. Consequently, strands were tested at higher stress ranges to confirm that the strands had normal fatigue characteristics. Table 2-1 summarizes the test results. Strand specimens labeled with an "A" were additional specimens obtained from the same reel of prestressing strand that was used for beam construction and were numbered sequentially.

32

Table 2-3 Strand Fatigue Test Results

Strand Number	Mean Stress (ksi)	Stress Range (ksi)	Cycles
A15	153	48	181,668
A16	153	48	561,414
A17	153	48	720,707
A18	153	48	464,364
4L	150	40	* 4,262,345
3L	150	40	* 3,995,123
A19	150	65	137,283
A20	150	65	124,005
A24	150	65	157,755
A25	150	65	132,489
A26	150	80	88,824
A27	150	80	97,706
A28	150	80	91,763
5L	150	80	38,914
* Test stopped before failure, run-out.			

At first glance, one might suspect that the run-outs of strands 4L and 3L show unusual strand characteristics. Upon further review of the data collected by Paulson, et al. (1983), one will find numerous cases of nonfailure tests at these stress ranges. It should be understood that Paulson's models and data are appropriately based solely on tests resulting in fatigue failures. This is certainly the most conservative approach, though it doesn't take into account that many strands actually performed better than his model indicates.

33

2.6 COMPARISON OF ACTUAL PROPERTIES WITH EXPECTED PROPERTIES

Based on the results of the tests, the strand appears normal in all respects, and, being stored indoors, appears by visual inspection to be without noticeable corrosion or defect.

2.6.1 Apparent Modulus

Although there were no specified values to compare against, the apparent modulus information was obtained to evaluate the response of the beams, especially for determining prestress losses.

2.6.2 Tensile Strength

As shown in Figure 2-1, the tensile strength and stress-strain response appear to be within standards. The yield stress was almost exactly the required 245 ksi, while the tensile strength was slightly above the required 270 ksi at 275 ksi. Since the strain measurements were based on machine head displacement, actual strain can only be smaller than that measured (due to the possibility of slip). Consequently, the yield stress value is a conservative value. It cannot be stated conclusively that the strand met the elongation rupture requirements because of the method of measurement, even though it appears satisfactory.

2.6.3 Strand Modulus of Elasticity

The measured strand modulus of elasticity at 29,400 ksi is slightly above the range of values typically used for design, 28,500 to 29,000 ksi (PCI 1992)

2.6.4 Fatigue

As can be seen in Figure 2-5, all of the fatigue specimens tested to failure broke within the expected range of cycles given by Paulson, et al. (1983). The two specimens that did not fail in fatigue are also shown for reference, but as was

34

noted earlier, Paulson, et al. (1983) did not include any runout specimens, although reasonably common.
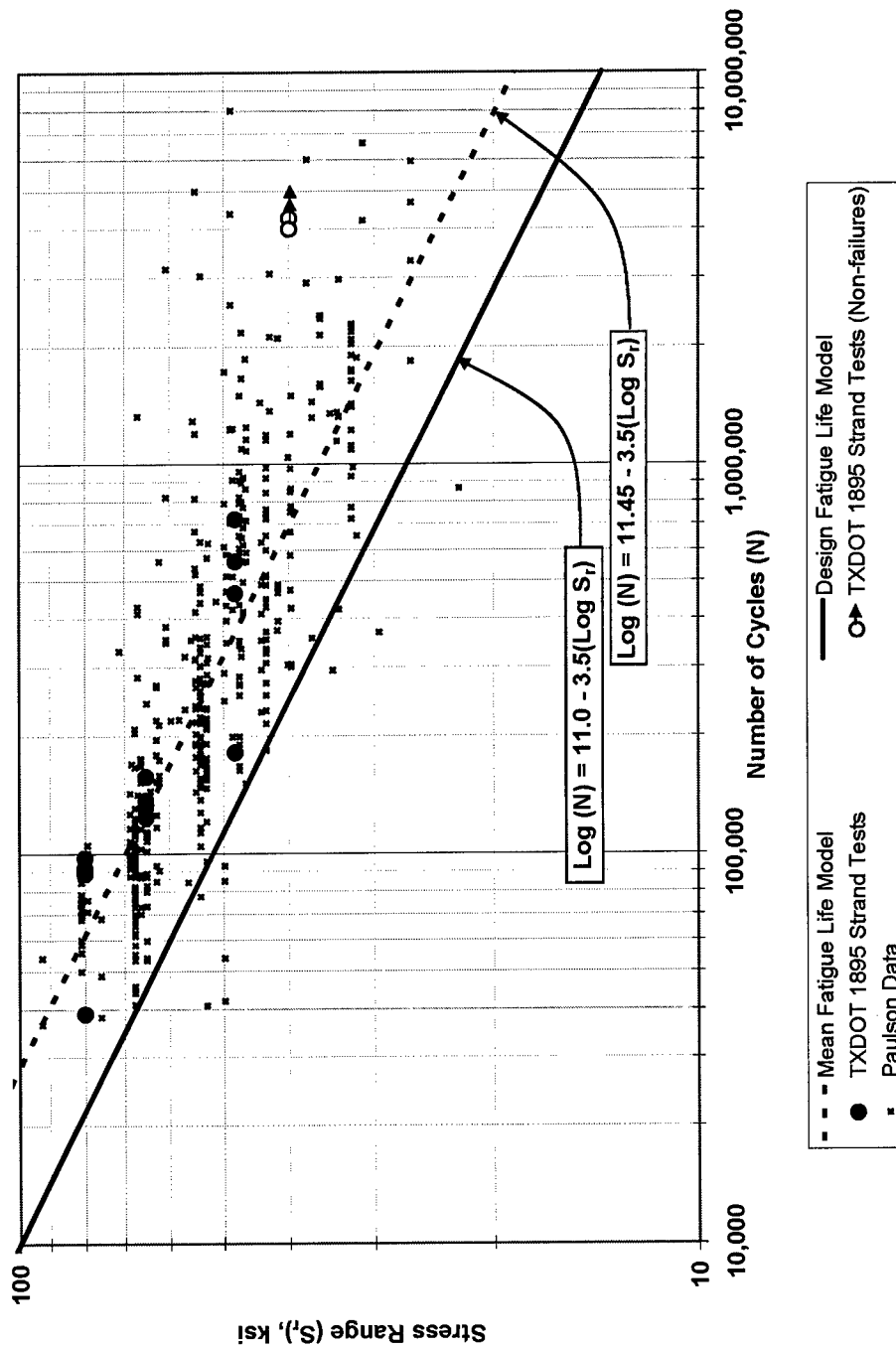
Figure 2-5 Plot of Test Results Compared to Paulson's Models and Data

36

CHAPTER 3

Beam Test Setup and Procedures

3.1 BEAM CONSTRUCTION AND MATERIALS

Six beams, labeled Beam 1 through 6, were constructed and tested as a part of the TXDOT 1895 project. The response of the first four beams tested (Beams 2 through 5) will be discussed in this paper. Hagenberger (2003) will discuss the response of the remaining two beams. While construction details and analyses of all six beams are provided in detail by Hagenberger (2003), a brief description is given here for the convenience of the reader.

3.1.1 Geometric Properties

The beams were T-shaped, pretensioned, prestressed concrete beams. They were built to model a highway bridge, with higher strength concrete in the girder and lower strength concrete in the slab/flange. The entire cross section was designed to act as a composite section. The beams were 15 ft long with a cross section as shown in Figure 3-1.
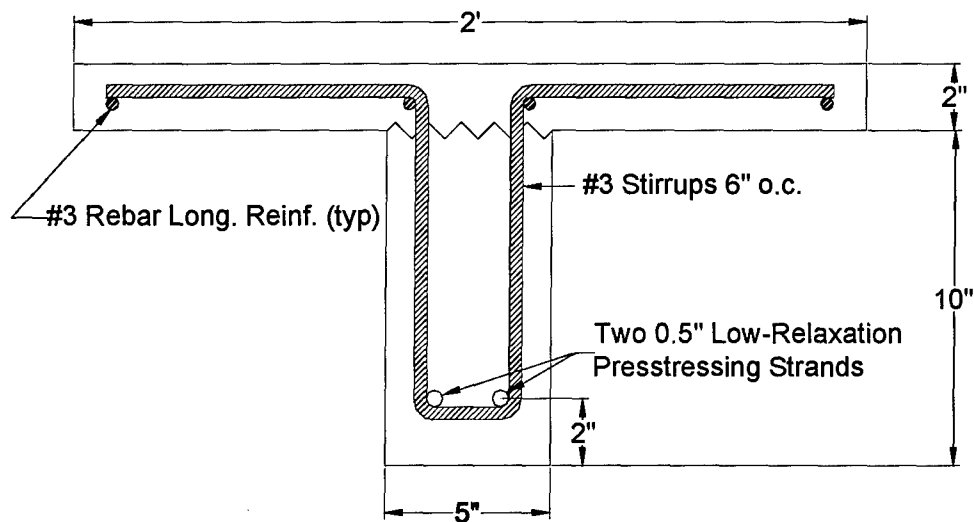
Figure 3-1 Typical Beam Cross-Section

3.1.2 Material Properties

3.1.2.1 Concrete

The concrete in the flanges was placed two days after the concrete in the web and the compressive strengths were intentionally different. During design, the compressive strength of the concrete in the webs was assumed to be 10,000 psi, and the compressive strength of the concrete in the flanges was assumed to be 6000 psi. However, the measured strengths of both concretes exceeded the design strengths by considerable amounts. At the time of the beam tests, the compressive strength of the web concrete was approximately 12,000 psi, while the compressive strength of the flange concrete was approximately 6,700 psi.

3.1.2.2 Prestressing Strand

The measured material properties of the prestressing strand are discussed in detail in Chapter 2. Two prestressing strands ran straight through all beams.

The strands were centered horizontally and were 2 in. apart and located 2 in. from the bottom of the beam.

3.1.2.3 Reinforcing Steel

The stirrups and longitudinal bars in the flange were typical #3 Grade 60 deformed reinforcing bars (ASTM A 615). The stirrups were placed 6 in. on center along the length of the beam, except within 1 ft of midspan, where they were omitted near the internal strain gages. The longitudinal steel was provided as shown in Figure 3-1 to facilitate placement of the stirrups.

3.1.3 Prestressing

The prestressing strand was initially tensioned to 150 ksi. Ten strain gages were used on the strands in each beam to provide prestress loss data. The apparent modulus of elasticity discussed in Chapter 2 was used to determine the prestress losses from strains measured after release of the strands. Effective prestress after losses will be stated with the results of each beam. The effective prestress ranged from 127 to 135 ksi.

3.2 TEST SETUP

3.2.1 General Geometry

The physical layout of the testing frame and supports was simple, with the beam being supported on elastomeric pads at the ends and the two point loads symmetrically placed 2 ft from midspan. The test setup is shown in Figure 3-2. Figure 3-3 provides a schematic of the test setup.
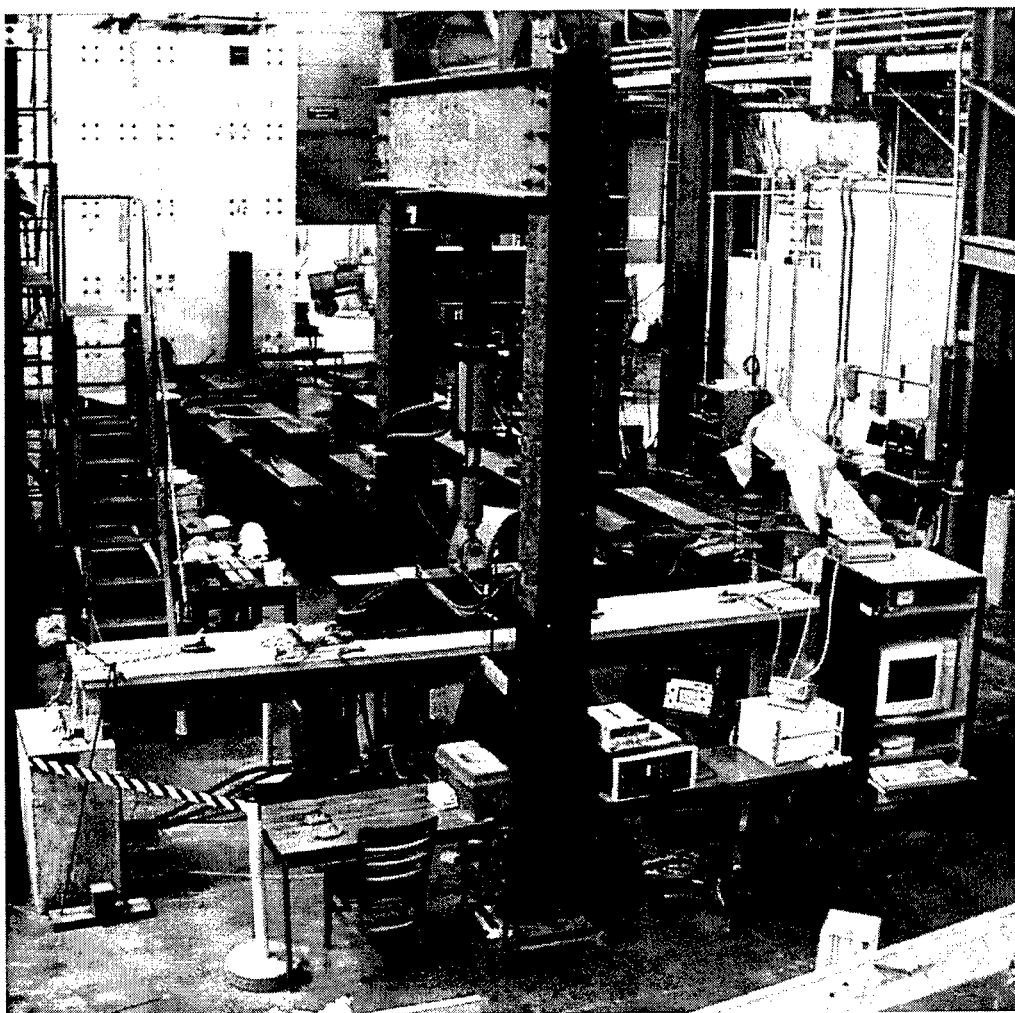
Figure 3-2 Beam Test Setup

40
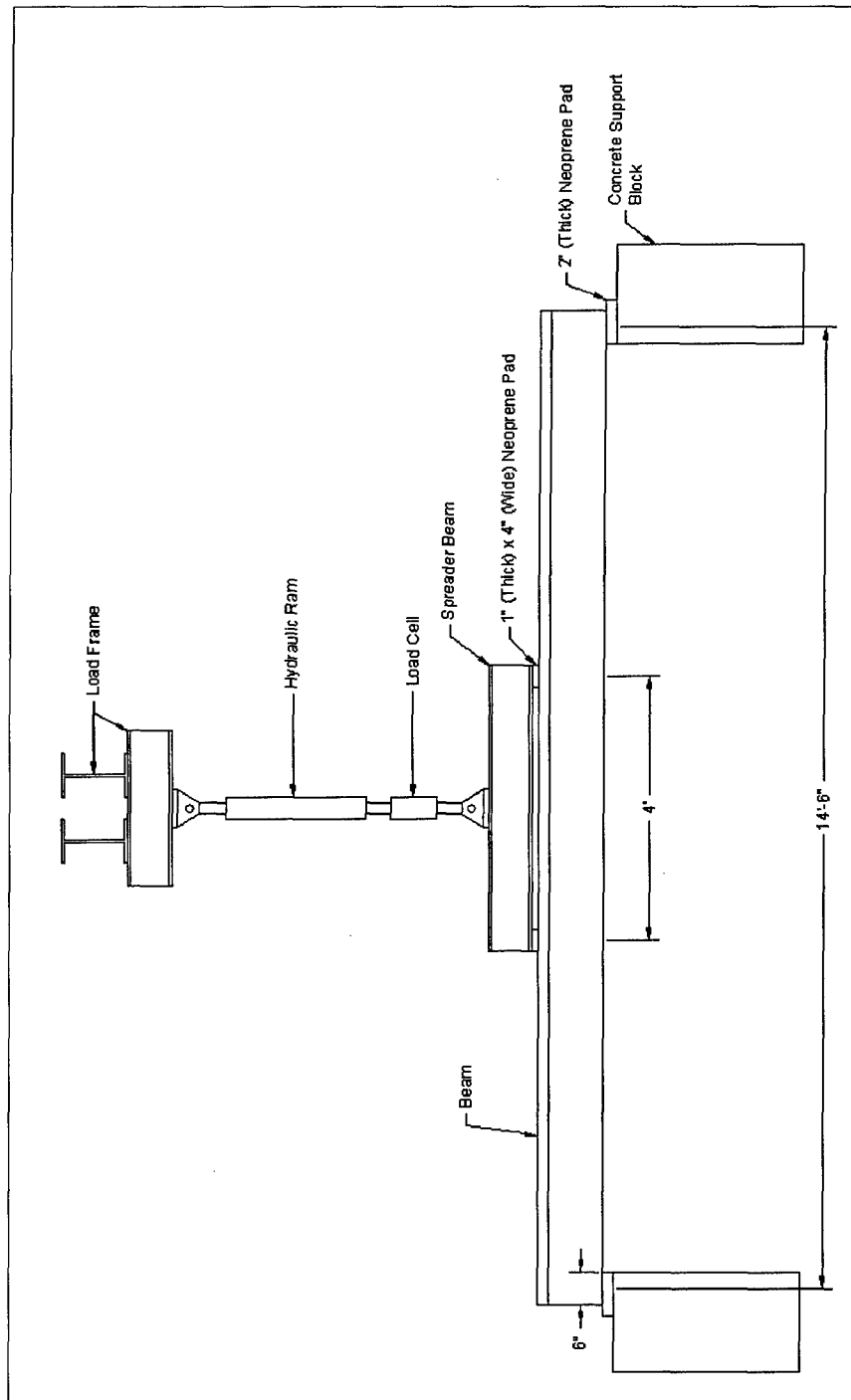
Figure 3-3 Beam Test Setup Schematic Diagram

41

The two point loads created a 4-ft constant moment region. Because fatigue failures initiate from material flaws, a constant moment region provides a finite length along which fatigue cracks may develop. As the length of the constant moment region increases, the expected fatigue life decreases because the likelihood that a significant flaw is located within the constant moment region increases. Thus, full-sized beams with more strands in their cross sections will generally have shorter fatigue lives than smaller test specimens.

The beams were 15 ft long, resting on a 6-in. neoprene pad at the supports. Effective beam length was then taken as the center-to-center distance between the pads, or 14.5 ft. The spreader beam split the single load provided by the hydraulic ram into two equal loads. The two loads were applied through 1-in. thick neoprene pads that were 4 in. long. The 4-ft constant moment region length was the center to center distance between these two neoprene loading pads. Neoprene bearing pads were used to prevent damage from local stress raisers (concrete surface flaws) and to allow reasonably free rotation over the small angles produced due to bending.

3.2.2 Instrumentation

Several types of instruments were used to measure displacements and strains. All instruments were connected to the data acquisition system for automatic reading.

Each beam had ten 5-mm strain gages attached to the prestressing strands within 12 in. of midspan. Located at the same depth, each beam also had one 60-mm embedded concrete strain gage between the two prestressing strands near midspan.

Figure 3-4 shows the placement of the vertical displacement transducers used to measure midspan and end deflections.

42
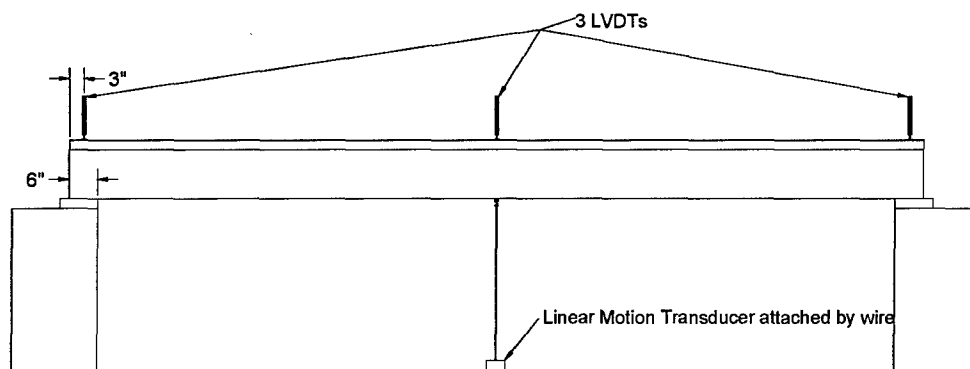
Figure 3-4 Placement of Vertical Displacement Transducers

Three direct current linear variable differential transformers (LVDTs) were used to measure vertical displacement. One was used to measure midspan deflection, while the two others were used to measure deflection at the ends due to the compression of the neoprene bearing pads. These three LVDTs were TRANS-TEK Model 0352-0000. In addition to the three LVDTs, an Ametek Rayelco linear motion transducer was connected to the bottom of the beam as a second reference for midspan deflection. Midspan deflection values reported in this paper are corrected for average bearing pad compression displacement.

Once a crack formed, two more strain gages were attached to the bottom surface of the concrete, and a fourth LVDT was placed across the crack. The strain gages were 60-mm gages attached along the longitudinal axis of the beam on either side of the crack. The LVDT was attached using two short pieces of L1½ x 1½ x ⅛ angles on the side of the beam approximately at the same height as the bottom of the beam as shown in Figure 3-5. This LVDT was a TRANS-TEK Model 0350-0000. Since the steel angels are separated by about ½ in., the LVDT indicates both the crack width and the elastic deformation of the ½ in. of concrete. The purpose of the LVDT was not to measure the crack width, rather to indicate when the crack opens. The surface strain gages were used for the same purpose.

43

Figure 3-5 LVDT Across Crack (Crack Displacement Gage)

Applied load was measured using a Lebow model 3117-104 load cell. The load cell had a capacity of 100 kips.

3.2.3 Test Control

3.2.3.1 Data Acquisition

All gages and transducers were connected to a desktop computer through a data logger input/output system for data acquisition. The gages and transducers were connected to a Hewlett Packard 75000 Series B Data Logger through circuit completion boxes. The desktop computer recorded the data using the Ferguson Structural Engineering Laboratory Data Acquisition add-in to Microsoft Excel.

Voltage data from the linear motion transducer were also recorded manually for Beams 2, 3, and 5. After analyzing the information from Beam 4 (the first beam tested), it was recognized that permanent offset in the midspan deflection was not being recorded. The external transducers were removed during the fatigue loading to reduce transducer wear. Because the transducers could not be repositioned exactly the same each time, the acquisition software was zeroed before each test after the external transducers were reattached. A highly accurate

44

multimeter was then attached to the output of the linear motion transducer for later tests so that the deflection at zero load could be monitored over the entire life of the beam.

3.2.3.2 Test Control Method

Static tests and fatigue tests were controlled using an MTS 458.10 Microconsole controller. The tests were run in load-control mode.

3.2.3.3 Methods of Stopping Fatigue Tests

Four error signals were monitored to ensure that the test was running at the desired loads. The first was an input to output error signal that compared the command signal from the signal generator with the output of the load cell. Changes in this error signal indicated changes in the beam response. Beam response changes are indicative of material changes such as cracking of the concrete or fracture of the wires. This error signal will also stop the test if the hydraulic pressure to the ram is lost.

Two of the error signals were high and low load error signals, which stopped the test if the load cell output was outside of the set range. These signals prevented beam damage in the event that the MTS controller signal generator produced erroneously high command signals. Additionally, these error signals stopped the test if the hydraulic pressure to the ram was lost, preventing errant fatigue cycle counts.

The last error signal was produced by a limit switch placed just under the beam flange at midspan. The limit switch (Figure 3-6) was set such that if the midspan deflection increased by the limit switch travel length, then the switch opened a circuit and caused an emergency stop in the MTS controller. The travel length was just less than 1/16 in. and was found to be very effective in detecting

45

increased deflection caused by concrete cracking and wire breaks within the prestressing strand.
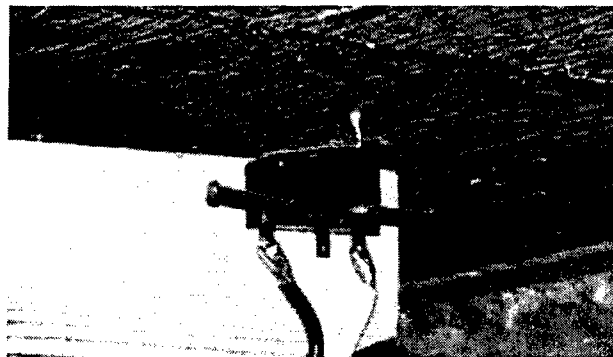
Figure 3-6 Limit Switch Under Flange

3.3 TEST PROCEDURES

Prior to running fatigue tests, concrete compressive strengths and modulus of elasticity were measured for both the web (girder) concrete and the flange (slab) concrete. Additionally, prestress loss data were used to calculate the effective prestress. Then, static tests were run to document baseline response. Periodically during the fatigue tests and when an error signal interrupted a fatigue test, fatigue loading was stopped and a static test was run to verify beam response characteristics. Finally, after the conclusion of each fatigue test, the concrete was removed to expose the strand near midspan so that the number of wire breaks could be determined.

3.3.1 Concrete Cylinder/Modulus Tests

Immediately before each beam test, the compressive strength of the concrete was determined in accordance with ASTM C 39/C 39M. Additionally, the modulus of elasticity of the concrete was measured using the methods described in ASTM C 469. Cylinder testing was conducted on a Forney model LT-0806-01 test machine at the Concrete Durability Center Laboratory in

46

Building 18B of the J. J. Pickle Research Campus of the University of Texas at Austin.

3.3.2 Determination of Prestress Losses

Ten 5-mm strain gages were attached to the prestressing strands and monitored by Hagenberger (2003) continuously from the initial prestressing until just before the beam testing. Based on the apparent modulus of elasticity described in Chapter 2 and the changes in the average observed strains, prestress losses were calculated and used in the analyses by Hagenberger (2003).

3.3.3 Initial Static Tests

Before beginning the fatigue loading, each beam was subjected to two static tests. Concrete cracks formed during the first static load except in Beam 3. For Beams 2, 4, and 5, the concrete surface strain gages and crack displacement gage were applied after the first static test. Beam 3 cracked during the first 25 cycles of fatigue loading. The strain gages and crack displacement gage were applied to Beam 3 after 100 cycles, at the time that a prominent crack could be identified.

At the beginning of all static tests, the displacement transducers were positioned and zeroed. The data acquisition system was started in automatic mode and several readings were obtained at zero load. The load was usually increased in 1-kip increments until the flexural tensile stresses were approximately equal to the precompression stress at the bottom fiber at midspan. The loading increment was reduced after this point as the cracks opened. During the initial tests, a loading increment of 0.25 kip was used and 0.5 kip was used in subsequent tests. During the initial tests, these smaller load increments were continued until the maximum test load was reached. In subsequent tests, if the beam was loaded significantly above the decompression load, 1-kip increments

47

were again used in this region of linear response. Data were recorded during unloading as well.

The beam was inspected for cracks during loading. Cracks were marked at load increments with colored markers.

During each static test, data were recorded from all available strand strain gages, the embedded concrete gage, and the vertical displacement transducers. After the crack gages were installed, data were also recorded from the concrete surface strain gages and the crack displacement gage.

3.3.4 Fatigue Tests

During the fatigue tests, a sinusoidal command signal was used to apply cyclic loads to the beam. The maximum and minimum loads were determined from analyses conducted by Hagenberger (2003) to provide stress ranges in the prestressing strands similar to those experienced by the prototype highway bridge being studied in this project. The critical parameter in evaluating the highway bridge was the calculated tensile stress in the extreme fiber of the girders using an uncracked section analysis. Two levels of tensile stress were considered: $12\sqrt{f_c'}$ and $7.5\sqrt{f_c'}$. Throughout the remainder of this thesis, reference will be made to these two stress indices.

The applied loads for each test beam were selected such that the calculated stress range in the strand was the same as the calculated stress range in the center of gravity of the strand profile in the prototype highway bridge girders at one of the two stress indices described above. Additionally, the calculated minimum stress in the test beam strand was the same as the calculated minimum stress in the extreme layer of strand in the prototype highway bridge girders. For Beams 4 and 5, the stress index was $12\sqrt{f_c'}$. For Beams 2 and 3, the stress index was

$7.5\sqrt{f'_c}$. Figure 3-7 provides a summary of how the strand stresses in the test beam were selected.

(a) Prototype Highway Bridge Girder

Midspan

Deck Slab

Girder

Center of Strand Profile $\rightarrow$

f_{ps-DL}

$\Delta f_{ps-prototype}$

Index Stress = Bottom Fiber Stress = $12\sqrt{f'_c}$ or $7.5\sqrt{f'_c}$

(b) Test Beam

Midspan

Strand $\rightarrow$

f_{ps-min}

$\Delta f_{ps-test}$
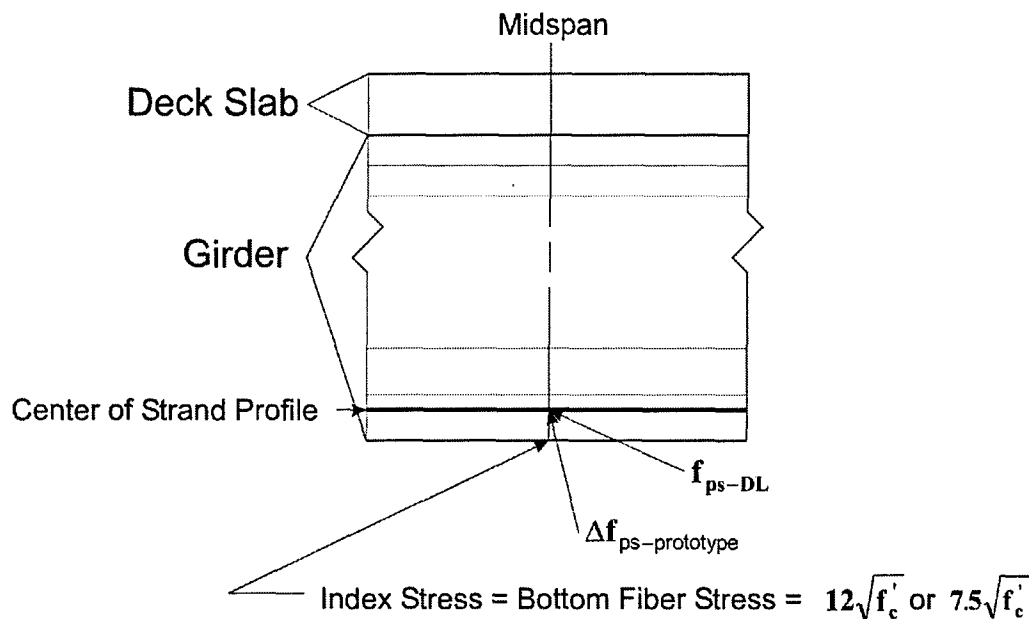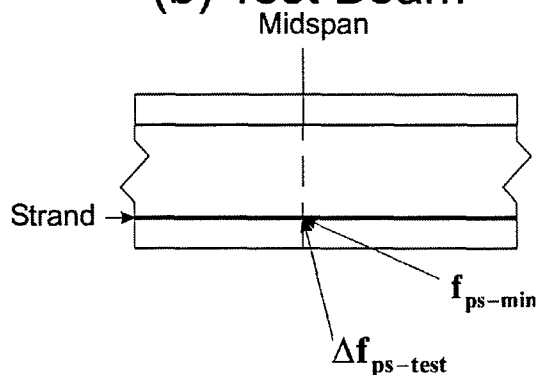
Figure 3-7 Idealized Stresses in Prototype Bridge Girder and Test Beam

49

For the given index stress, $12\sqrt{f_c'}$ or $7.5\sqrt{f_c'}$, the stress in the strand in the prototype bridge under dead load, $f_{ps\text{-}DL}$, and full service load, $f_{ps\text{-}SL}$, were calculated. The stress range, $\Delta f_{ps\text{-}prototype}$, was then determined as:

$$\Delta f_{ps\text{-}prototype} = f_{ps\text{-}SL} - f_{ps\text{-}DL} \qquad (3\text{-}1)$$

The applied loads for the test beams were established such that the minimum strand stress, $f_{ps\text{-}min}$, was equal to $f_{ps\text{-}DL}$ and the stress range, $\Delta f_{ps\text{-}test}$, was equal to $\Delta f_{ps\text{-}prototype}$.

3.3.4.1 Establishing Load Settings

The load settings for the MTS controller were analog and set using dials. The dial markings gave no indication of the load being applied. One dial was used to adjust the mean load and another dial was used to adjust the span or amplitude of the load variation. Because the loads could not be set using the dial faces, loads had to be adjusted based on the output of the load cell. This occurred over the initial cycles of the test. The set point of the mean load was easily set prior to cycling by calculating the average of the maximum and minimum loads. The amplitude was adjusted during the initial cycles, which were loaded at a frequency of approximately 1/3 Hz, to allow adjustment. Using this method, the load settings were able to be properly set within the first 25 cycles. These initial 25 cycles are included in the fatigue life values given later in Chapters 4 and 5, but are obviously insignificant.

Load settings did not need to be reset after periodic static tests. The mean load set point was recorded and then returned after the static test. Because the

span or amplitude dial was not used in the static tests, it remained in position, correctly set when the fatigue testing was resumed.

3.3.4.2 Selecting Cycle Frequency

Once the load settings were established, the load cycle frequency was increased slowly until the quality of the test system response began to deteriorate. The quality of the test system response is indicated by magnitude and shape of the input to output error signal described in Section 3.2.3.3. An oscilloscope was used to monitor this error signal. The system response could be tuned by adjusting controller gain. However, for a given amount of hydraulic ram stroke (midspan deflection), a critical point was reached when the frequency became too high for the hydraulics to respond properly. After this point, either the full desired load range was not achieved, or, if the span dial was adjusted to provide more load range, the curve was no longer sinusoidal. Once the critical point was found, the frequency was lowered to provide acceptable system response.

For Beams 4 and 5, load cycle frequency was initially about 2 Hz. For Beams 2 and 3, the load cycle frequency was initially about 4 Hz. Late in the fatigue life, as beam stiffness began to degrade, the frequency was reduced to maintain satisfactory system response.

3.3.5 Periodic Static Tests

Periodically during the fatigue life of the beam, static tests were performed to verify the condition of the prestressing strands. As opposed to the in-air tests described in Chapter 2, one cannot see the prestressing strands to inspect them. Therefore, the condition of the strand was inferred from the response of the beams during the static tests.

Each time an error signal stopped the test, a static test was performed. The displacement limit switch generated the error signal that stopped the test, and

51

signified a reduction in stiffness. During the late stages of the fatigue tests, these signals usually indicated a broken prestressing strand wire, although the displacement limit also indicated growth of concrete cracks. The procedure used to load the specimens and record data during the periodic static tests was the same as those for the initial static tests.

3.3.6 Post-Mortem Investigation

Fatigue testing was continued well past the first suspected wire failure. Tests were continued until the midspan deflection increased dramatically and collapse was deemed imminent. As will be discussed in Chapter 4, the specimens sustained a significant number of cycles after the initial wire break. Figure 3-8 shows a photograph of typical wire fatigue failures. Fatigue failures generally occurred in the same region, which is expected because a broken wire will rub against the remaining wires and will reduce the effective cross section of the strand, increasing both the mean stress and the stress range in that region.
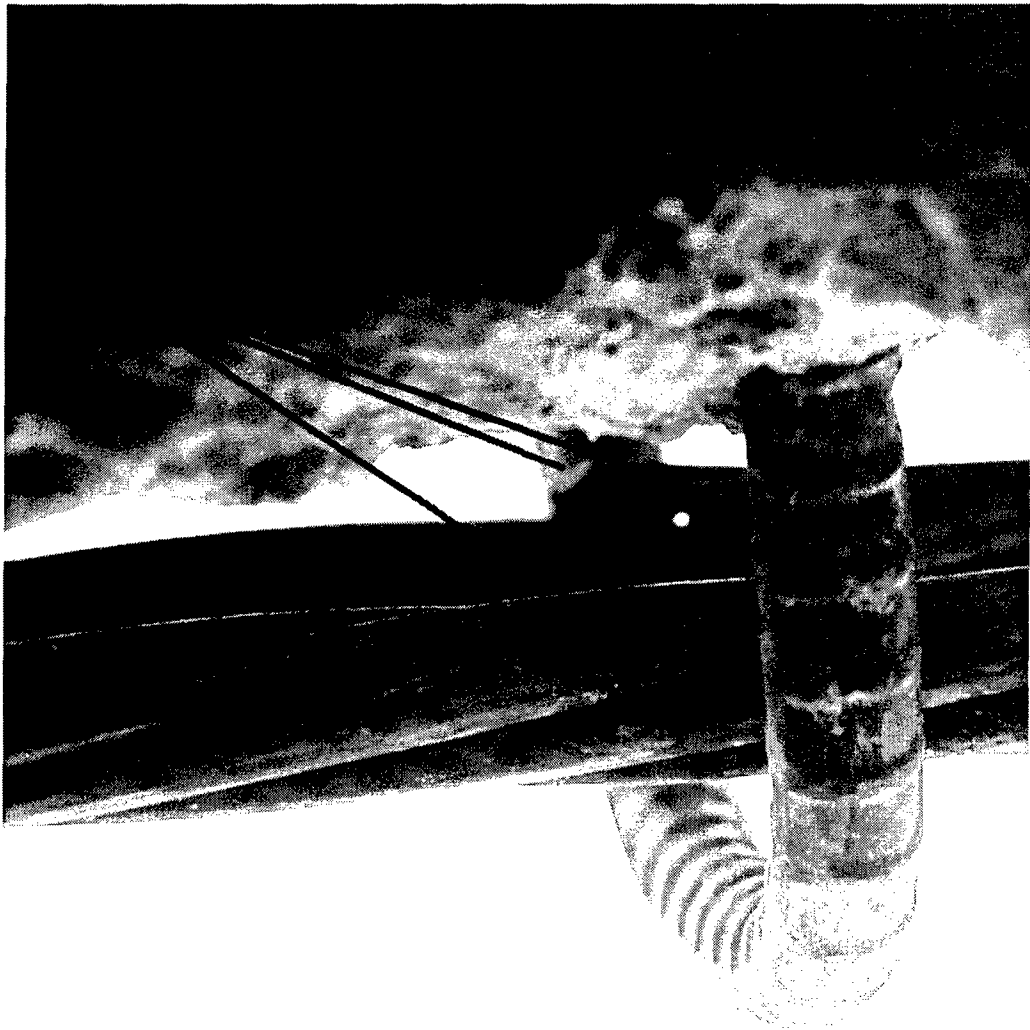
Figure 3-8 Typical Prestressing Strand Fatigue Failures

CHAPTER 4

Results From Fatigue Tests of Beams

As discussed in Chapter 3, a total of six prestressed concrete beams were subjected to fatigue loads as part of TXDOT Project 1895. The measured response of four of those beams is discussed in this chapter. Table 4-1 summarizes the beam tests. All tests were performed in 2003.

Table 4-1 Overview of Beam Tests

Beam	Index Stress	Date Fatigue Tests Started	Date Fatigue Tests Completed	Min. Load (kip)	Max. Load (kip)	Initial Cycle Freq. (Hz)	Calculated Stress Range (ksi)
2	$7.5\sqrt{f_c'}$	10 Apr.	5 May	3.41	11.71	4	21.7
3	$7.5\sqrt{f_c'}$	22 Mar.	8 Apr.	2.27	11.85	4	23.3
4	$12\sqrt{f_c'}$	17 Feb.	27 Feb.	1.21	14.20	2	43.2
5	$12\sqrt{f_c'}$	10 Mar.	19 Mar.	0.60	14.25	2	42.0

The applied loads for each beam were selected such that the calculated stress range in the strand was the same as the calculated stress range in the center of gravity of the strand profile in the prototype highway bridge. Calculated tensile stress in the extreme tension fiber of the concrete in the highway bridge girders was used as the index stress, which served as the basis for all calculations (Figure 3-7). The details of all calculations are summarized by Hagenberger (2003).

54

Response of the specimens are presented in the order that they were tested. Beams 4, 5, 3, and 2 are discussed in Sections 4.1, 4.2, 4.3, and 4.4, respectively.

4.1   BEAM 4

The loading sequence for Beam 4 was designed to crack the beam during the initial static tests and then subject the specimen to fatigue stress ranges of $12\sqrt{f_c'}$ for the index stress and approximately 43 ksi for the strand.

4.1.1   Initial Static Tests

Beam 4 was loaded from zero to 18 kip during the first static test. The maximum load was reduced to 17 kip following the first static test.

Initial cracking was apparent from the change in slope of the midspan deflection and strand strain gage plots at an applied load of approximately 11 kip, but cracks were not observed until the applied load reached 13 kip. The cracking load calculated using a modulus of rupture of $7.5\sqrt{f_c'}$ was 11.9 kip. Crack patterns observed during the initial static test are shown in Figure 4-1. Numbers shown along the cracks correspond to magnitude of the applied load during the loading increment in which the crack was observed.
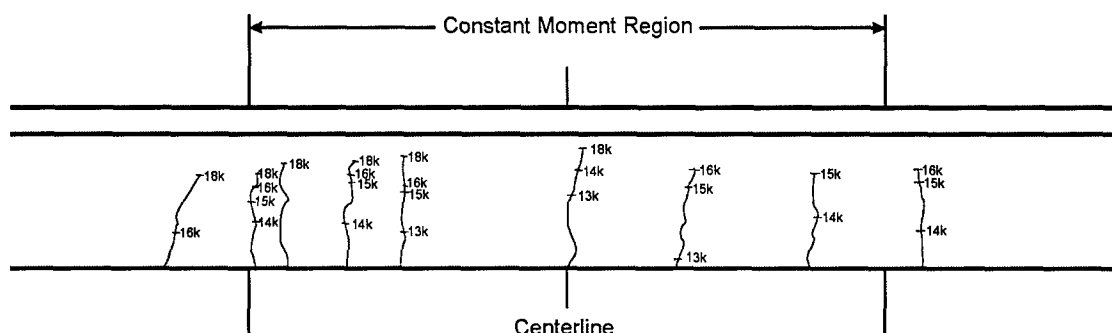
Figure 4-1   Crack Pattern Following Initial Static Test—Beam 4

55

4.1.2 Decompression Load

The decompression load is the applied load at which the bottom fiber concrete transitions from compression due to the prestress to tension due to flexure. The calculated decompression load for Beam 4 was 8.7 kip. The decompression load can be estimated from the measured response using the strand strain (Fig. 4-2), midspan deflection (Fig. 4-3), and crack gage displacement (Fig. 4-4). As can be seen in these figures, changes in stiffness in the vicinity of the decompression load are easily identified, but determining a unique value is not possible. For the purposes of this project, lines were fit to the measured data above and below the decompression load. The decompression load was then assumed to be the point at which the two lines intersected. Data from the third static test were used for this analysis. The results from this test were representative of all subsequent static tests conducted before the wires began to fail in fatigue.
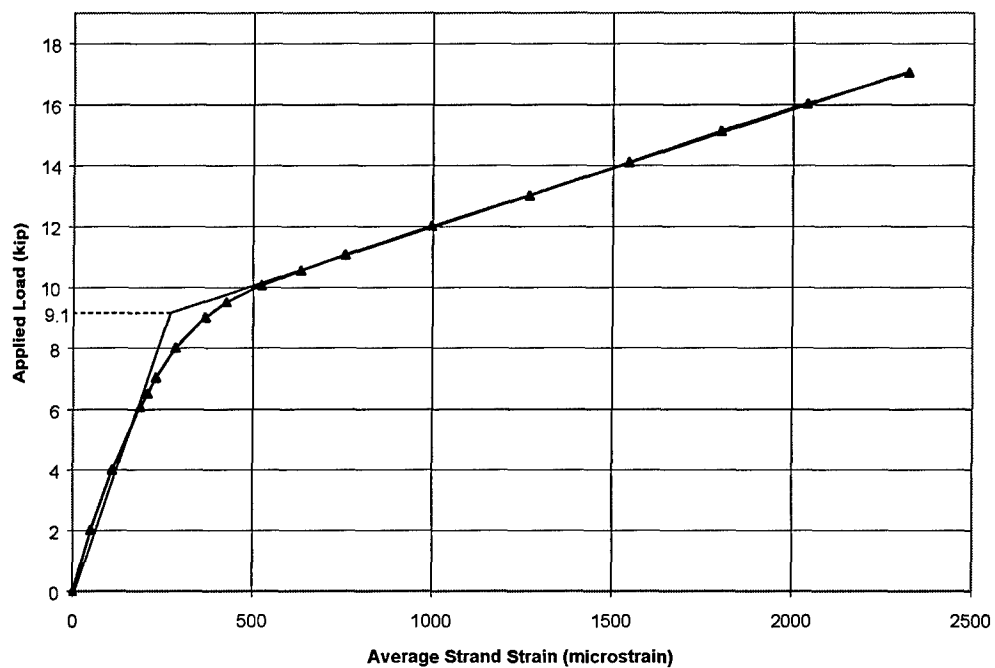
Figure 4-2 Estimated Decompression Load Using Average Strand Strain—

Beam 4

Figure 4-2 shows the plot of applied load versus average strand strain. Based on these data, the decompression load is estimated to be 9.1 kip.
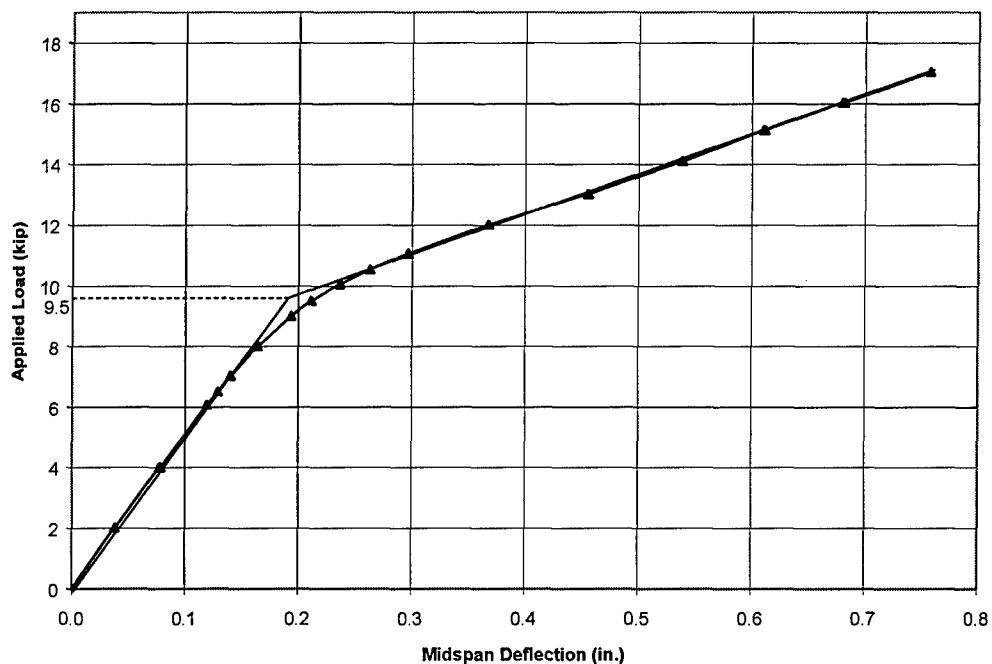
Figure 4-3 Estimated Decompression Load Using Midspan Deflection—Beam 4

Figure 4-3 shows the plot of applied load versus midspan deflection. Based on these data, the decompression load is estimated to be 9.5 kip.

Figure 4-4 displays the plot of applied load versus the crack LVDT displacement. Based on these data, the decompression load is estimated to be 9.6 kip. Averaging the values from these three sets of data, the decompression load for Beam 4 is approximately 9.4 kip, which is slightly higher than the value predicted by Hagenberger (2003).
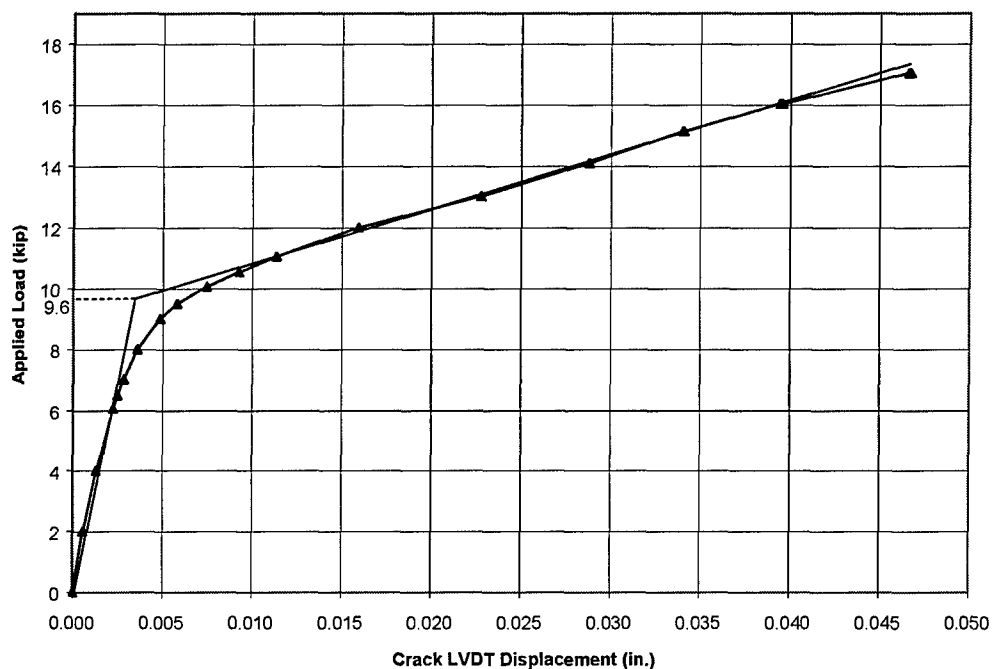
Figure 4-4 Estimated Decompression Load Using Crack LVDT
Displacement—Beam 4

4.1.3   Fatigue Loads

Beam 4 was loaded using a minimum applied load of 1.21 kip and a maximum of 14.20 kip.   Based on the analyses by Hagenberger (2003), the prestressing strand (with an effective prestress of 132 ksi) should have experienced a stress range of 43.2 ksi with a minimum stress of 133 ksi.

4.1.4   Fatigue Behavior

This section presents data from a variety of instruments to demonstrate how the response of the beam changed during the fatigue tests. Some of the strain gages failed during the tests; therefore, data are not available from all instruments throughout the tests. The fatigue tests were stopped periodically, and static tests

59

were conducted to verify the response of the beam at various points in the fatigue life of the beam. Data from the static tests are presented in this section. As wires began to fail in fatigue, the maximum applied load was further reduced to avoid exceeding the stroke of the displacement transducers.
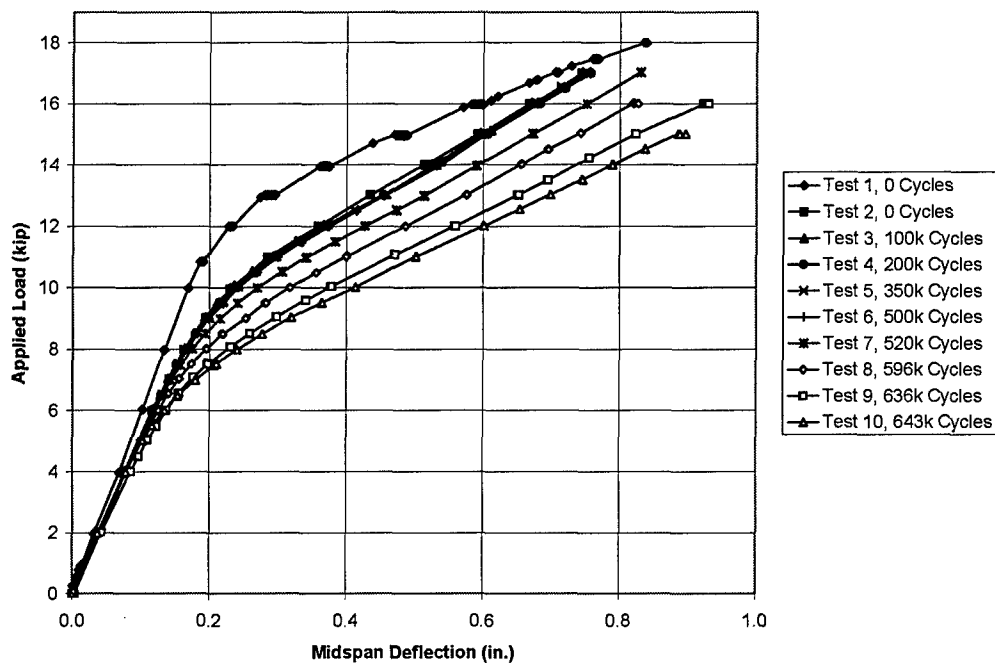
Figure 4-5 Variation of Midspan Deflection During Fatigue Tests—Beam 4

Midspan deflection is presented in Fig. 4-5. As expected, the beam is stiffer during the initial static test prior to cracking. After cracking, the beam experienced larger displacements at each applied load. The response of the beam did not change appreciably during the first 500,000 cycles. The stiffness began to degrade after 520,000 cycles, however.

60
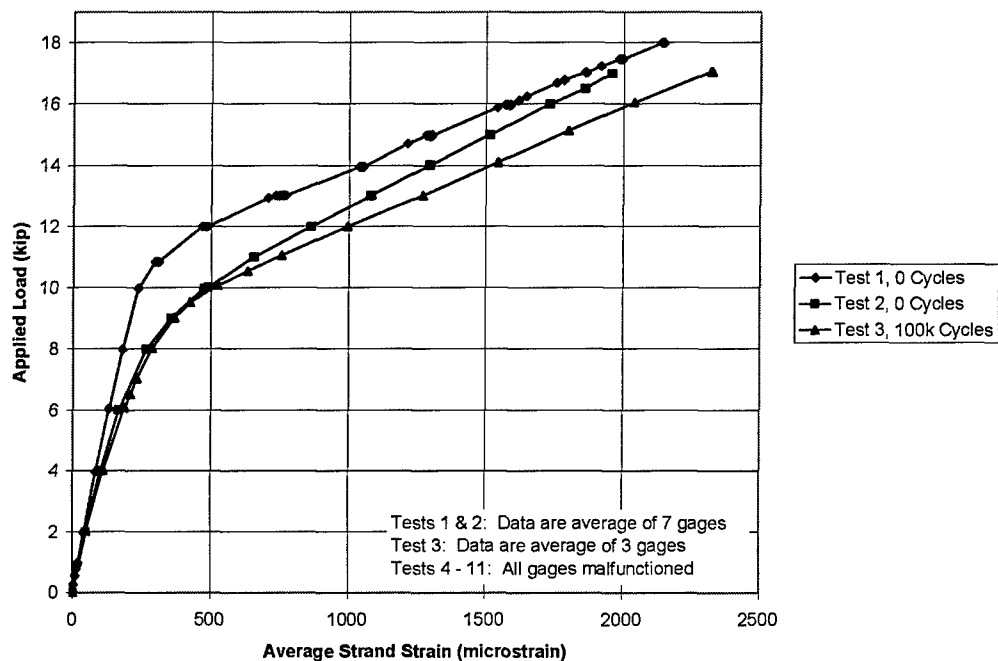
Figure 4-6 Variation of Average Strand Strain During Fatigue Tests—Beam 4

Average strand strain is presented in Fig. 4-6. During the first two tests, three of the strain gages failed. After 100,000 cycles, 4 additional strain gages had failed. By static test 4, all gages had malfunctioned.

61
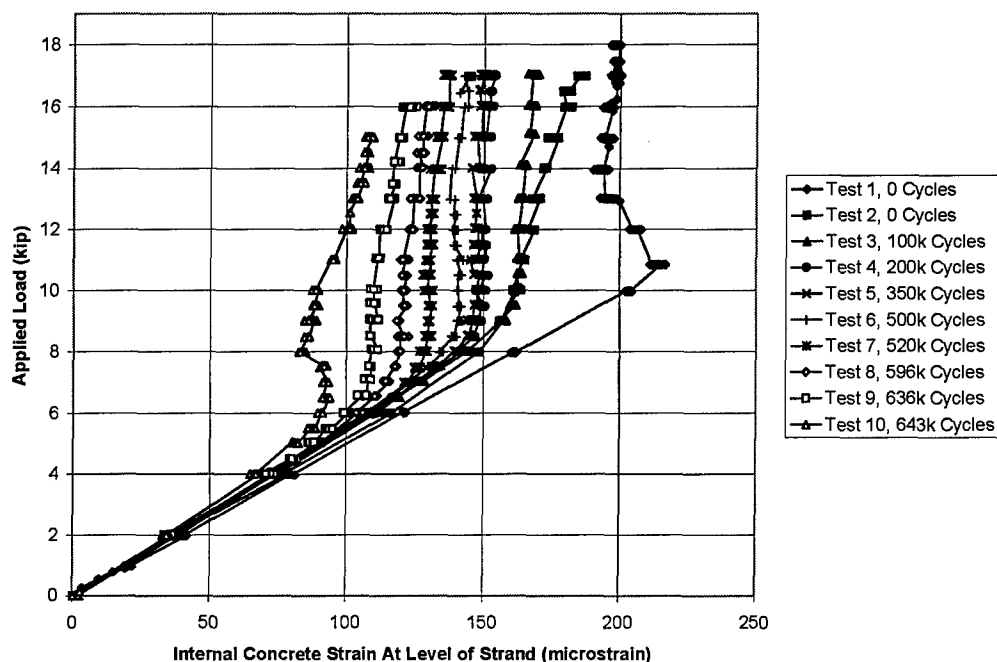
Figure 4-7 Variation of Embedded Concrete Strain During Fatigue Tests—
Beam 4

A concrete strain gage was embedded in the beam near midspan between the two strands. This gage was located just to the right of the centerline crack (Figure 4-1). Figure 4-7 is the plot of applied load as a function of the concrete gage readings over the fatigue life of the beam. For a given applied load, the concrete strain decreased in amplitude throughout the tests. Differences were most noticeable at applied loads above the decompression load.

62
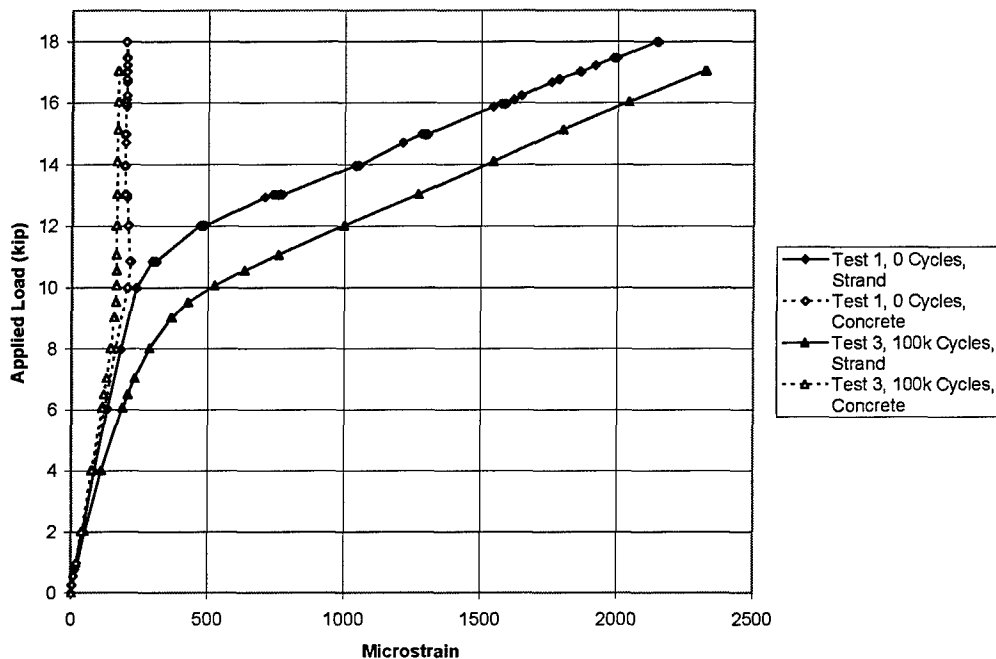
Figure 4-8 Comparison of Strand Strain and Concrete Strain—Beam 4

Figure 4-8 compares the average strand strain and concrete strain for Static Tests 1 and 3. As expected, the data from the strands and the concrete are initially very similar and begin to vary as the cracking load is approached. Once the beam cracks, the strains in the strand and surrounding concrete vary dramatically.

After the initial static test, three instruments were attached to the beam in the vicinity of the most prominent crack (Section 3.2.2). In the case of Beam 4, the most prominent crack was nearly at midspan. The plots from these three instruments are shown in Figures 4-9, 4-10, and 4-11.

63
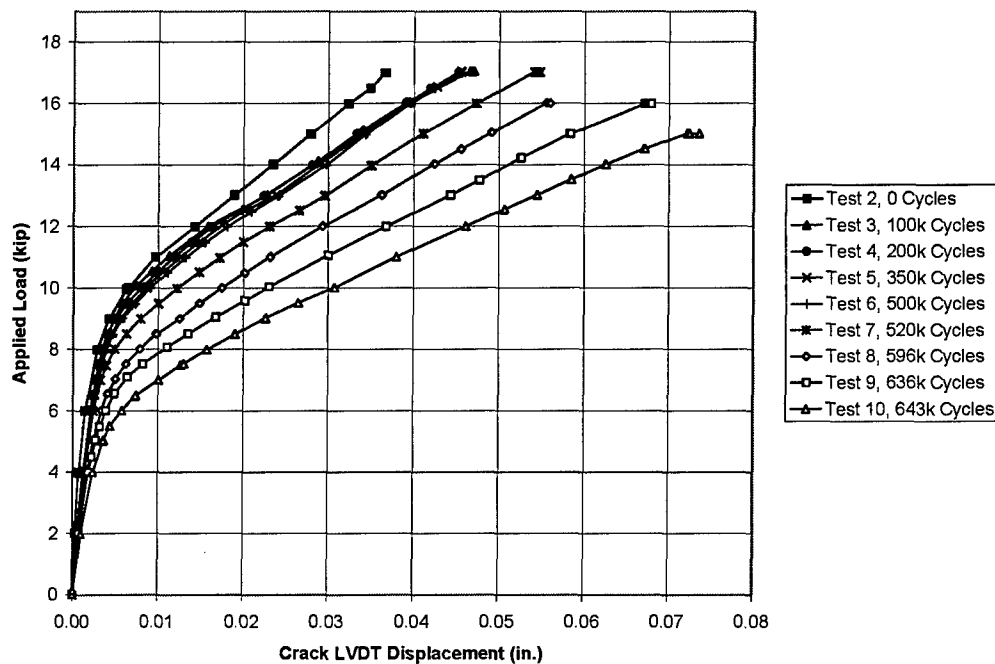
**Figure 4-9 Variation of Crack Gage Displacement During Fatigue Tests—
Beam 4**

Figure 4-9 shows the plot of applied load vs. the crack LVDT displacement. This plot corresponds remarkably well with Figure 4-5, and both show distinct changes in displacement at the same points in fatigue life. From these two sets of data, four wire breaks were expected. Abrupt changes in stiffness may be observed at 520,000, 596,000, 636,000, and 643,000 cycles. It is likely that wire breaks triggered these changes.

It should be noted that after initial cycling, the beam response is repeatable, as can be seen in most of the plots of Tests 3 through 6. Early changes in response are most likely attributed to concrete creep and debonding of the strand near the cracks.
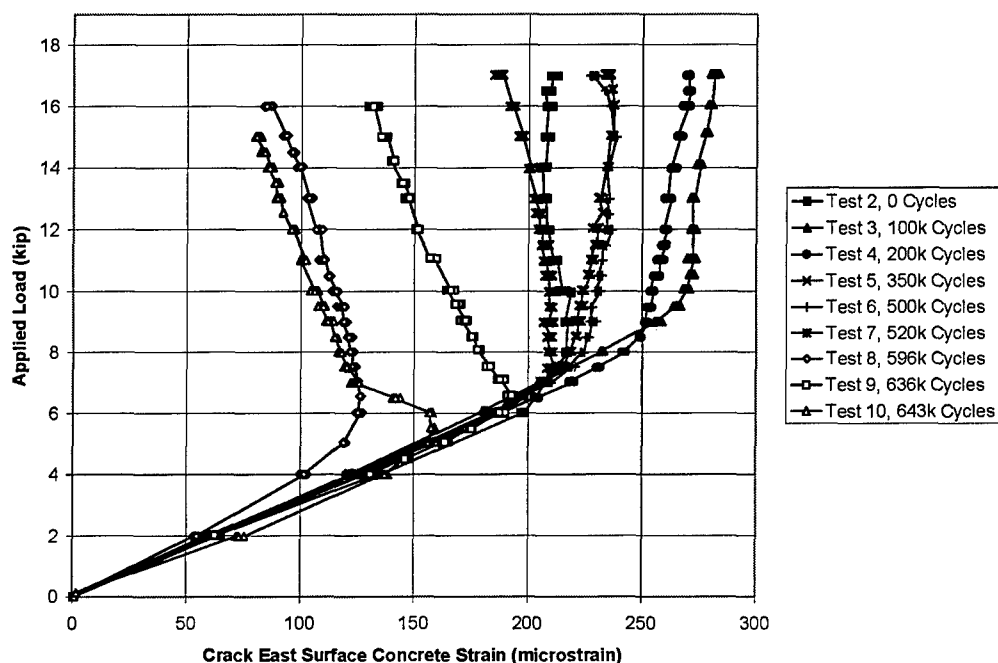
Figure 4-10 Variation of Concrete Surface Strain East of Crack During Fatigue Tests—Beam 4

Figures 4-10 and 4-11 are plots of the applied load vs. the concrete surface strain gage readings on either side of the prominent crack. All diagrams and photographs of beam crack patterns shown in this chapter show the south side of the beam (a north facing view), thus the east surface concrete gage was on the right of the prominent crack in these figures and the west surface concrete gage was on the left.

65
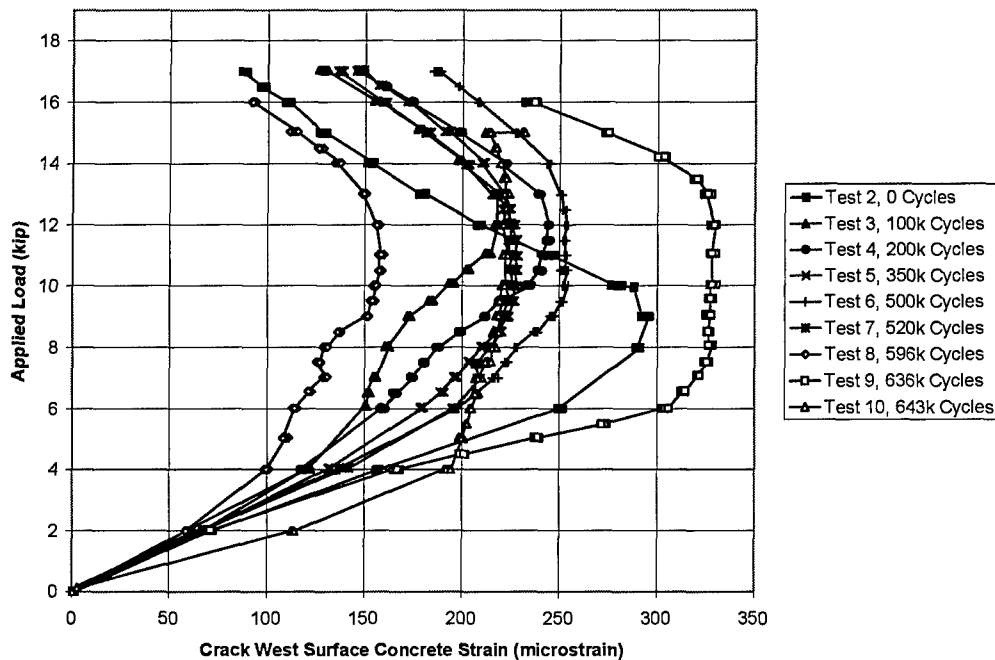
Figure 4-11 Variation of Concrete Surface Strain West of Crack During

Fatigue Tests—Beam 4

Prior to testing, it was expected that these surface strain gages near the crack would show an increase in strain as the prestress compression was released. Once the decompression load was reached, it was expected that the strain would stop increasing (the curve would plot vertically) or increase slightly if the debonding length was shorter than the strain gage. However, during this and other tests, the strain behaved as expected initially, but then often decreased at higher loads. This behavior was not expected. One possible hypothesis to explain the observed response is explained in the following paragraph.

Concrete strain is affected by several influences. Initially, concrete strains from its original compressive state because of the applied bending moment. Once the cracks open, the concrete is pulled into tension because of the deformation of

66

the strand, which is in the shape of a straight center wire surrounded by 6 outer wires with helical twists. If the strand is pulled sufficiently, the diameter of the strand will reduce due to Poisson's ratio, and the debonded concrete will slip relative to the strand, thereby decreasing the tensile stress. Once strand wires break, the area increases due to the loss of tension, and the broken wire presses against the other wires encased in the concrete. This radial force keeps the concrete in that local area against the steel, forcing it into greater tension than in previous tests. Once the diameter of the remaining wires reduces enough to compensate for the expansion of the broken wires, the debonded concrete can once again slip relative to the strand, decreasing its tensile stress.
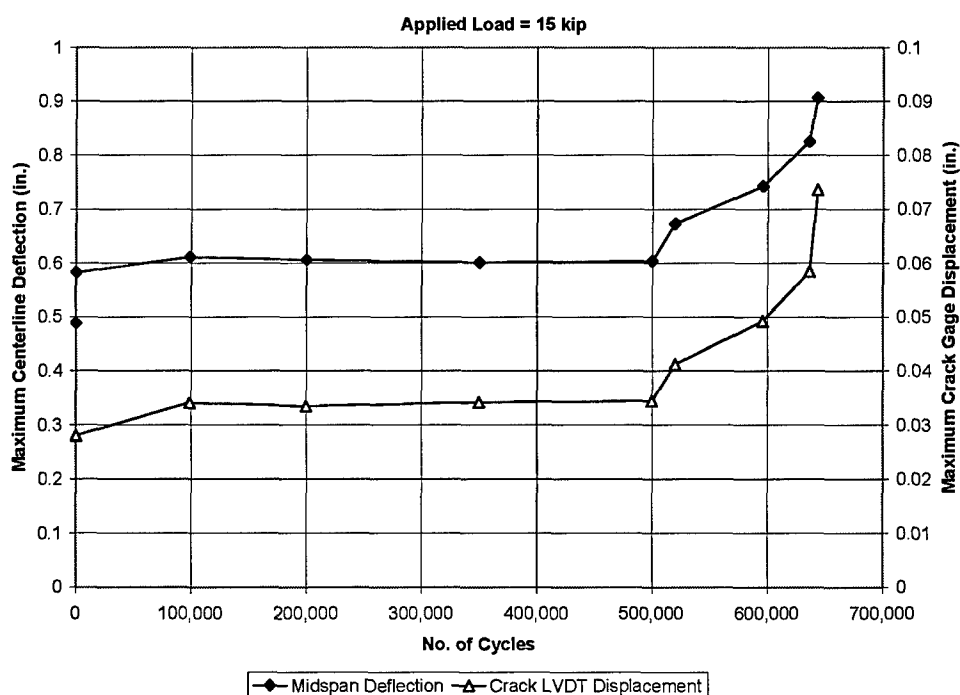
Figure 4-12 Variation of Midspan Deflection and Crack Gage Displacement
with Number of Cycles—Beam 4

67

For comparison purposes, midspan deflection and crack gage displacement at an applied load of 15 kip are plotted as a function of the number of load cycles in Figure 4-12. These plots show the characteristic fatigue life phases, showing an initial degradation, a steady state plateau, and then dramatic degradation after initial fatigue failure. It should be noted that there is no indication prior to the onset of fatigue failure that such failure is imminent. However, the beam still carried the applied load for many cycles after initial wire fracture.

Figure 4-13 shows the final crack pattern at the end of testing. The numbers shown by the cracks represent the number of cycles experienced by the beam at the time that the crack had propagated to that point. For example, 0 is the initial static test, 100k is the third static test at 100,000 cycles, and so forth. Figure 4-14 is a photograph showing the actual crack markings. Changes in beam coloring are the result of combining separate close-up photographs into one composite image, not anomalies in beam construction. Obtaining a single image was not possible because of the presence of the test frame and other laboratory equipment.
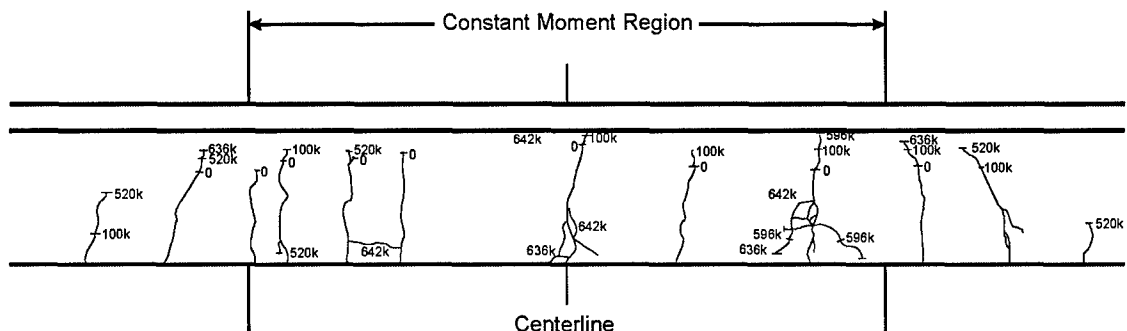
Figure 4-13 Observed Crack Pattern at End of Fatigue Tests—Beam 4

Figure 4-14 Composite Photograph of Beam 4 at End of Fatigue Tests

4.1.5 Post-Mortem Investigation

After testing, the condition of the strand was investigated by carefully removing the concrete around the prestressing strands. Four wires (two on each strand) failed in fatigue. Failures were identified approximately 8 in. west of midspan. Figure 4-15 shows a photograph of the beam at the conclusion of the post-mortem investigation. Figure 4-16 shows the end of fatigue life crack pattern with the location of the failures indicated.
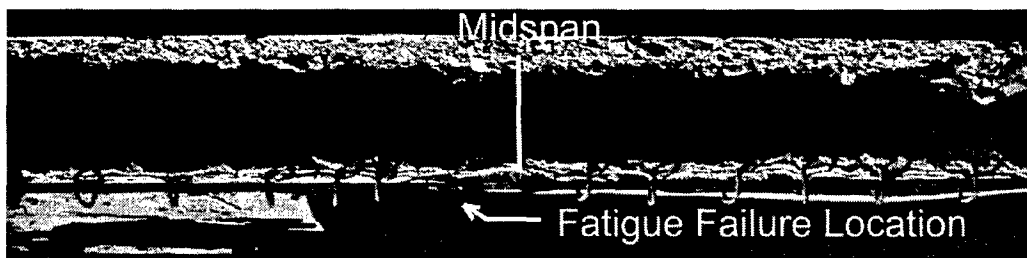
Figure 4-15 Photograph of Beam 4 After Removal of Concrete to Expose Strand

69
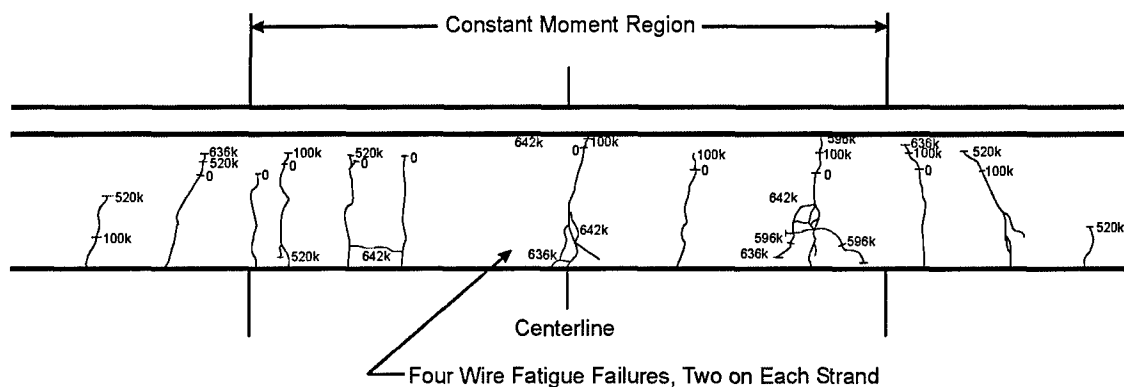
Figure 4-16 Location of Wire Failures—Beam 4

The four wire failures identified during the post-mortem investigation correlate very well with the four distinct changes in the midspan deflection and crack gage displacement (Figures 4-5 and 4-9). This initial test demonstrated that the limit switch used to stop the fatigue tests was sufficiently sensitive to stop a test because of the increased deflection caused by the failure of one of the 14 wires (two seven-wire strands).

4.2 BEAM 5

The loading sequence for Beam 5 was designed to crack the beam during the initial static tests and then subject the specimen to fatigue stress ranges of $12\sqrt{f_c'}$ for the index stress and approximately 42 ksi for the strand.

4.2.1 Initial Static Tests

Beam 5 was loaded from zero to 14.5 kip during all static tests. Initial cracking was apparent from the change in slope of the midspan deflection and strand strain gage plots at an applied load of approximately 10 kip, but visual cracks were not observed until the applied load reached 11.25 kip. The cracking load calculated using a modulus of rupture of $7.5\sqrt{f_c'}$ was 12.2 kip. Crack

70

patterns observed during the initial static test are shown in Figure 4-17. Numbers shown along the cracks correspond to the magnitude of the applied load during the increment in which the crack was observed.
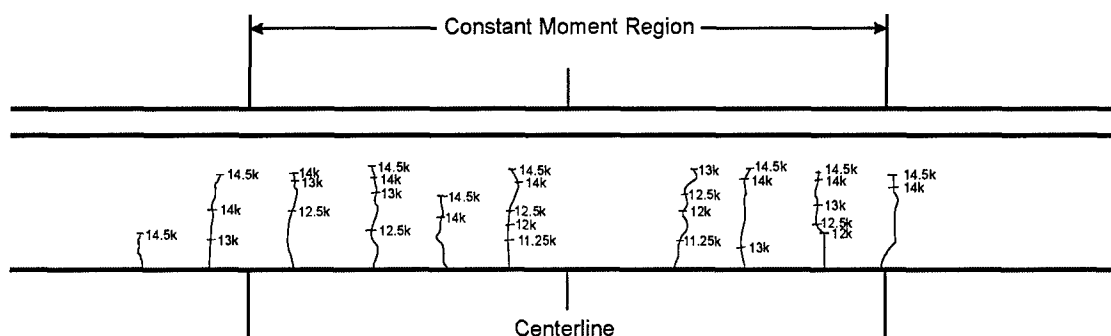
Figure 4-17 Crack Pattern Following Initial Static Test—Beam 5

4.2.2 Decompression Load

The calculated decompression load for Beam 5 was 8.9 kip. The decompression load can be estimated from the measured response using the strand strain (Fig. 4-18), midspan deflection (Fig. 4-19), and crack gage displacement (Fig. 4-20). Data from the third static test were used for this analysis. The results from this test were representative of all subsequent static tests conducted before the wires began to fail in fatigue.

71
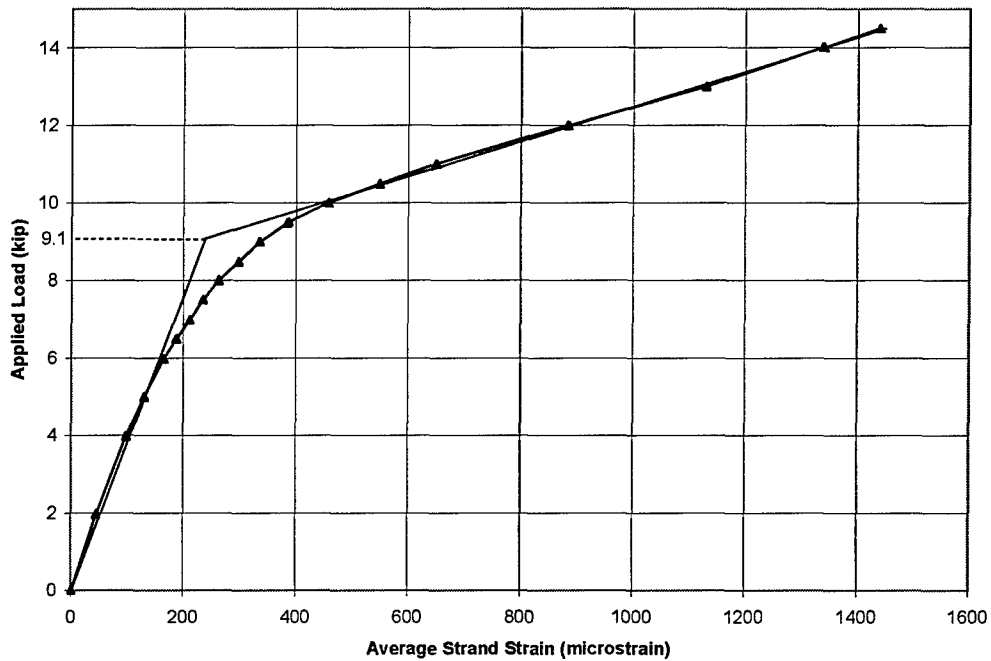
Figure 4-18 Estimated Decompression Load Using Average Strand Strain—
Beam 5

Figure 4-18 shows the plot of applied load versus average strand strain. Based on these data, the decompression load is estimated to be 9.1 kip.
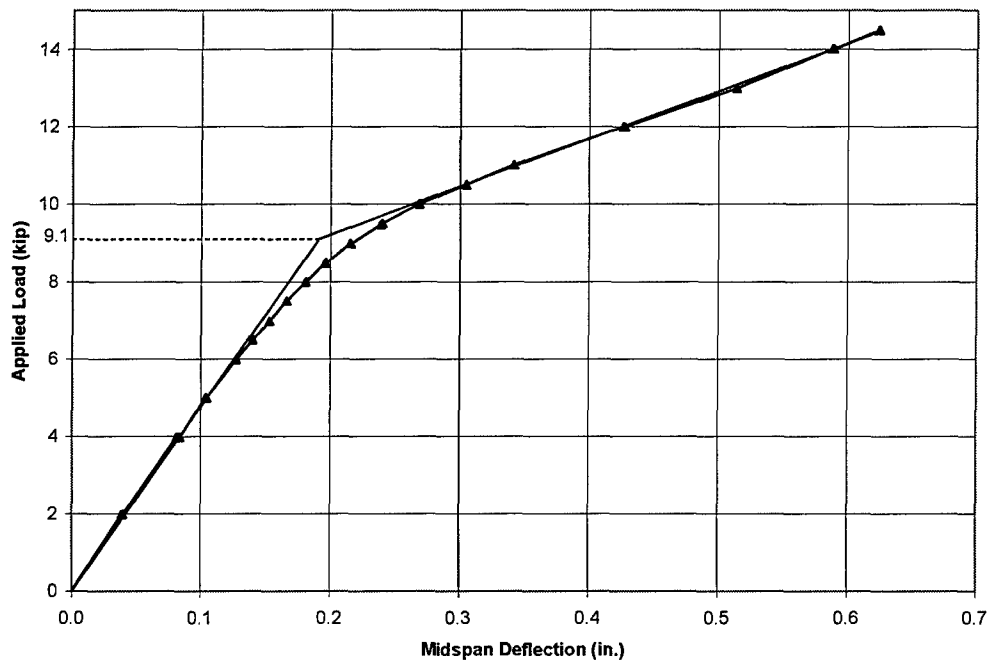
Figure 4-19 Estimated Decompression Load Using Midspan Deflection—Beam 5

Figure 4-19 shows the plot of applied load versus midspan deflection. Based on these data, the decompression load is estimated to be 9.1 kip.

Figure 4-20 displays the plot of applied load versus the crack LVDT displacement. Based on these data, the decompression load is estimated to be 9.1 kip. Averaging the values from these three sets of data, the decompression load for Beam 5 is approximately 9.1 kip, which is slightly higher than the value predicted by Hagenberger (2003).
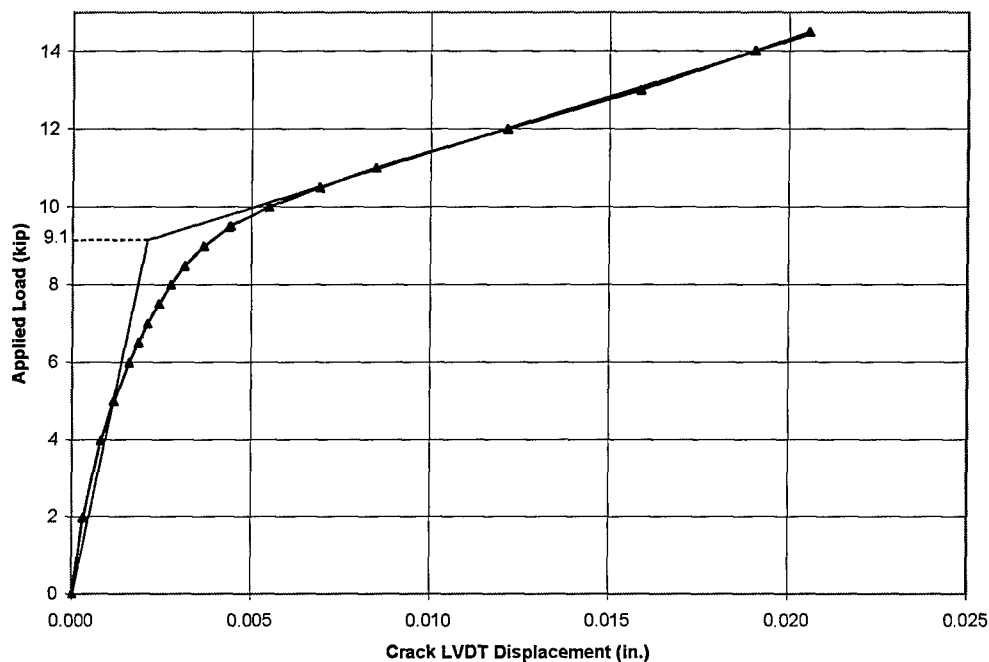
Figure 4-20 Estimated Decompression Load Using Crack LVDT Displacement—Beam 5

4.2.3 Fatigue Loads

Beam 5 was loaded using a minimum applied load of 0.60 kip and a maximum of 14.25 kip. Based on the analyses by Hagenberger (2003), the prestressing strand (with an effective prestress of 135 ksi) should have experienced a stress range of 42.0 ksi with a minimum stress of 135.2 ksi.

4.2.4 Fatigue Behavior

This section presents data from a variety of instruments to demonstrate how the response of the beam changed during the fatigue tests. Some of the strain gages failed during the tests; therefore, data are not available from all instruments throughout the tests.

74
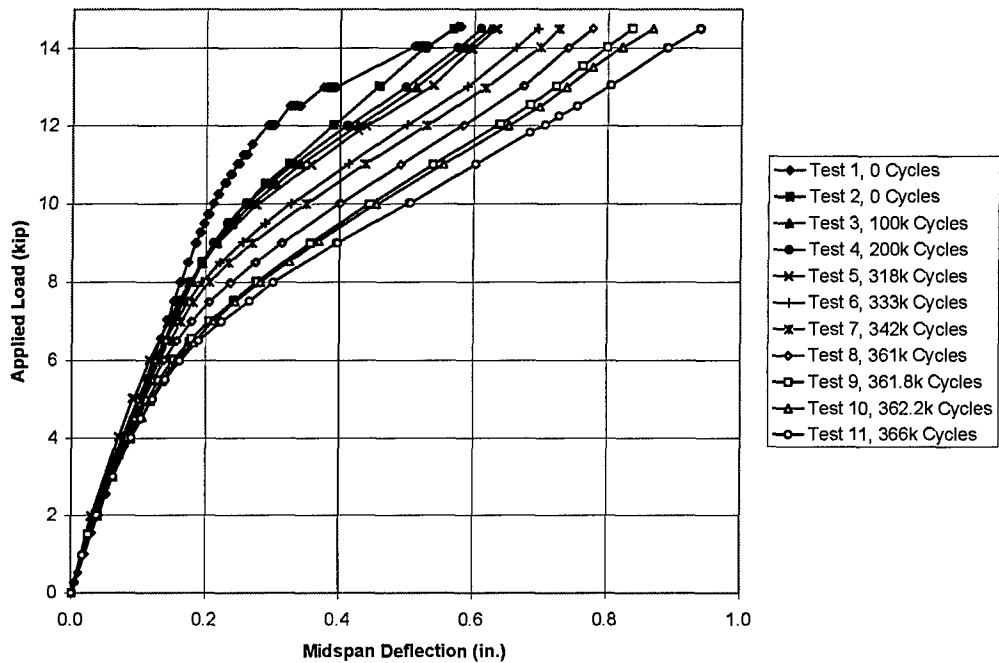
Figure 4-21 Variation of Midspan Displacement During Fatigue Tests—Beam 5

Applied load versus midspan deflection is presented in Fig. 4-21. The response of the beam did not change appreciably during the first 200,000 cycles. The stiffness began to degrade after 318,000 cycles, however.

75
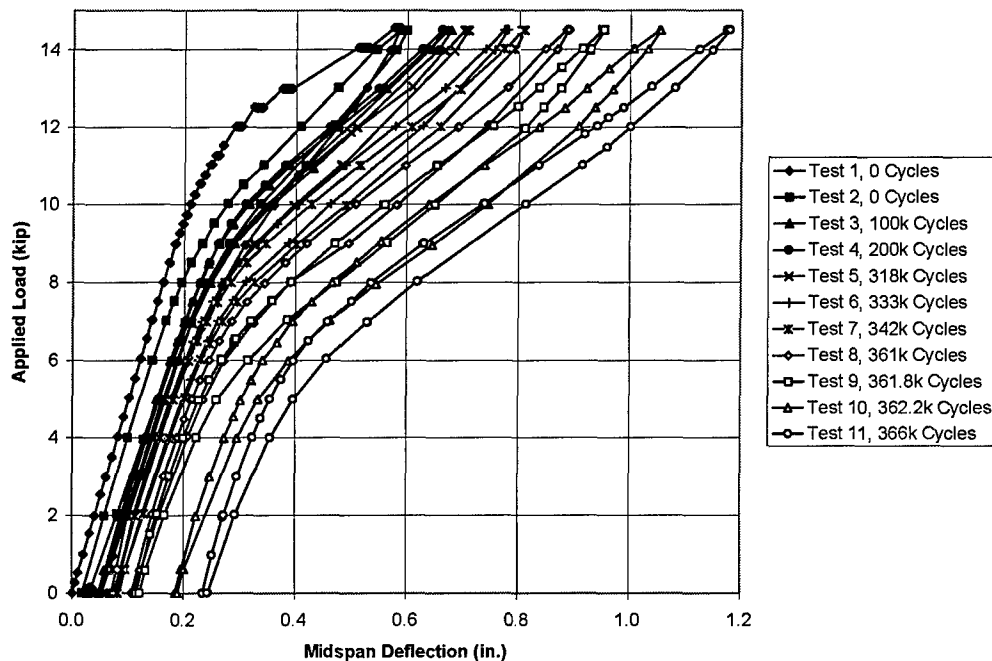
***Figure 4-22 Variation of Midspan Displacement, Including Permanent
Offset—Beam 5***

Because the external transducers were removed from the specimen during
the fatigue tests and could not be returned to their exact previous positions at the
beginning of each static test, the permanent offset of the beam was not recorded.
Beginning with beam 5, a voltage meter was attached to the output of the linear
motion transducer that was attached by wire to the bottom of the beam, and
voltages were manually recorded throughout the entire series of static tests. The
changes in voltage readings were correlated to changes in displacement, and were
then added to the displacements read using the data acquisition system. Figure 4-
22 presents the results. With the permanent offset included in the data, it is
possible to show a continuous loading/unloading path for the entire series of tests.

Data from the unloading sequences were removed from other plots because the large number of intersecting lines made the plots unreadable.
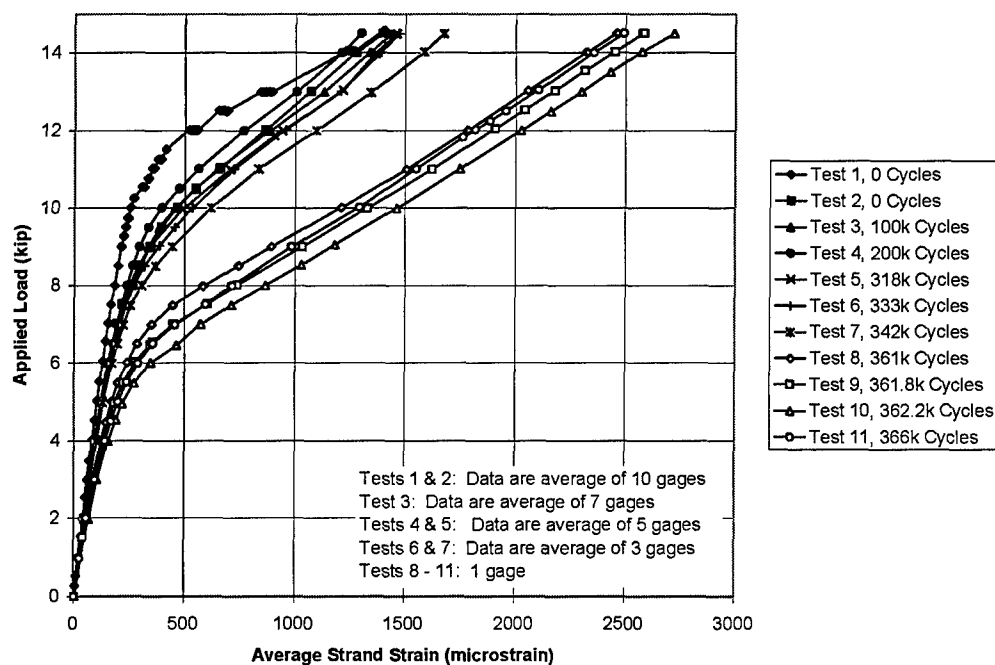
Figure 4-23 Variation of Average Strand Strain During Fatigue Tests—Beam 5

Applied load versus average strand strain is presented in Fig. 4-23. Comparison between tests is complicated by the fact that over the fatigue life of the beam, gages began to malfunction. The number of surviving gages is shown on the figure.
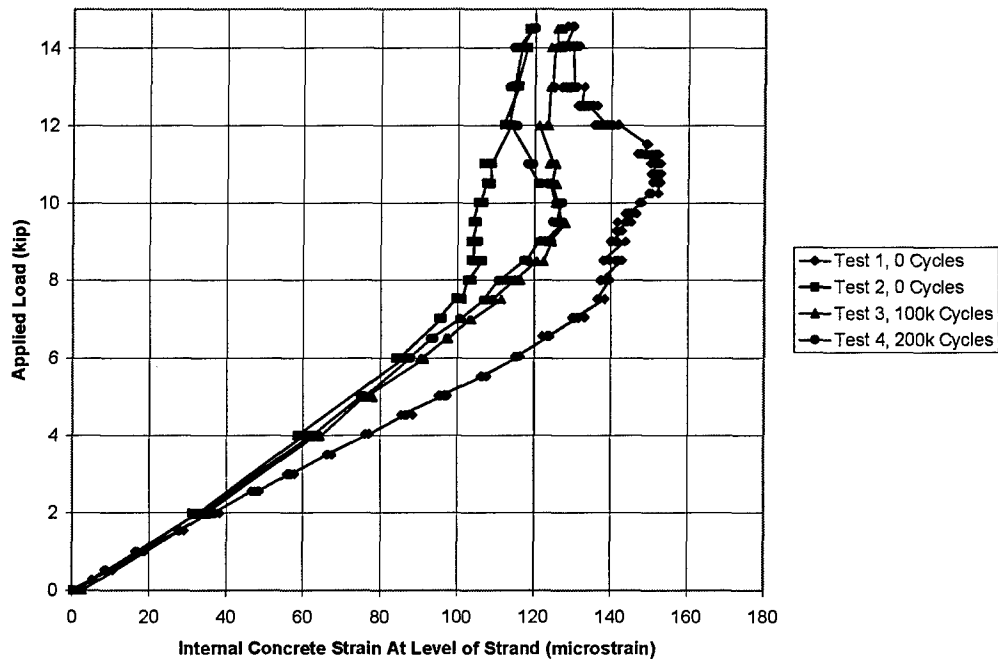
Figure 4-24 Variation of Embedded Concrete Strain During Fatigue Tests—

Beam 5

A concrete strain gage was embedded in the beam between the two strands near midspan. This gage was located just to the left of centerline (Figure 4-17). Figure 4-24 is the plot of applied load as a function of the concrete gage readings over the first 200,000 cycles of the beam. After static test 4, the gage failed. Once again, the concrete strain decreased in amplitude throughout the tests. Differences were most noticeable at applied loads above the decompression load.
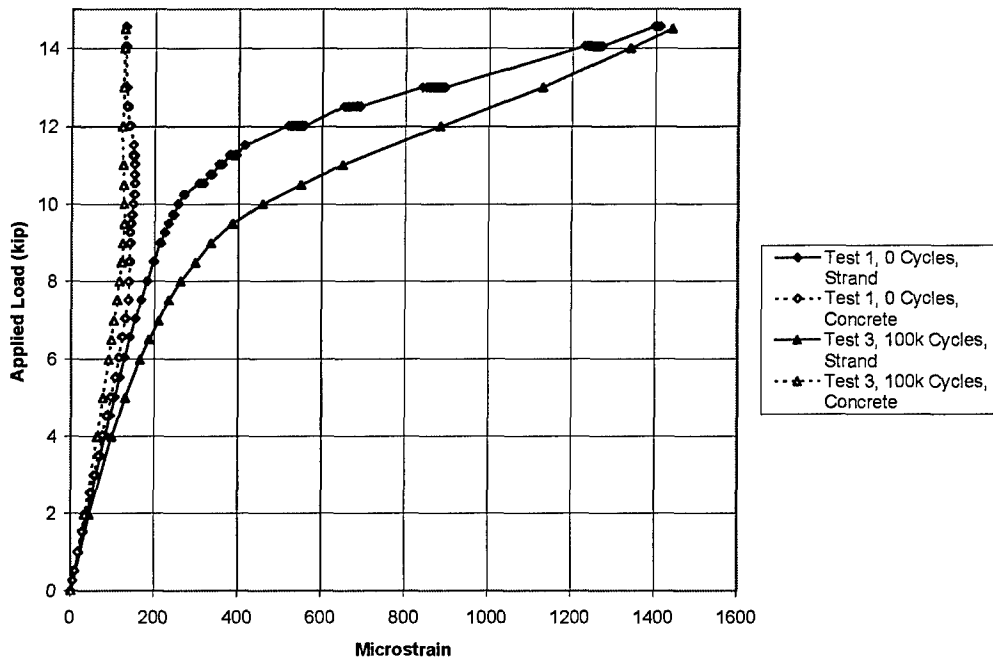
Figure 4-25 Comparison of Strand Strain and Concrete Strain—Beam 5

Figure 4-25 compares the average strand strain and concrete strain for Static Tests 1 and 3. As expected, the data from the strands and the concrete are initially very similar and begin to vary as the cracking load is approached. Once the beam cracks, the strains in the strand and surrounding concrete vary dramatically.

After the initial test, three instruments were attached to the beam in the vicinity of the most prominent crack (Section 3.2.2). In the case of Beam 5, the most prominent crack was approximately 8 in. east (to the right) of midspan. The plots from these three instruments are shown in Figures 4-26, 4-27, and 4-28.

79
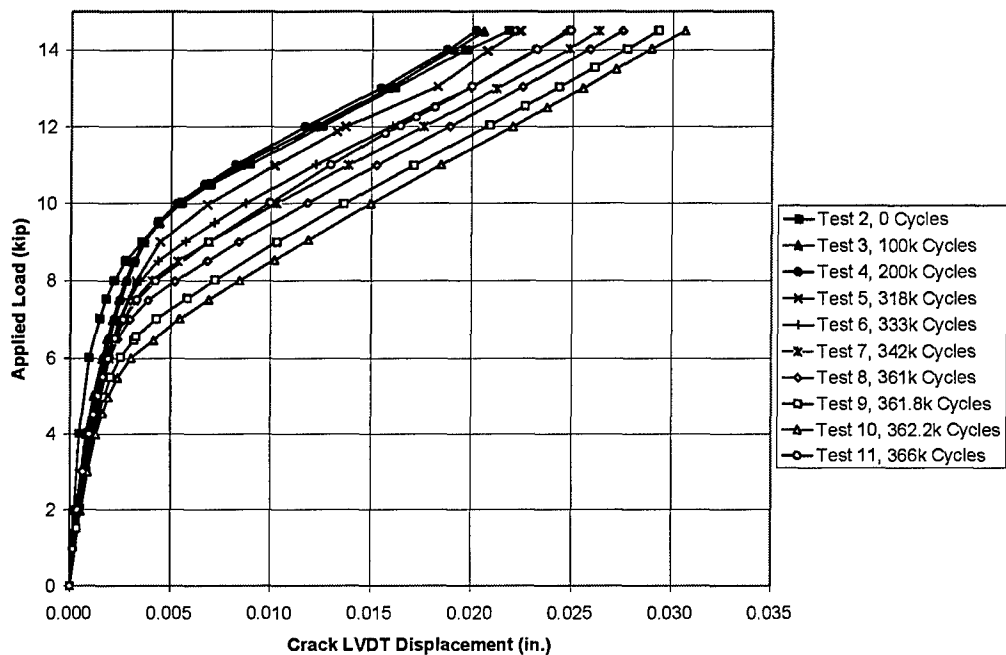
Figure 4-26 Variation of Crack Gage Displacement During Fatigue Tests—
Beam 5

Figure 4-26 shows the plot of applied load vs. the crack LVDT displacement readings. This plot corresponds reasonably well with Figures 4-21 and 4-22, and each show distinct changes in displacement at the same points in fatigue life. From these three sets of data, seven wire breaks were expected. Abrupt changes in stiffness are best observed in Figure 4-22 at 318,000, 333,000, 342,000, 361,000, 361,800, 362,200, and 366,000 cycles. It is likely that wire breaks triggered these changes.
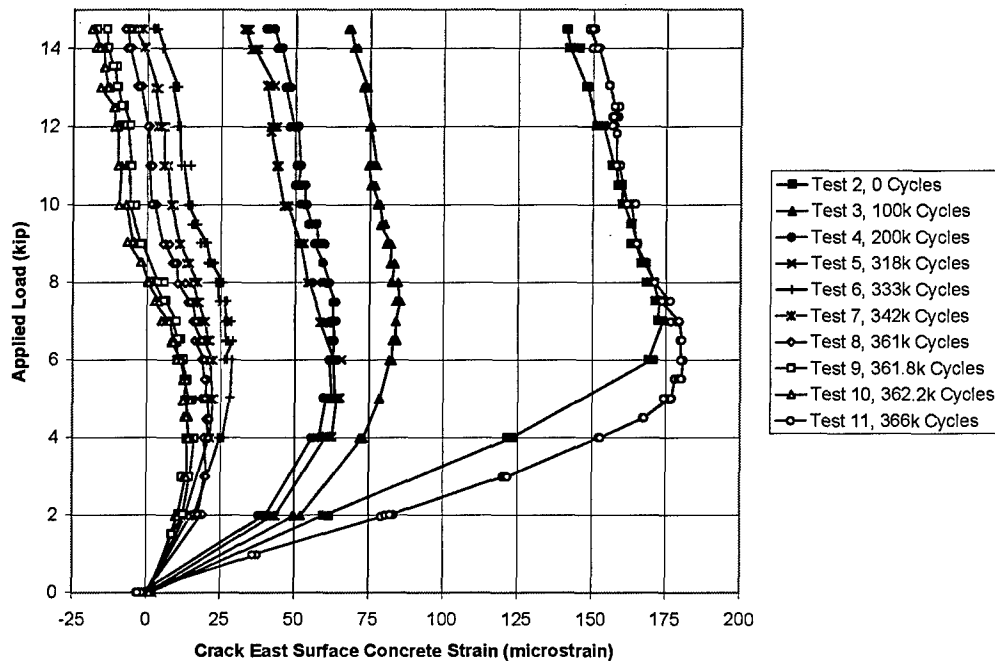
Figure 4-27 Variation of Concrete Surface Strain East of Crack During Fatigue Tests—Beam 5

Figures 4-27 and 4-28 are plots of the applied load vs. the concrete surface strain gage readings on either side of the prominent crack. All diagrams and photographs of beam crack patterns shown in this chapter show the south side of the beam (a north facing view), thus the east surface concrete gage was on the right of the prominent crack in these figures and the west surface concrete gage was on the left.
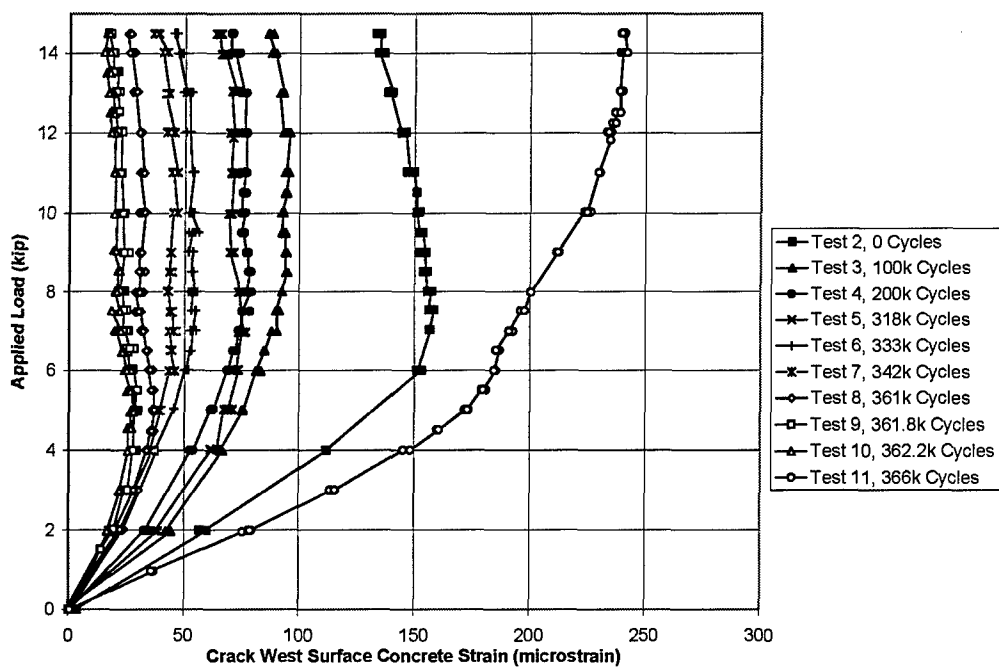
Figure 4-28 Variation of Concrete Surface Strain West of Crack During
Fatigue Tests—Beam 5

The concrete surface gages on this beam experienced behavior similar to that of Beam 4 and was discussed in more detail in Section 4.1.4. Although these gages were originally intended to help define the decompression load, the many factors affecting the strain of the concrete in this region minimize the effectiveness in using these gages for that purpose.

82

Applied Load = 14.5 kip
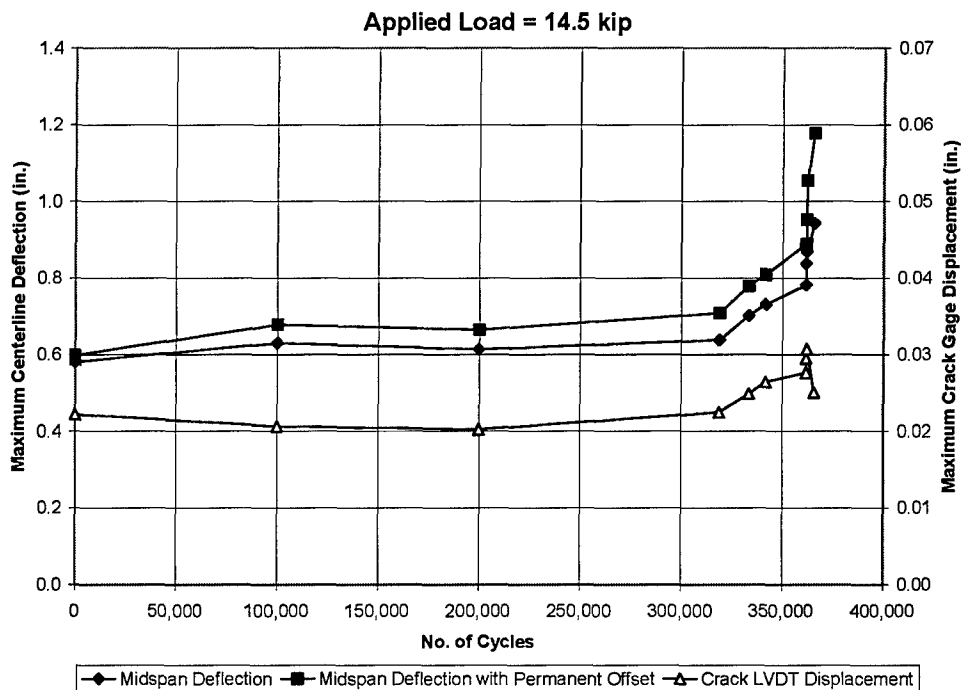
*Figure 4-29 Variation of Midspan Deflection and Crack Gage Displacement
with Number of Cycles—Beam 5*

For comparison purposes, midspan deflection, midspan deflection with permanent offset, and crack gage displacement at an applied load of 14.5 kip are plotted as a function of the number of load cycles in Figure 4-12. These plots show the characteristic fatigue life phases, showing an initial degradation, a steady-state plateau, and then dramatic degradation after initial fatigue failure. It should be noted that there is no indication prior to the onset of fatigue failure that such failure is imminent. However, the beam still carried the applied load for many cycles after initial wire fracture.

Figure 4-30 shows the final crack pattern at the end of testing. The numbers shown by the cracks corresponds with the number of load cycles experienced by the beam at the time that the crack had propagated to that point.

83

For example, 0 is the initial static test, 100k is the third static test at 100,000 cycles, and so forth. Figure 4-31 is a photograph showing the actual crack markings. Changes in beam coloring are the result of combining separate close-up photographs into one composite image, not anomalies in beam construction. Obtaining a single image was not possible because of the presence of the test frame and other laboratory equipment.

Figure 4-30 Observed Crack Pattern at End of Fatigue Tests—Beam 5

Figure 4-31 Composite Photograph of Beam 5 at End of Fatigue Tests

4.2.5   Post-Mortem Investigation

After testing, the condition of the strand was investigated by carefully removing the concrete around the prestressing strands. Seven wires failed in fatigue and were identified at three separate locations along the beam. Figure 4-32 shows a photograph of the beam at the end of the post-mortem investigation.

84

Figure 4-33 shows the crack pattern at the conclusion of fatigue testing with the location of the failures indicated.
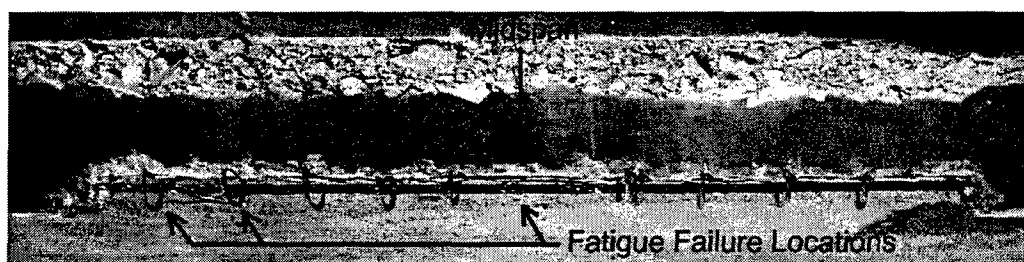
Figure 4-32 Photograph of Beam 5 After Removal of Concrete to Expose Strand
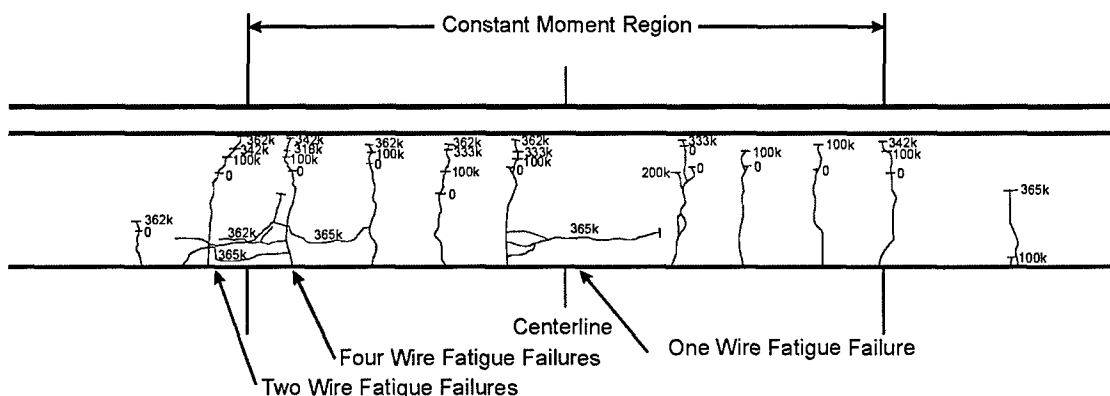
Figure 4-33 Location of Wire Failures—Beam 5

The seven fatigue failures identified during post-mortem investigation correlate very well with the seven distinct changes in the midspan deflection and crack gage displacement plots shown in Figures 4-21, 4-22 and 4-26.

4.3   BEAM 3

The loading sequence for Beam 3 was expected to crack the beam during the initial static tests and then subject the specimen to fatigue stress ranges of $7.5\sqrt{f_c'}$ for the index stress and approximately 23 ksi for the strand.

4.3.1 Initial Static Tests

Beam 3 was loaded from zero to 11.85 kip during all static tests. No cracking was observed either visually or in the plots of midspan deflection or strand strain gage readings during the initial static tests. Given that cracking theoretically should have occurred, initial cycling was begun, estimating that the beam would soon crack under cyclic loading. During the first 25 cycles (run at slow frequencies while setting the applied loads), noise associated with cracking was heard. A third static test was then conducted, and cracking was apparent from the change in slope of the midspan deflection and the strand strain gage plots at an applied load of about 8.5 kip, and visual cracks were first observed when the applied load reached 9 kip. The cracking load calculated using a modulus of rupture of $7.5\sqrt{f_c'}$ was 11.5 kip, but comparison is not possible, because the beam did not crack during static loading. Crack patterns observed during the third static test are shown in Figure 4-34. Numbers shown along the cracks correspond to the magnitude of the applied load during the loading increment in which the crack was observed.
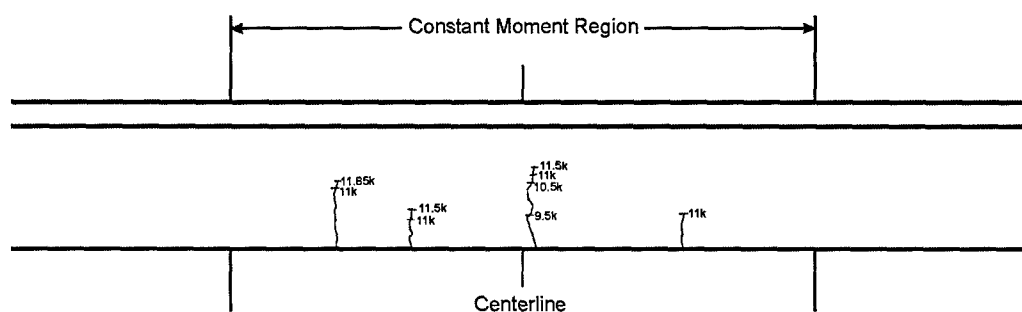
Figure 4-34 Crack Pattern Following Third Static Test—Beam 3

4.3.2 Decompression Load

The calculated decompression load for Beam 3 was 8.2 kip. The decompression load can be estimated from the measured response using the strand strain (Fig. 4-35), midspan deflection (Fig. 4-36), and crack gage displacement (Fig. 4-37). Data from the fifth static test was used for this analysis. The results from this test were representative of all subsequent static tests conducted before the wires began to fail in fatigue.
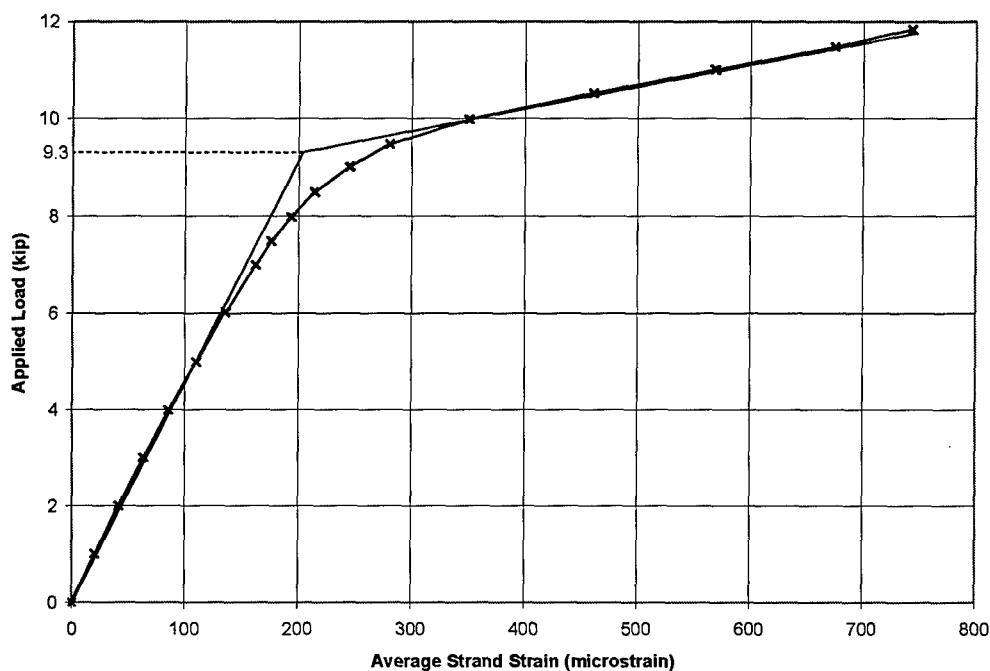
Figure 4-35 Estimated Decompression Load Using Average Strand Strain—

Beam 3

Figure 4-35 shows the plot of applied load versus average strand strain. Based on these data, the decompression load is estimated to be 9.3 kip.
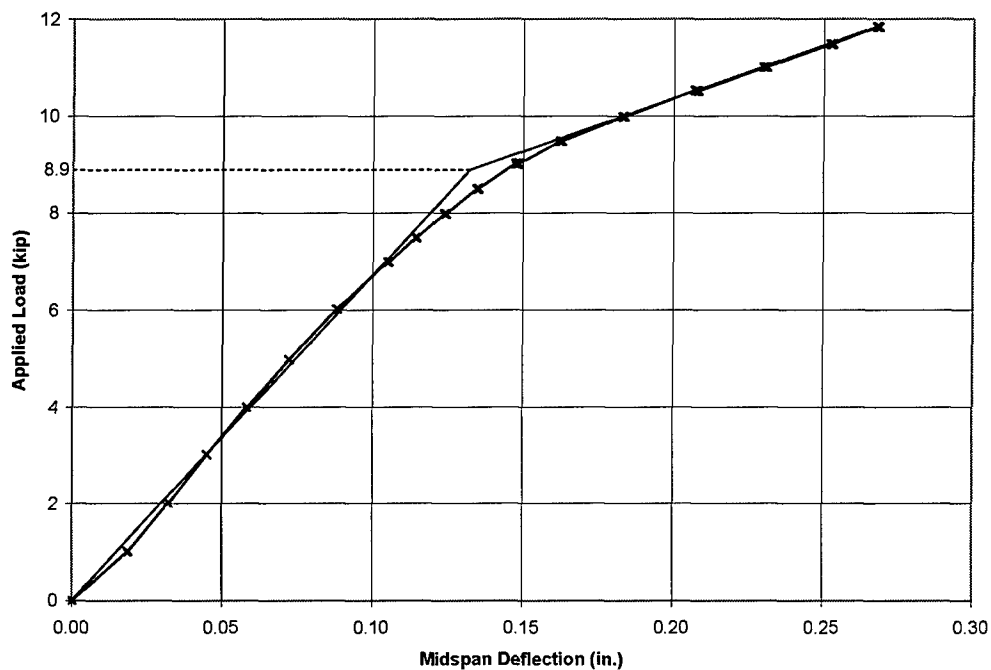
Figure 4-36 Estimated Decompression Load Using Midspan Deflection—Beam 5

Figure 4-36 shows the plot of applied load versus midspan deflection. Based on these data, the decompression load is estimated to be 8.9 kip.

Figure 4-37 displays the plot of applied load versus the crack LVDT displacement. Based on these data, the decompression load is estimated to be 9.1 kip. Averaging the values from these three data sets, the decompression load for Beam 3 is approximately 9.1 kip, which is slightly higher than the value predicted by Hagenberger (2003).
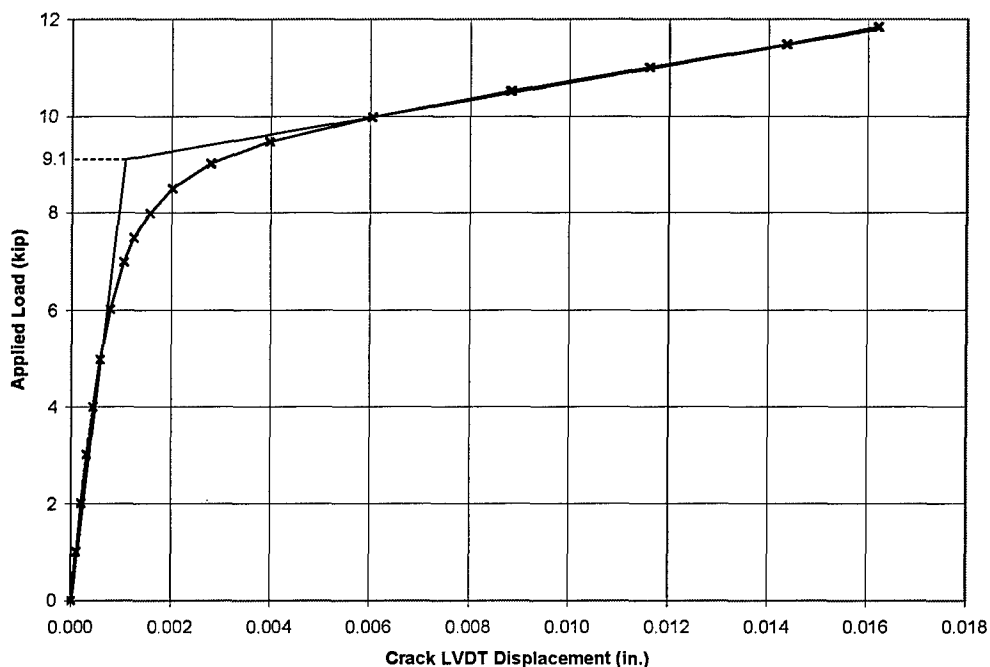
Figure 4-37 Estimated Decompression Load Using Crack LVDT

Displacement—Beam 3

4.3.3 Fatigue Loads

Beam 3 was loaded using a minimum applied load of 2.27 kip and a maximum of 11.85 kip. Based on the analysis by Hagenberger (2003), the prestressing strand (with an effective prestress of 128 ksi) should have experienced a stress range of 23.3 ksi with a minimum stress of 130 ksi.

4.3.4 Fatigue Behavior

This section presents data from a variety of instruments to demonstrate how the response of the beam changed during the fatigue tests. Some of the strain gages failed during the tests; therefore, data are not available from all instruments throughout the tests.

89
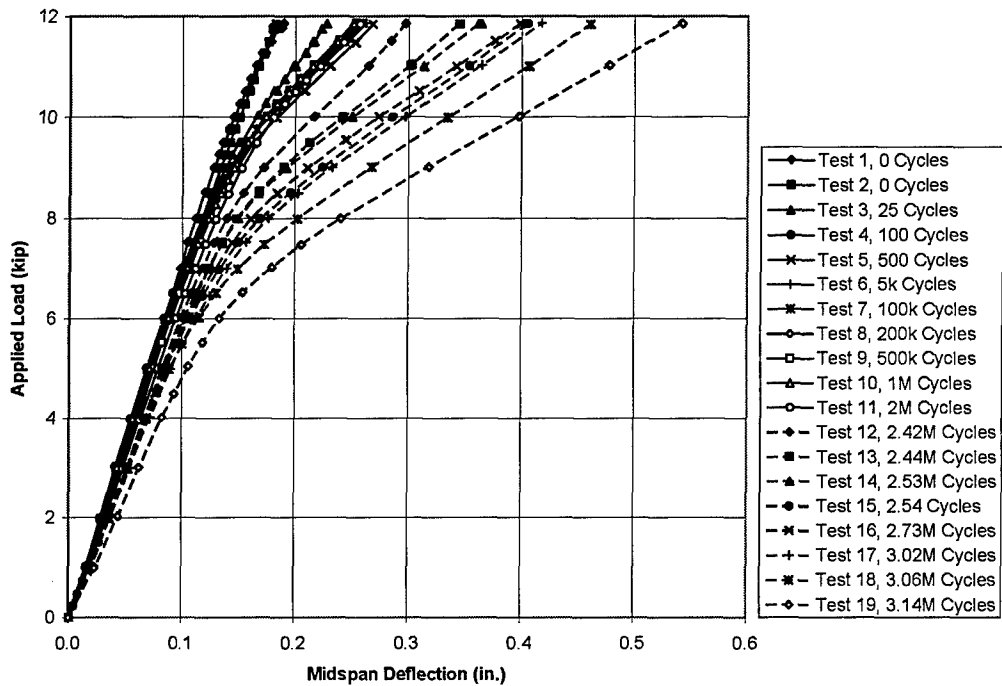
Figure 4-38 Variation of Midspan Displacement During Fatigue Tests—Beam 3

Applied load versus midspan deflection is presented in Figure 4-38. The response of the beam did not change appreciably during the first 2,000,000 cycles. The stiffness began to degrade after 2,420,000 cycles, however.
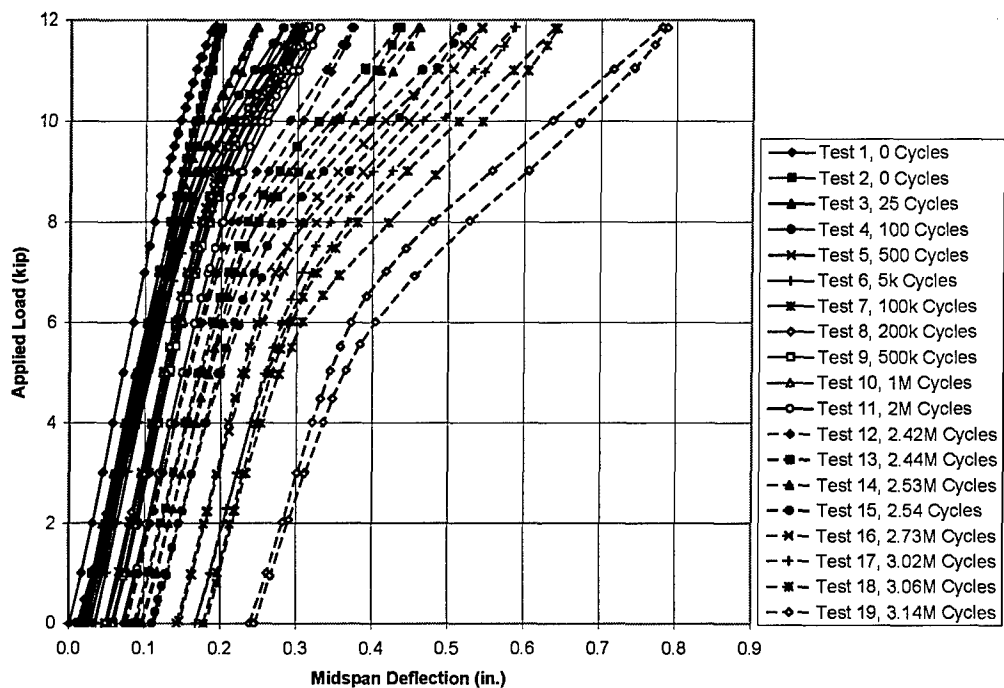
*Figure 4-39 Variation of Midspan Displacement, Including Permanent
Offset—Beam 3*

Applied load versus midspan deflection, including permanent offset, is
presented in Figure 4-39.
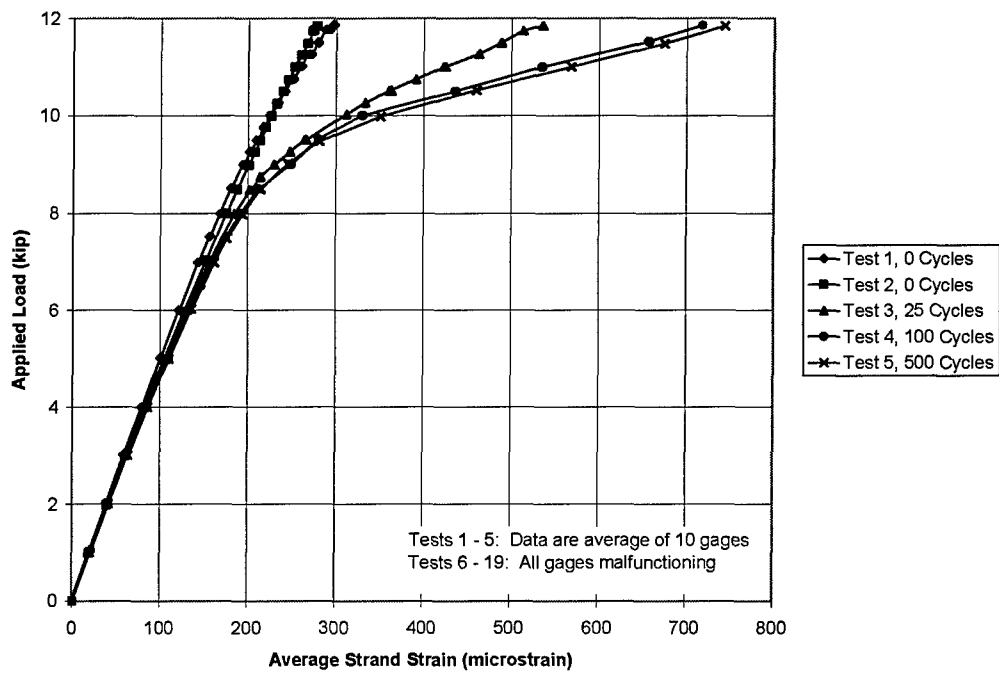
Figure 4-40 Variation of Average Strand Strain During Fatigue Tests—Beam 3

Applied load versus average strand strain is presented in Fig. 4-40. During these fatigue tests, all 10 strand strain gages malfunctioned after Static Test 5.
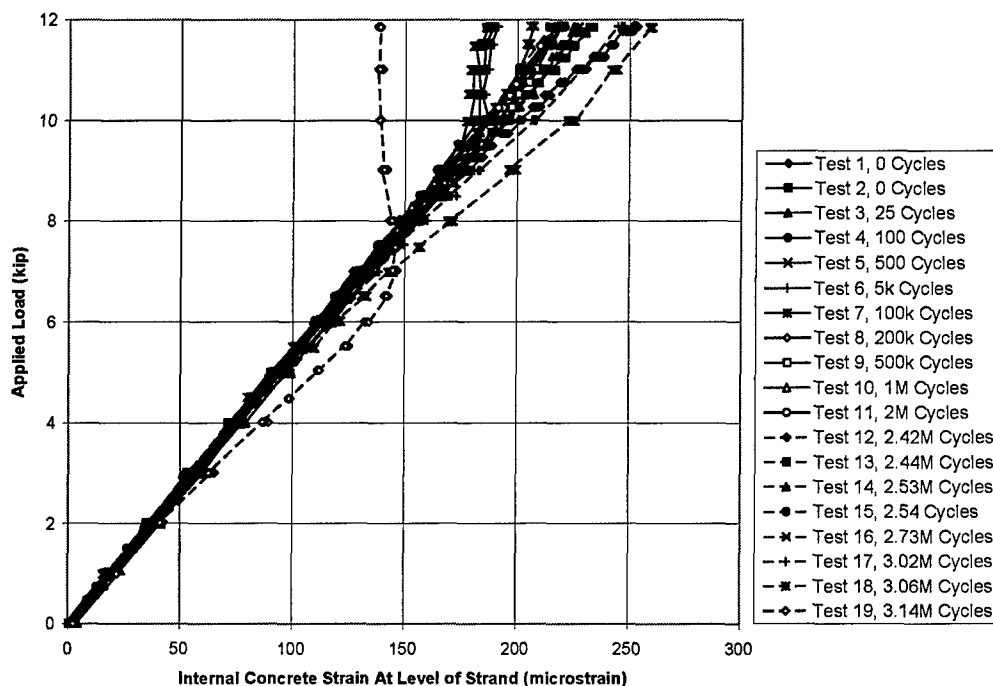
Figure 4-41   Variation of Embedded Concrete Strain During Fatigue Tests—
Beam 3

A concrete strain gage was embedded in the beam between the two strands near midspan. This gage was located about 5 in. to the left of centerline, about half way between the two center cracks (Figure 4-34). Figure 4-41 is the plot of applied load as a function of the concrete gage readings over the fatigue life of the beam. Initially, the behavior of this gage was similar to that of the embedded concrete gages in Beams 4 and 5, with the concrete strain decreasing in amplitude throughout the tests. However, after 100,000 cycles, the amplitude above the decompression load increased. Through most of the fatigue life, the response of this gage was almost linear. This behavior was unique to Beam 3, and a hypothesis to explain the observed behavior has not been developed.
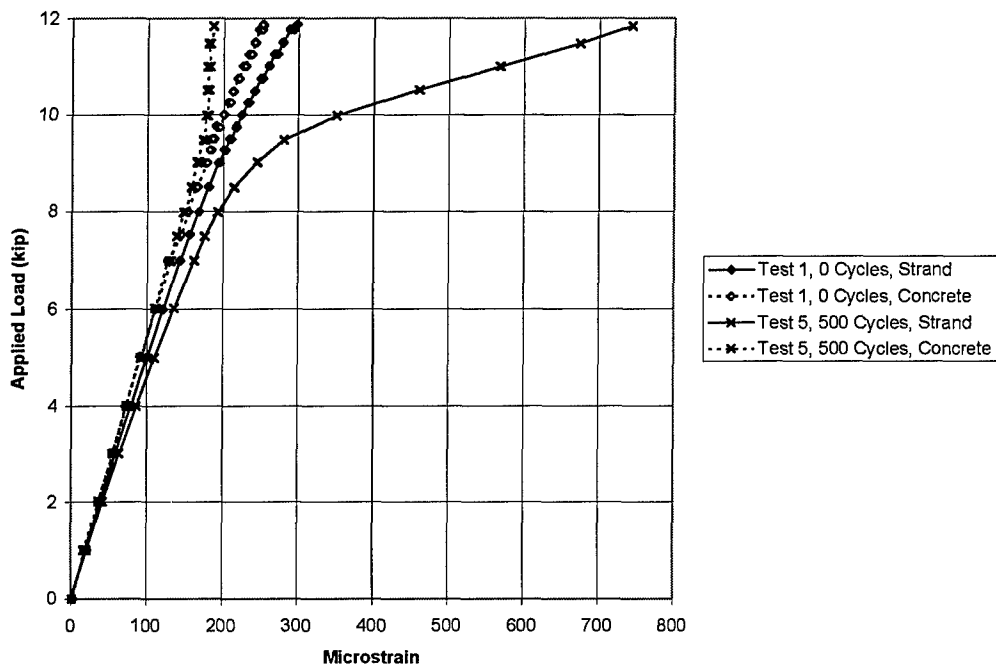
Figure 4-42 Comparison of Strand Strain and Concrete Strain—Beam 3

Figure 4-42 compares the average strand strain and concrete strain for Static Tests 1 and 5. As expected, the data from the strands and the concrete are very similar in the uncracked state and vary dramatically once cracked.

After the static test 4, three instruments were attached to the beam in the vicinity of the most prominent crack (Section 3.2.2). In the case of Beam 3, the most prominent crack was approximately 2 in. east (to the right) of midspan. The plots from these three instruments are shown in Figures 4-43, 4-44, and 4-45.

94

Figure 4-43 graph legend:
- —×— Test 5, 500 Cycles
- —+— Test 6, 5k Cycles
- —*— Test 7, 100k Cycles
- —◇— Test 8, 200k Cycles
- —□— Test 9, 500k Cycles
- —▲— Test 10, 1M Cycles
- —○— Test 11, 2M Cycles
- – ◆ – Test 12, 2.42M Cycles
- – ■ – Test 13, 2.44M Cycles
- – ▲ – Test 14, 2.53M Cycles
- – ● – Test 15, 2.54 Cycles
- – ✱ – Test 16, 2.73M Cycles
- – + – Test 17, 3.02M Cycles
- – ✻ – Test 18, 3.06M Cycles
- – ◇ – Test 19, 3.14M Cycles
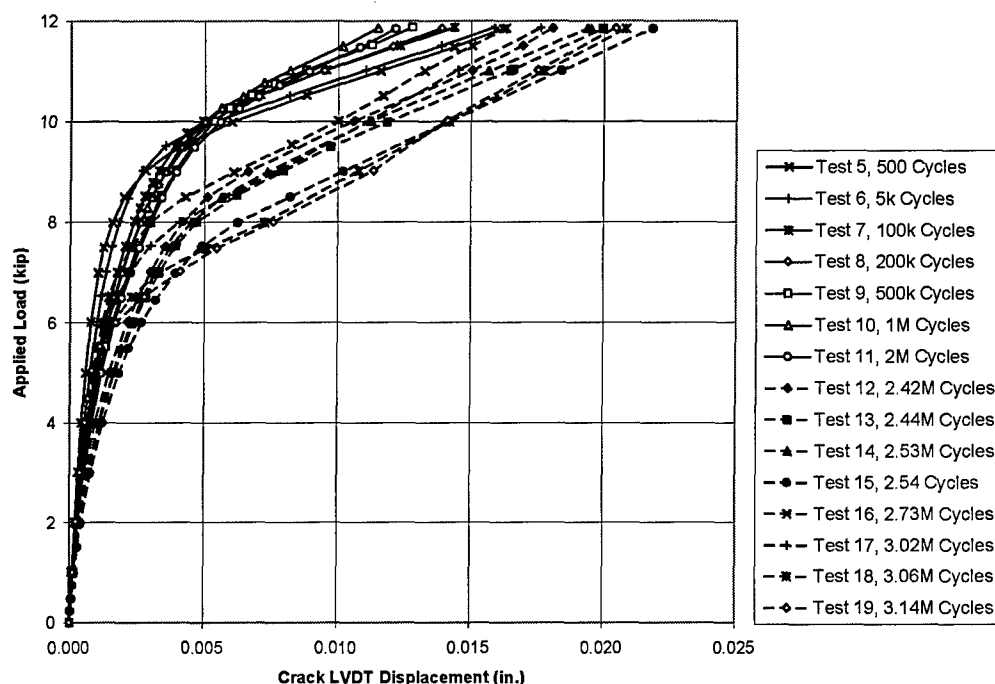
Figure 4-43 Variation of Crack Gage Displacement During Fatigue Tests—

Beam 3

Figure 4-43 shows the plot of applied load vs. the crack LVDT displacement readings. This plot is more difficult to correlate with the midspan deflection plots than were the data from Beams 4 and 5. This is probably because of the limited cracking in the beam initially. Crack widths can become narrower if new cracks form in the surrounding concrete, thereby "sharing" beam curvature. However, from the midspan deflection data (Figures 4-38 and 4-39), especially with the permanent offset included, six wire breaks are expected. Abrupt changes in stiffness were observed at 2,420,000, 2,440,000, 2,540,000, 3,020,000, 3,060,000 and 3,140,000 cycles. It is likely that wire breaks triggered these changes.
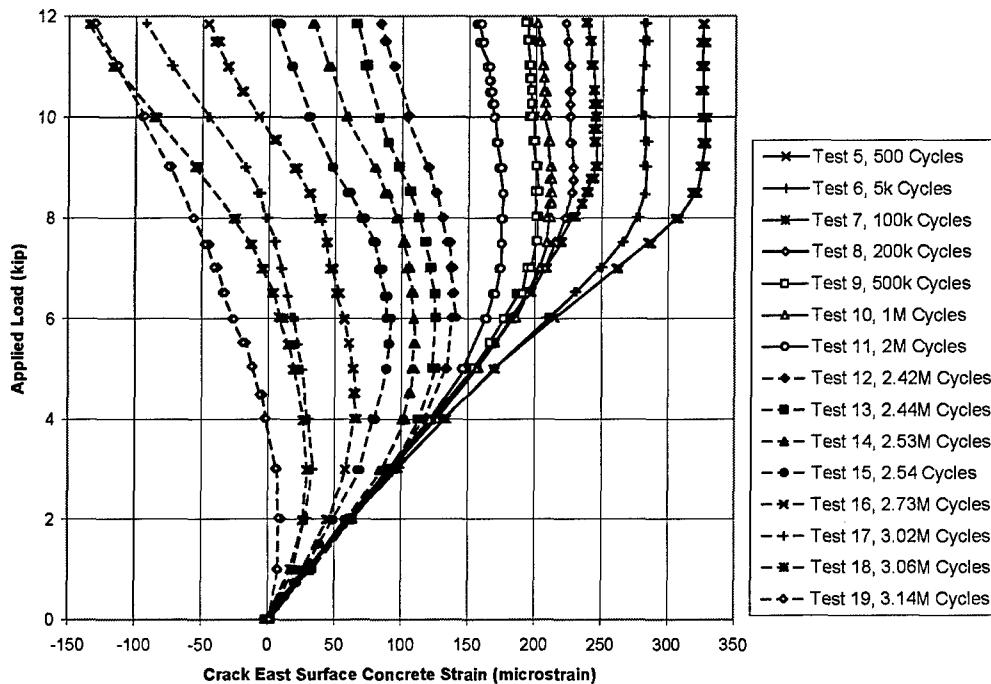
Figure 4-44 Variation of Concrete Surface Strain East of Crack During Fatigue Tests—Beam 3

Figures 4-44 and 4-45 are plots of the applied load vs. the concrete surface strain gage readings on either side of the prominent crack. All diagrams and photographs of beam crack patterns shown in this chapter show the south side of the beam (a north facing view), thus the east surface concrete gage was on the right of the prominent crack in these figures and the west surface concrete gage was on the left.
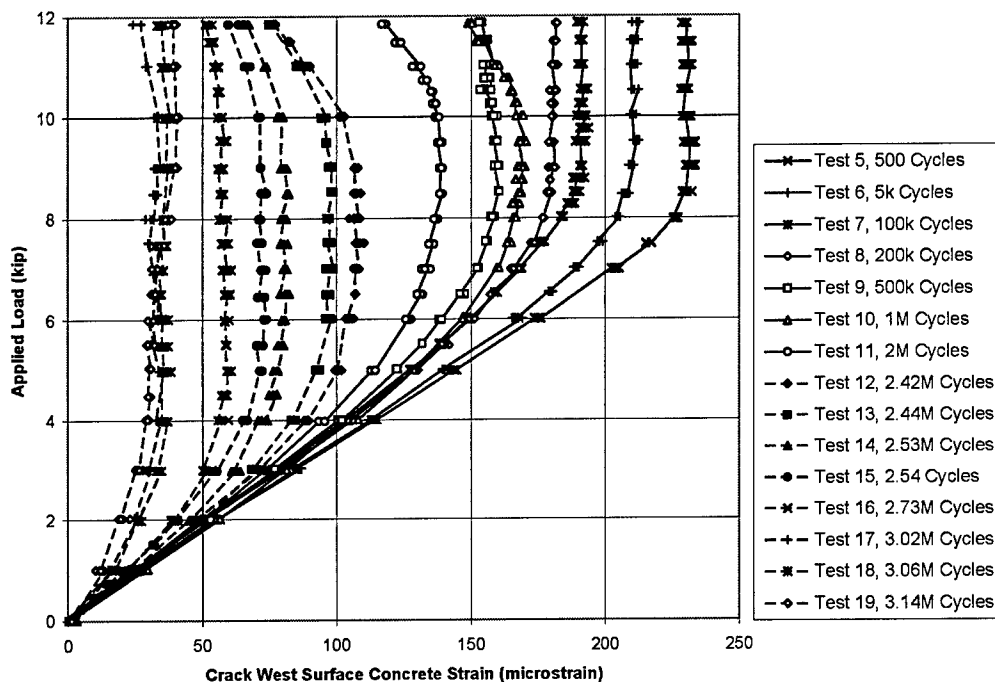
Figure 4-45   Variation of Concrete Surface Strain West of Crack During

Fatigue Tests—Beam 3

The concrete surface strain gages for Beam 3 exhibited the same general response as those for Beams 4 and 5, but the response became more exaggerated as the number of loading cycles increased. When interpreting these data, it is important to remember that the strains represent the change in strain relative to the beginning of the individual static test. The initial strain due to prestressing, and accumulated strains are not included in these plots. After numerous strand wires are broken in a local region, that region will be very close to the decompression load when the beam is subjected to its own self weight. This is believed to be the reason why a few of the curves late in life show negative (compressive) strain.

97

Applied Load = 11.85 kip
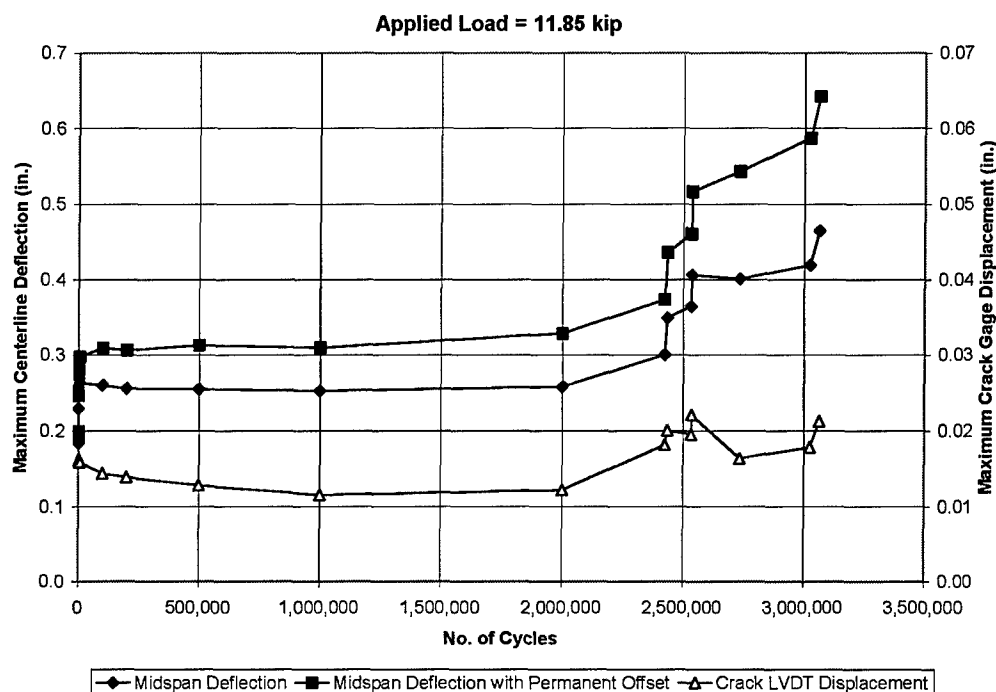
*Figure 4-46 Variation of Midspan Deflection and Crack Gage Displacement
with Number of Cycles—Beam 3*

For comparison purposes, midspan deflection, midspan deflection with permanent offset, and crack gage displacement at an applied load of 11.85 kip are plotted as a function of the number of load cycles and are shown in Figure 4-46. These curves show the characteristic fatigue life phases, showing an initial degradation, a steady-state plateau, and then dramatic degradation after the initial fatigue failure. It should be noted that there is no indication prior to the onset of fatigue failure that such failure is imminent. However, the beam still carried the applied load for many cycles after initial wire fracture.

Figure 4-47 shows the final crack pattern at the end of testing. The numbers shown by the cracks correspond with the number of load cycles experienced by the beam at the time that the crack had propagated to that point.

98

For example, 0 is the initial static test, 100k is the third static test at 100,000 cycles, and so forth. Figure 4-48 is a photograph showing the actual crack markings. Changes in beam coloring are the result of combining separate close-up photographs into one composite image, not anomalies in beam construction. Obtaining a single image was not possible because of the presence of the test frame and other laboratory equipment.
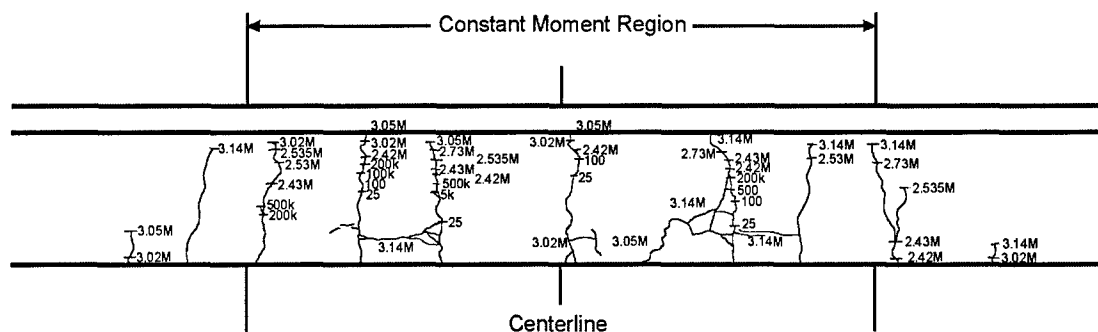
Figure 4-47 Observed Crack Pattern at End of Fatigue Tests—Beam 3
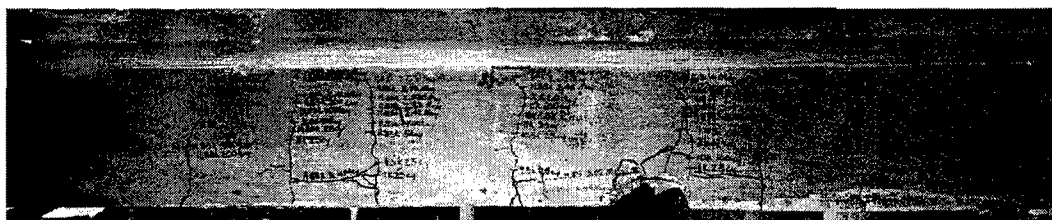
Figure 4-48 Composite Photograph of Beam 3 at End of Fatigue Tests

4.3.5   Post-Mortem Investigation

After testing, the condition of the strand was investigated by carefully removing the concrete around the prestressing strands without damaging the strands. Six wires failed in fatigue and were identified in two separate locations along the beam. Figure 4-49 shows a photograph of the beam at the conclusion of

the post mortem investigation. Figure 4-50 shows the crack pattern at the conclusion of fatigue testing with the location of the failures indicated.

Figure 4-49 Photograph of Beam 3 After Removal of Concrete to Expose Strand

Figure 4-50 Locations of Wire Failures—Beam 3

The six fatigue failures identified during the post-mortem investigation are more difficult to correlate with the deflection plots than for Beams 4 and 5. The crack gage displacements shown in Figure 4-43 are more erratic, and are thus more difficult to correlate to wire failures. The best correlation can be seen in Figure 4-39, the midspan deflection plot that includes permanent offset. Here one can reasonably group curves together and find 6 significant changes in midspan deflection.

100

4.4 BEAM 2

The loading sequence for Beam 2 was expected to crack the beam during the initial static tests and then subject the specimen to fatigue stress ranges of $7.5\sqrt{f_c'}$ for the index stress and approximately 22 ksi for the strand.

4.4.1 Initial Static Tests

Beam 2 was loaded from zero to 11.71 kip during all static tests. Initial cracking was apparent from the change in slope of the midspan deflection and the strand strain gage plots at an applied load of approximately 10 kip, but cracks were not observed until the applied load reached 11 kip. The cracking load calculated using a modulus of rupture of $7.5\sqrt{f_c'}$ was 12.9 kip. The maximum applied load theoretically correlated to a concrete extreme fiber tensile stress of $5.5\sqrt{f_c'}$. Consequently, very little cracking was initially observed. Crack patterns observed during the initial static test are shown in Figure 4-51. Numbers shown along the cracks correspond to magnitude of the applied load during the loading increment in which the crack was observed.
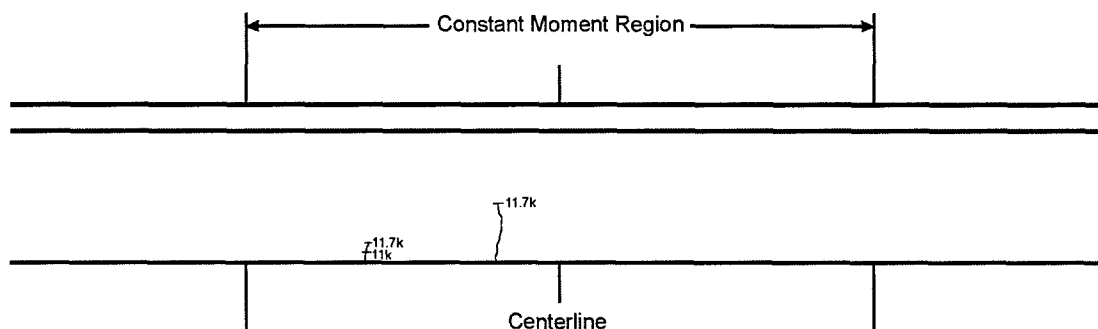
Figure 4-51 Crack Pattern Following Initial Static Test—Beam 2

101

4.4.2 Decompression Load

The calculated decompression load for Beam 2 was 9.5 kip. The decompression load can be estimated from the measured response using the strand strain (Fig. 4-52), midspan deflection (Fig. 4-53), and crack gage displacement (Fig. 4-54). Data from the fourth static test was used for this analysis. The results from this test were representative of all subsequent static tests conducted before the wires began to fail in fatigue.
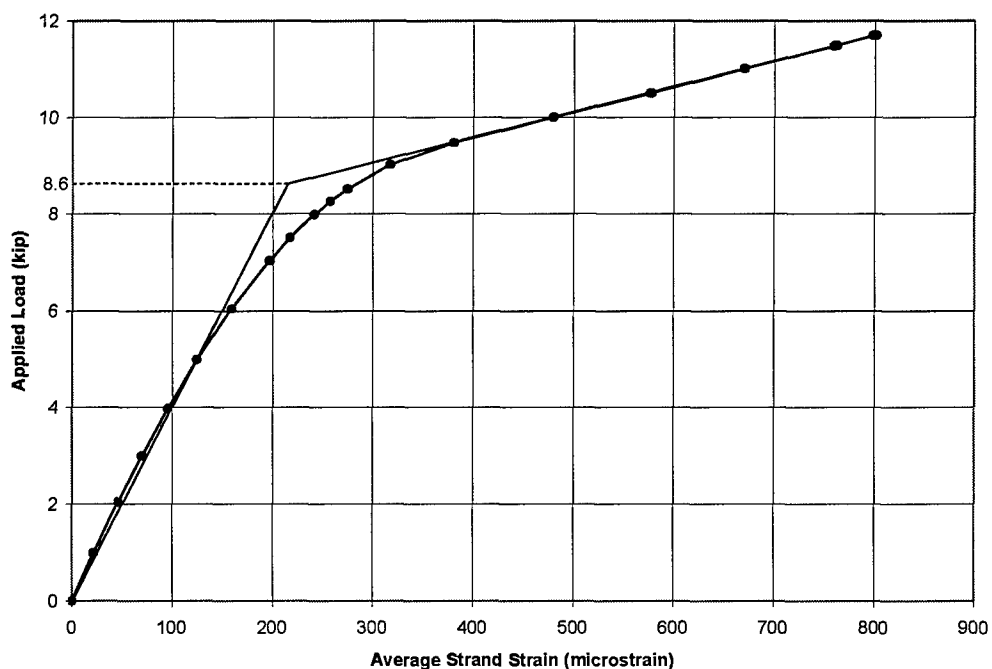
Figure 4-52 Estimated Decompression Load Using Average Strand Strain—

Beam 2

Figure 4-52 shows the plot of applied load versus average strand strain. Based on these data, the decompression load is estimated to be 8.6 kip.
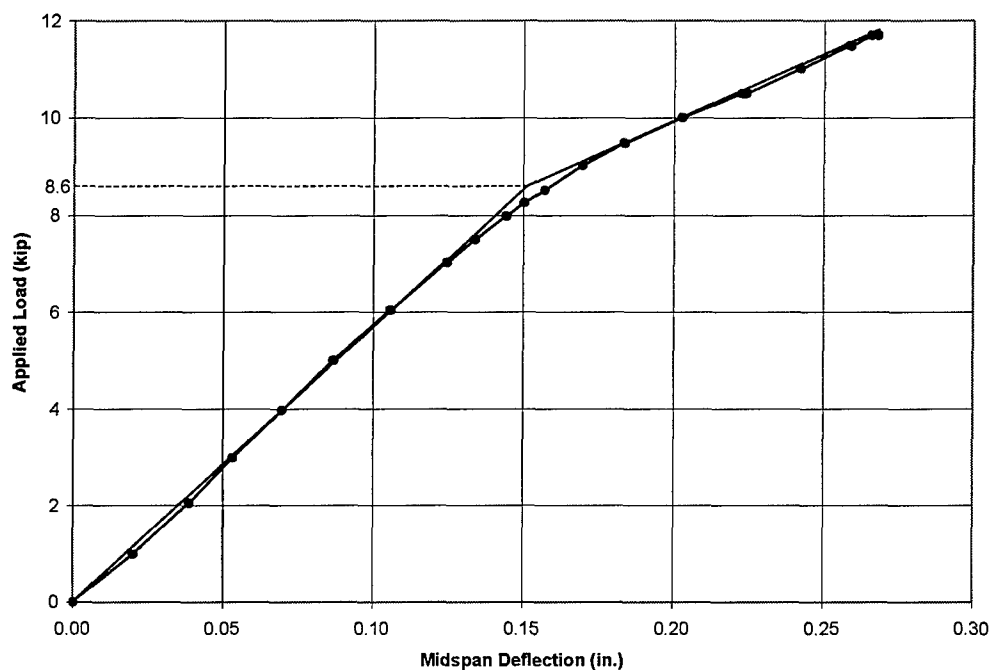
Figure 4-53 Estimated Decompression Load Using Midspan Deflection—Beam 2

Figure 4-53 shows the plot of applied load versus midspan deflection. Based on these data, the decompression load is estimated to be 8.6 kip.

Figure 4-54 displays the plot of applied load versus the crack LVDT displacement. Based on this plot, the zero tension load is estimated to be 8.8 kip. Averaging the values from these three sets of data, the decompression load for Beam 2 is approximately 8.7 kip, which is slightly lower than the value predicted by Hagenberger (2003).

103
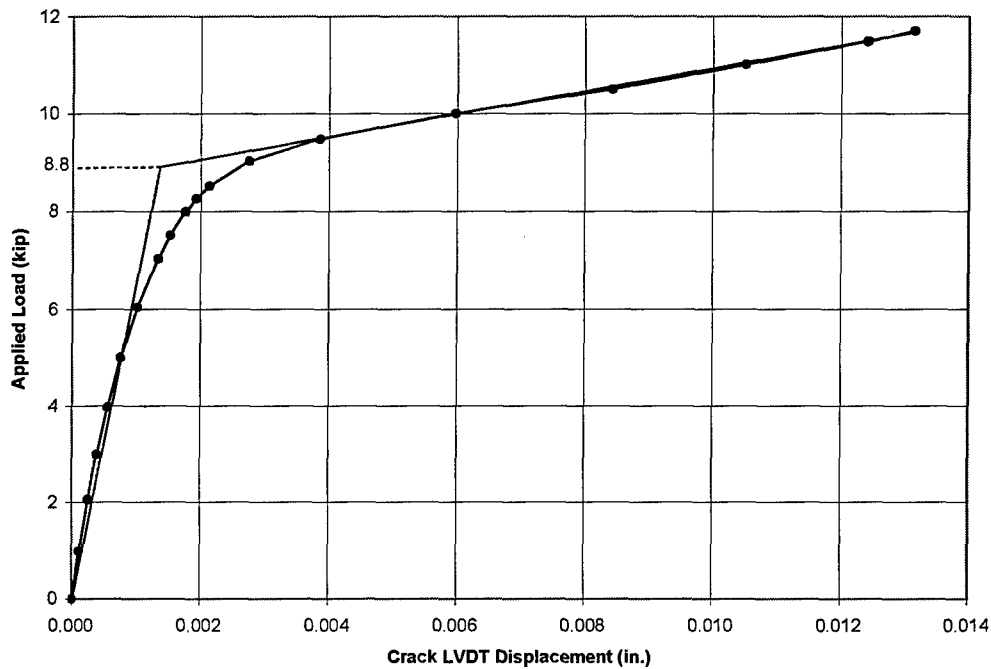
Figure 4-54 Estimated Decompression Load Using Crack LVDT Displacement—Beam 2

4.4.3 Fatigue Loads

Beam 2 was loaded using a minimum applied load of 3.41 kip and a maximum of 11.71 kip. Based on the analyses by Hagenberger (2003), the prestressing strand (with an effective prestress of 127 ksi) should have experienced a stress range of 21.7 ksi with a minimum stress of 130 ksi.

4.4.4 Fatigue Behavior

This section presents data from a variety of instruments to demonstrate how the response of the beam changed during the fatigue tests. Some of the strain gages failed during the tests; therefore, data are not available from all instruments throughout the tests.

104
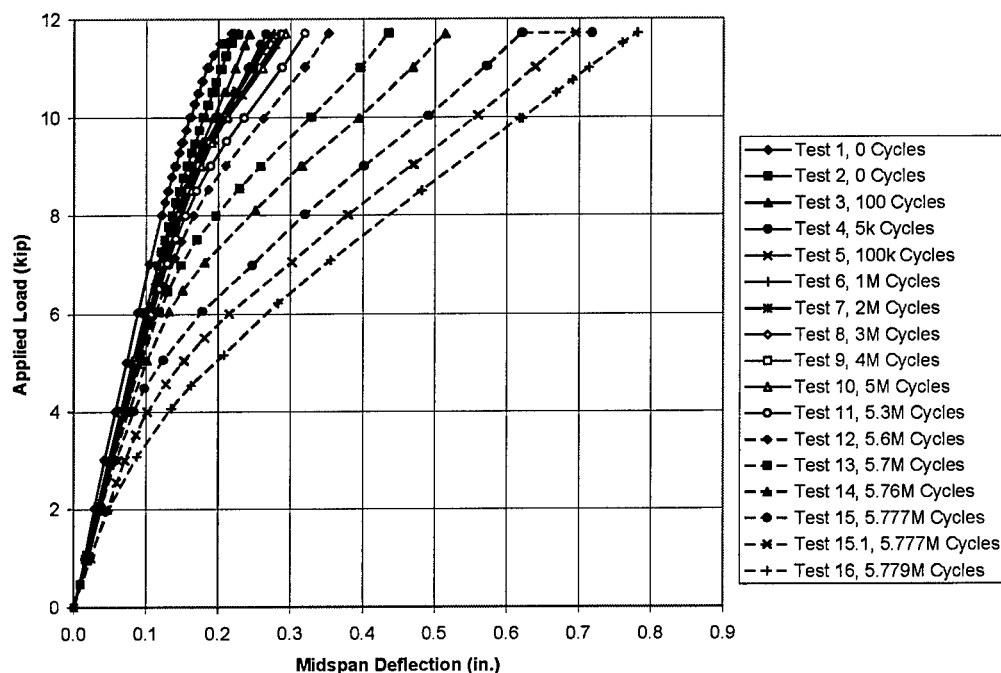
Figure 4-55 Variation of Midspan Deflection During Fatigue Tests—Beam 2

Applied load versus midspan deflection is presented in Fig. 4-55. The response of the beam did not change appreciably during the first 5,000,000 cycles. The stiffness began to degrade after 5,300,000 cycles.

It should be noted that while marking cracks with the beam loaded during static test 15, the beam emitted a loud, percussive noise, which was assumed to be a wire breaking. An additional static test, 15.1, was then run to evaluate suspected changes in the response of the beam, which appeared to confirm a new wire break.

105
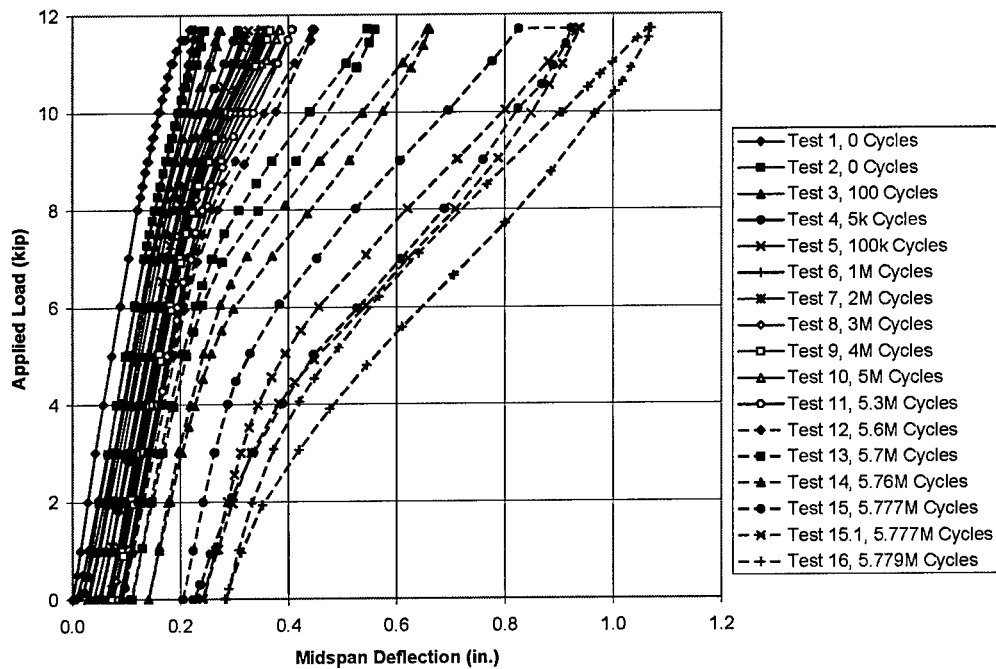
Figure 4-56 Variation of Midspan Displacement, Including Permanent

Offset—Beam 2

Applied load versus midspan deflection, including offset, is presented in Figure 4-56.
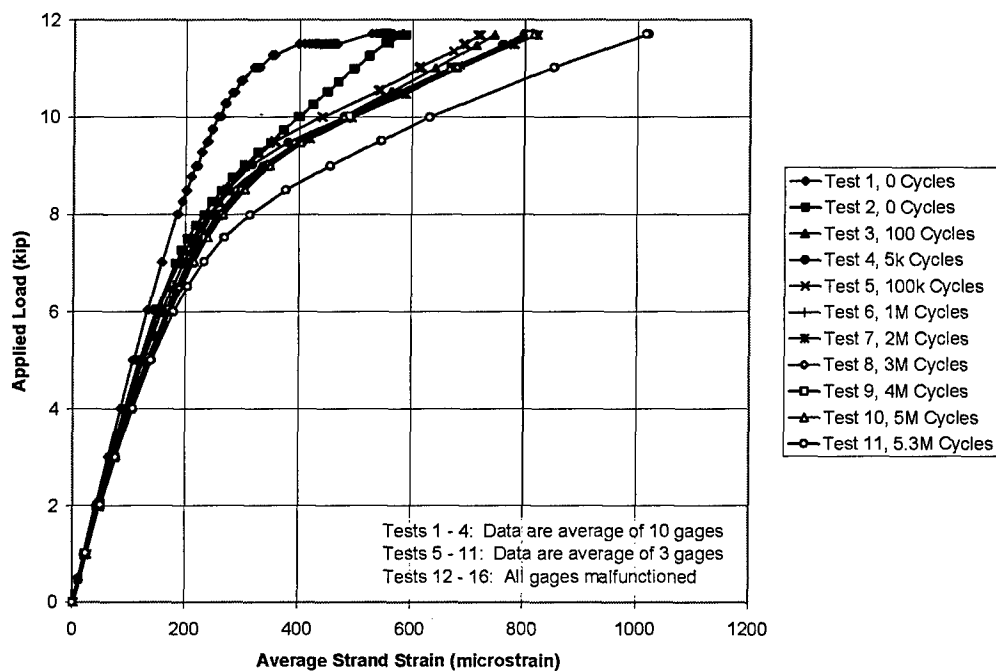
Figure 4-57 Beam 2 Load vs. Average Strand Strain Over Fatigue Life

Applied load versus average strand strain is presented in Fig. 4-57. After static test 4, only 3 gages were functioning, and after test 11, all 10 strand strain gages had malfunctioned.

107
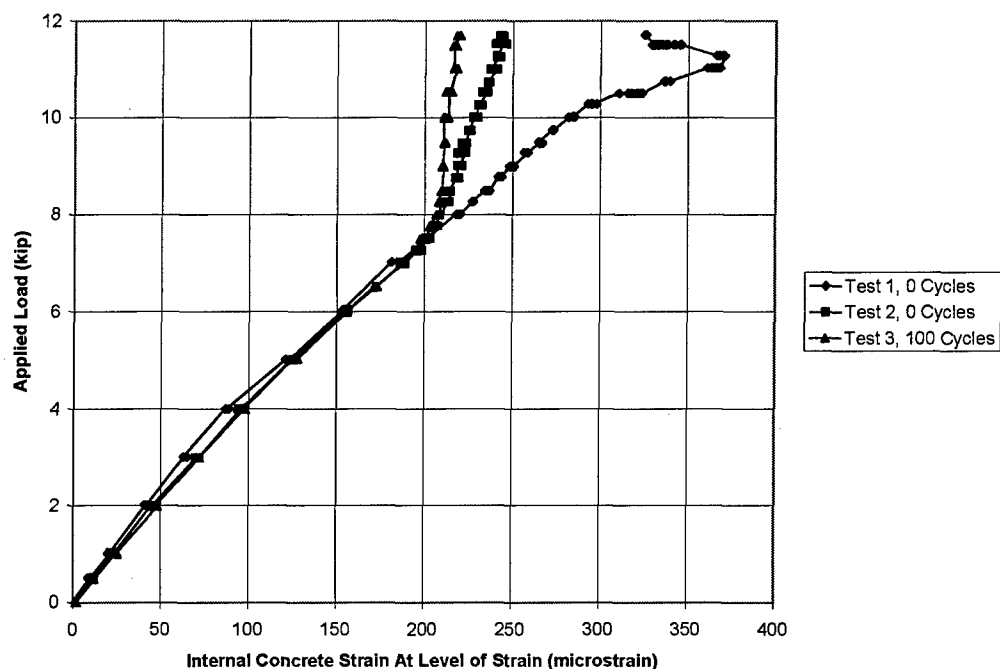
Figure 4-58 Variation of Embedded Concrete Strain During Fatigue Tests—
Beam 2

A concrete strain gage was embedded in the beam between the two strands near midspan. This gage was located just to the right of the smaller, left-most crack (Figure 4-51). Figure 4-58 is the plot of applied load as a function of the concrete gage readings over the first 100 cycles of the beam. After static test 3, the gage failed.
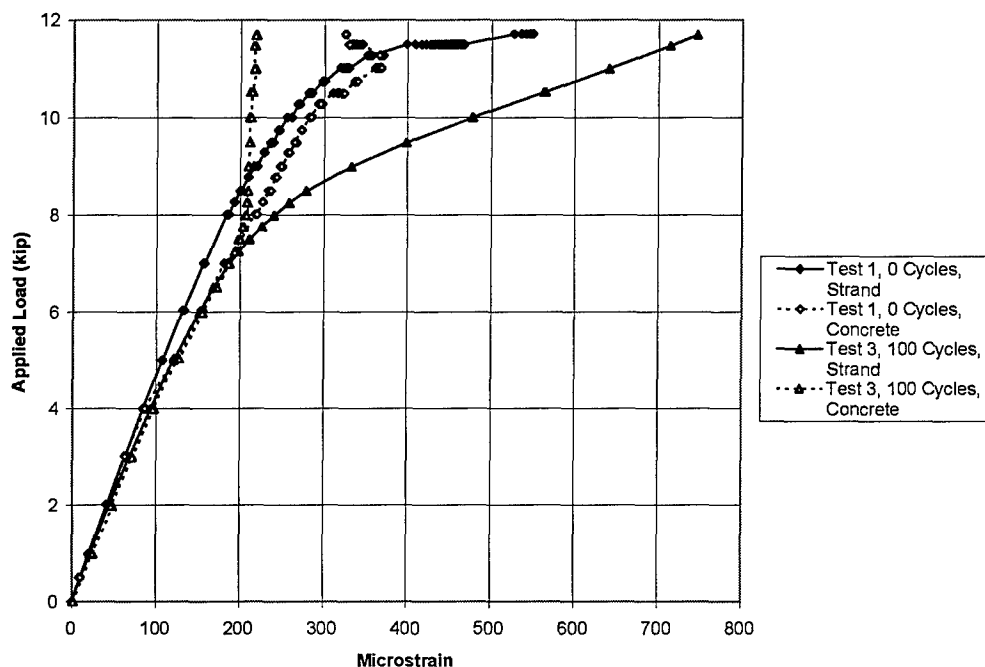
Figure 4-59 Comparison of Strand Strain and Concrete Strain—Beam 2

Figure 4-59 compares the average strand strain and concrete strain for static tests 1 and 3. As expected, the data from the strands and the concrete are initially very similar and begin to vary as the cracking load is approached. Once the beam cracks, the strains in the strand and surrounding concrete vary dramatically.

After the initial test, three instruments were attached to the beam in the vicinity of the most prominent crack (Section 3.2.2). In the case of Beam 2, the most prominent crack was approximately 5 in. west (to the left) of midspan. The plots from these three devices are shown in Figures 4-60, 4-61, and 4-62.

109

Figure 4-60 shows the plot of applied load versus the crack LVDT displacement. The following is a legend for the figure:

- Test 2, 0 Cycles
- Test 3, 100 Cycles
- Test 4, 5k Cycles
- Test 5, 100k Cycles
- Test 6, 1M Cycles
- Test 7, 2M Cycles
- Test 8, 3M Cycles
- Test 9, 4M Cycles
- Test 10, 5M Cycles
- Test 11, 5.3M Cycles
- Test 12, 5.6M Cycles
- Test 13, 5.7M Cycles
- Test 14, 5.76M Cycles
- Test 15, 5.777M Cycles
- Test 15.1, 5.777M Cycles
- Test 16, 5.779M Cycles

Figure 4-60   Variation of Crack Gage Displacement During Fatigue Tests—
Beam 2

Figure 4-60 shows the plot of applied load versus the crack LVDT displacement. This plot again correlates very well with the midspan deflection plots in Figures 4-55 and 4-56, and each shows distinct changes in displacement at the same points in fatigue life. From these three sets of data, seven wire breaks were expected. Abrupt changes in stiffness may be observed at 5,300,000, 5,600,000, 5,700,000, 5,760,000, 5,777,000 (two times), and 5,779,000. It is likely that wire breaks triggered these changes

110
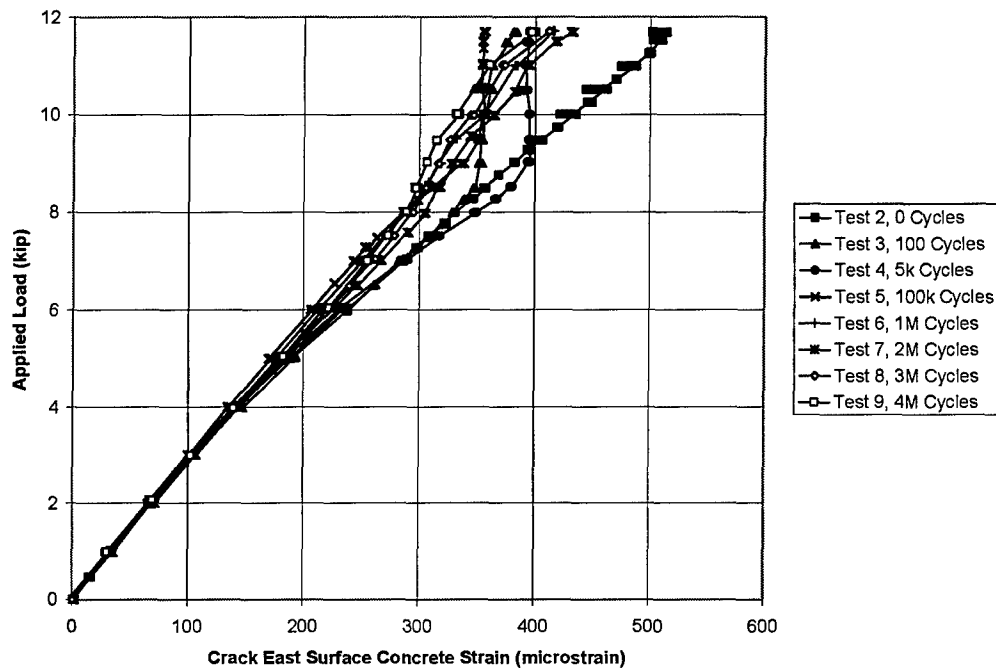
Figure 4-61 Variation of Concrete Surface Strain East of Crack During Fatigue Tests—Beam 2

Figures 4-61 and 4-62 are plots of the applied load vs. the concrete surface strain gage readings on either side of the prominent crack. All diagrams and photographs of beam crack patterns shown in this chapter show the south side of the beam (a north facing view), thus the east surface concrete gage was on the right of the prominent crack in these figures and the west surface concrete gage was on the left.

111
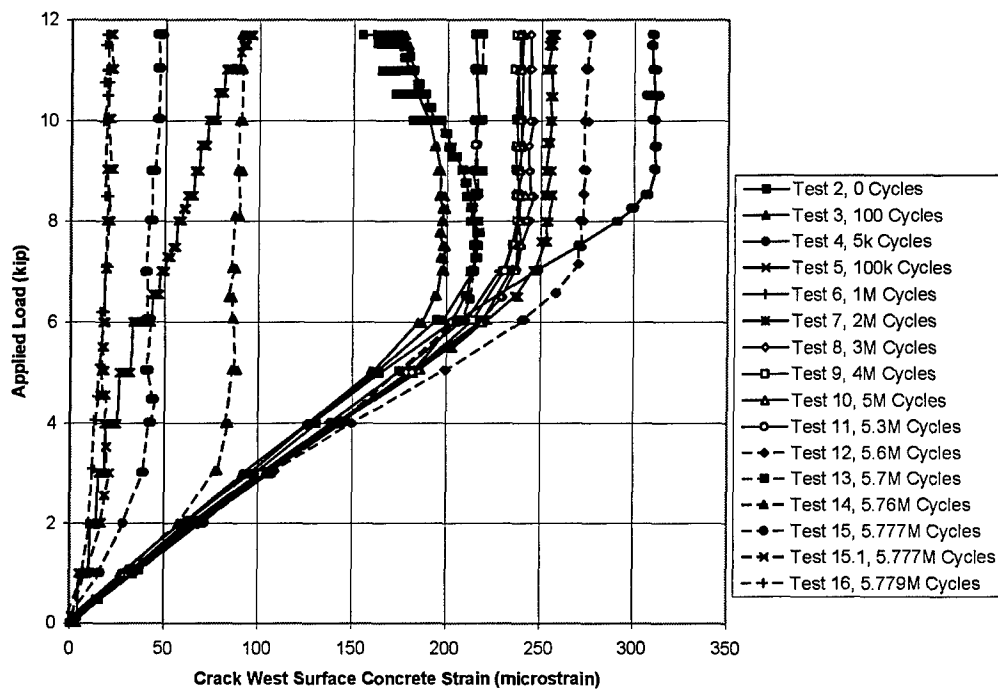
***Figure 4-62 Variation of Concrete Surface Strain West of Crack During
Fatigue Tests—Beam 2***

The concrete surface gages on this beam experienced behavior similar to that of Beam 4 and was discussed in more detail in Section 4.1.4. Unfortunately, the east gage failed after the ninth static test at 4 million cycles.
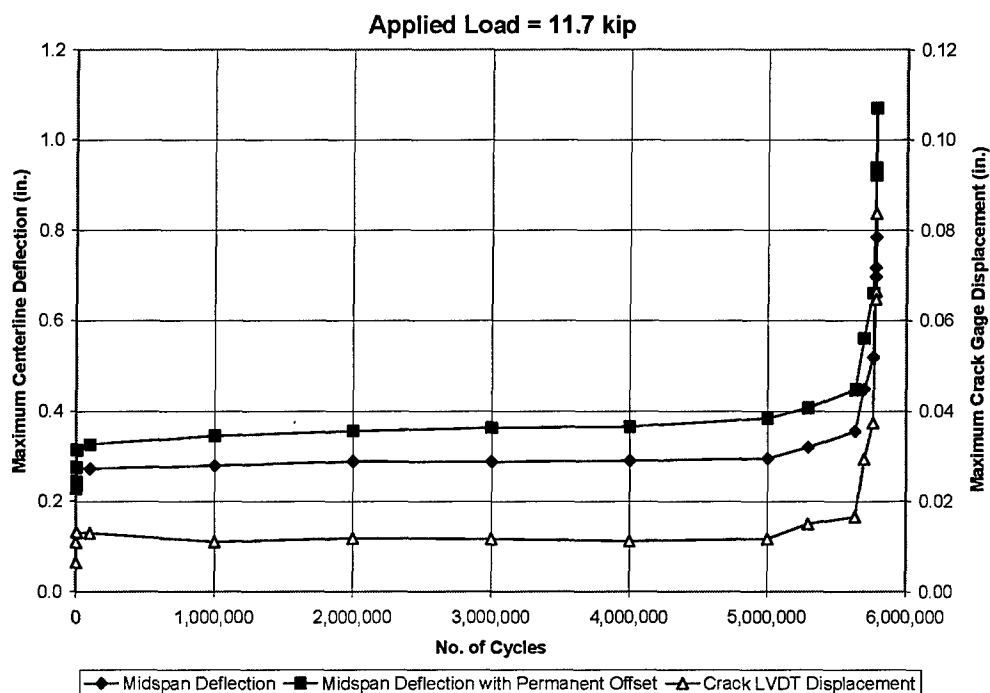
***Figure 4-63 Variation of Midspan Deflection and Crack Gage Displacement
with Number of Cycles—Beam 2***

For comparison purposes, maximum midspan deflection, midspan deflection with permanent offset, and crack gage displacement at an applied load of 11.7 kip are plotted as a function of the number of load cycles in Figure 4-63. These curves show the characteristic fatigue life phases, showing an initial degradation, a steady-state plateau, and then dramatic degradation after initial fatigue failure. It should be noted that there is no indication prior to the onset of fatigue failure that such failure is imminent. However, the beam still carried the applied load for many cycles after initial wire fracture.

Figure 4-64 shows the final crack pattern at the end of testing. The numbers shown by the cracks correspond with the number of fatigue cycles experienced by the beam at the time that the crack had propagated to that point.

113

For example, 0 is the initial static test, 100k is the third static test at 100,000 cycles, and so forth. Figure 4-65 is a photograph showing the actual crack markings. Changes in beam coloring are the result of combining separate close up photographs into one composite image, not anomalies in beam construction. Obtaining a single image was not possible because of the presence of the test frame and other laboratory equipment.

Figure 4-64 Observed Crack Pattern at End of Fatigue Tests—Beam 2

Figure 4-65 Composite Photograph of Beam 2 at End of Fatigue Tests

4.4.5   Post-Mortem Investigation

After testing, the condition of the strand was investigated by carefully removing the concrete around the prestressing strands without damaging the strands. Seven wires failed in fatigue and were identified in four separate locations along the beam. Figure 4-49 shows a photograph of the beam at the end

114

of post-mortem investigation. Figure 4-50 shows the crack pattern at the conclusion of fatigue testing with the location of the failures indicated.

Figure 4-66 Photograph of Beam 2 After Removal of Concrete to Expose Strand

Figure 4-67 Location of Wire Failures—Beam 2

The seven fatigue failures found during the post-mortem investigation correlate very well with the seven distinct changes in the midspan deflection and crack gage displacement plots shown in Figures 4-55, 4-56 and 4-66.

115

CHAPTER 5

Evaluation of Beam Tests

5.1 GENERAL SUMMARY

An overview of the results of the fatigue tests of Beams 2, 3, 4, and 5 is provided in Table 5-1.

Table 5-1 Overview of Beam Test Results

Beam	Index Stress	Calculated Bottom Fiber Tensile Stress	Calculated Strand Stress Range (ksi)	Experimental Strand Stress Range (ksi)	Crack Width Range (in.)	No. of Cycles to First Wire Break	No. of Cycles at End of Test	Total No. of Wire Breaks
2	$7.5\sqrt{f_c'}$	$5.5\sqrt{f_c'}$	21.7	22	0.011	5,293,703	5,778,707	7
3	$7.5\sqrt{f_c'}$	$8.2\sqrt{f_c'}$	23.3	21	0.014	2,424,121	3,142,804	6
4	$12\sqrt{f_c'}$	$11.6\sqrt{f_c'}$	43.2	45	0.025	519,799	642,964	7
5	$12\sqrt{f_c'}$	$11.1\sqrt{f_c'}$	42.0	42	0.017	318,958	365,576	4

As explained in Chapter 3, the applied loads for each beam were selected such that the calculated stress range in the strand was the same as the calculated stress range in the center of gravity of strand profile in the prototype highway bridge. Calculated tensile stress in the extreme tension fiber of the concrete in the highway bridge girders was used as the index stress, which served as the basis for all calculations (Figure 3-7). The details of all calculations are summarized in Hagenberger (2003).

The calculated bottom fiber tensile stress in the beams based upon uncracked section analysis, and the calculated strand stress range based on

116

cracked section analysis are reported in Table 5-1. The experimental strand stress ranges shown are based on the strand strain readings taken early in fatigue life (the first static test with more than 100 cycles). The change in strain between the minimum and maximum loads was multiplied by the apparent strand modulus of elasticity of 31,200 ksi. This value for apparent strand modulus of elasticity is based on experimental data, and is described in detail in Chapter 2. It relates the strain gage readings to average strand stress.

The values of Crack Width Range in Table 5-1 are approximate estimates of the change in crack width (between loaded and unloaded conditions) based on the crack displacement LVDT readings. During the literature review, a few authors stated that there might be a correlation between crack width ranges and strand fatigue. This effect was not thoroughly studied as a part of this project, but the data are provided for the benefit of future research.

The number of cycles to first wire fatigue failure is also provided in Table 5-1. Obviously, one cannot visually inspect the strand wires, and because these tests are conducted over a period of weeks, it is unlikely that a member of the research team will be present to hear the sound of a wire breaking. However, as discussed in Chapter 4, the limit switch under the beam was sufficiently sensitive to stop cyclic loading in the event of a wire break. Using the number of wire breaks found during the post-mortem investigation, the methods discussed in Section 5.3, and analysis of the data provided in Chapter 4, the number of cycles to first wire break can be determined with reasonable certainty. It should be realized, however, that because Wohler (S − N) diagrams are plotted on a logarithmic scale, the effect of a small error in the exact number of cycles is minimal. The number of cycles at the end of testing is also provided for reference.

5.2 DETERMINATION OF EXPERIMENTAL STRAND STRESS RANGES

As discussed in Section 5.1, experimental strand stress ranges were calculated using the strand strain gage readings measured during the static tests. At the beginning of fatigue testing there were ten active strain gages attached to the strands in each beam. Because the strain gages failed during the fatigue tests, it is not possible to determine how the strand strain varies with the number of loading cycles. Therefore, comparisons of stress range at the beginning and end of the fatigue tests are not possible.
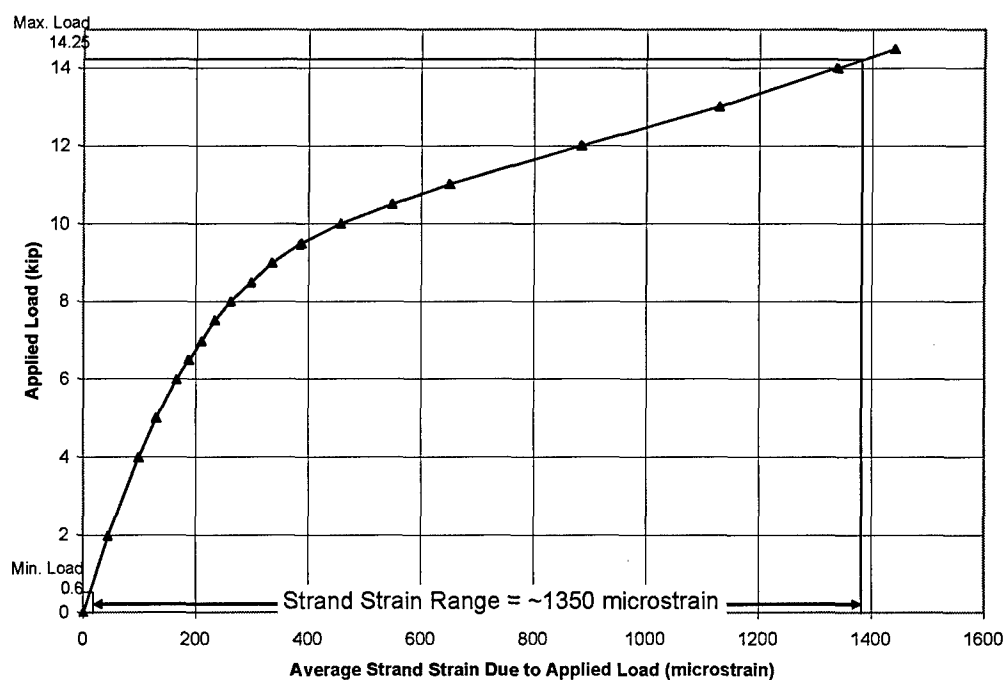
Figure 5-1 Example of Determining Strand Strain Range--Beam 5

Figure 5-1 illustrates the procedure used to calculate the experimental stress ranges. Beam 5 is used as an example. The cyclic loading of Beam 5 ranged from a minimum of 0.60 kip to a maximum of 14.25 kip. The corresponding strain values are then interpolated from the test data. The

118

difference between these strain values is the change in strain due to the applied load acting through one loading cycle, and is called the experimental strand strain range.

One should not be confused by the strain values. The point corresponding to zero strain in Figure 5-1 does not indicate that the strain in the strand is zero. Rather, the horizontal axis in Figure 5-1 represents the increase in strain due to the applied load. The strains due to the initial prestress and dead load must be added to this value to obtain the total strain.

Once the experimental strain range is determined from the beam response, the experimental stress range is calculated as

$$S_r = E_{pa} \times \varepsilon_r \qquad\qquad (5\text{-}1)$$

where S_r is the experimental strand stress range in ksi,

E_{pa} is the apparent modulus of elasticity of the strand in ksi, and

ε_r is the experimental strand strain range.

For example, for Beam 5 $S_r = E_{pa} \times \varepsilon_r = (31,200 \text{ ksi}) \times (0.001350) = 42$ ksi. Because of the scatter among the data from the strain gages, it is not possible to obtain an estimate of the stress range that is more precise. Section 2.3.1 of Chapter 2 contains a full discussion of the development of the apparent modulus of elasticity and why it is used instead of a nominal value for strand modulus of elasticity.

The nonlinear trends shown in Figure 5-1 do not invalidate the use of the linear relationship in Equation (5-1). The nonlinear relationship shown in Figure 5-1 is related to the decompression load. Once the applied load exceeds the decompression load, the concrete in the bottom portion of the section provides insignificant resistance to the tensile stresses, and the prestressing steel resists the tensile force required for equilibrium. Therefore, the strands are not yielding in

119

Figure 5-1, rather the concrete around the strands is no longer contributing to resisting the internal bending moment. The highest stress experienced by any strand during cyclic loading was about 177 ksi, which is about 73 percent of the nominal yield stress.

As is readily apparent in Table 5-1, the calculated strand stress ranges correlate extremely well with the values obtained using the measured strain data. This again provides validation of the analyses performed by Hagenberger (2003), and builds confidence in the results of these tests.

5.3   BEHAVIOR AFTER INITIAL WIRE FATIGUE FAILURE

This section describes methods used to determine that wire fatigue failures had occurred. While some of these methods would only be applicable to laboratory conditions where instrumentation can be permanently attached over the fatigue life of a beam, some indications could also be used by field inspection teams.

As indicated in Table 5-1 and Figures 4-12, 4-29, 4-46, and 4-63, the beams continued to support the applied loads well past the initial wire fatigue failure. In reviewing the general trends in the fatigue life plots, one can notice that after initial changes in midspan deflection, the midspan deflection is essentially independent of the number of loading cycles over most of the fatigue life of the beam. Certainly field inspectors would be extremely challenged to detect the small changes in midspan deflection over years of use. During these tests, no warning signs were observed that indicated that the first wire was about to fail in fatigue.

Once the initial wire failed, several different methods could be used to verify that a wire had failed. The first was used to stop the test: the midspan deflection increased due to the reduction in beam stiffness, allowing the beam to

120

touch the limit switch that stopped the test. However, crack growth or formation of new cracks also caused small changes in the beam stiffness. After the first wire break, there was no visual evidence of the damage when the beam was unloaded. Once the beam was loaded during the next static test, a significant amount of new cracking could be observed, both in the form of new cracks and as extensions of existing cracks.

From the data collected during the subsequent static test, one could observe three distinct changes in the midspan deflection data. First, the total deflection increased significantly compared with the very minor increases observed during the previous static tests. Second, when plotted against the applied load, the load at which the slope of the plot changed dramatically decreased, demonstrating a decrease in the decompression load. Additionally, looking at this same plot there was a very noticeable increase in the difference between the loading and the unloading curves. Prior to failure, but after initial cracking, the unloading curve was very close to the loading curve. After the first fatigue failure, hysteresis was observed, especially for loads above the decompression load. With each wire break, the differences between the loading and unloading curves increased.

Naturally, along with the increased cracking that was observed with wire breaks, the crack widths also increased. Crack gage displacement experienced changes very similar to the changes just described for midspan deflection, though sometimes not as reliably. The effects of adjacent cracks (especially new cracks forming) on the crack being measured can affect the trends in the width of the measured crack.

After several strands had broken in a beam, horizontal cracks were sometimes observed in the beam at the depth of the strand. This is caused by the radial expansion of the broken wires because of the loss of tension. The

121

horizontal cracking was not necessarily at the location of the wire fractures, but could be several inches away. For bridge field inspection crews, the presence of horizontal cracking would almost certainly be an indicator of a significant number of broken wires in the strands. In these tests, the horizontal cracking occurred at comparatively advanced stages of fatigue damage, shortly before the test was terminated. As can be seen in Figures 4-31 and 4-48, in two of the beams, a section of concrete separated and fell off of the bottom of the beam. While this is well past when a beam should be taken out of service, it is certainly notable that the beams still supported the applied loading in this condition.

A change in stiffness caused by a wire fatigue failure was also evident in the response of the test equipment. As described in Chapter 3, there was an error signal that measured the difference between the command signal of the signal generator and the output of the load cell. When a wire broke, this input-to-output error signal abruptly increased when cyclic loading was resumed. This increase was caused by the slower response of the beam due to a loss of stiffness. In order to restore the error signal to a satisfactory level, the cyclic loading frequency was reduced. While reducing the frequency was required after a loss of stiffness caused only by increased cracking, the amount by which the frequency had to be reduced was noticeably higher for wire breaks than for cracking.

Finally, the frequency at which the limit switch was triggered increased dramatically after the first wire break. In Chapter 3, it was discussed that a limit switch was placed under the beam to indicate when the midspan deflection had increased under load. During the early phases of the fatigue testing, the tests were interrupted once or twice due to increases in the midspan deflection, which were later correlated to cracking. Once the first wire breaks, the edges of the broken wire rub against the adjacent wires, which promotes fatigue crack formation in the remaining wires. Because the remaining prestressing strand area is reduced, and

the applied loads are maintained at the same levels, the stresses and stress ranges in the remaining wires increase. This leads to more rapid fatigue of the remaining wires in the vicinity of the initial wire break.

5.4 COMPARISON OF BEAM FATIGUE TESTS WITH EXPECTED RESULTS

Results reported in the literature were summarized in Chapter 1. If the beams followed the behavior of previously tested beams, and the expected correlation between stress range and number of cycles to failure was true, then Beams 2 and 3 would be expected to fail between 2,000,000 and 9,000,000 cycles, while Beams 4 and 5 would be expected to fail between 200,000 and 1,000,000 cycles. A comparison of expected results and test results is summarized in Table 5-2.

Table 5-2 Comparison of Test Results with Expected Results

Beam	Stress Index	Calculated Bottom Fiber Tensile Stress	Calculated Stress Range (ksi)	No. of Cycles to First Wire Failure	Expected Fatigue Life (Cycles)
2	$7.5\sqrt{f_c'}$	$5.5\sqrt{f_c'}$	21.7	5,293,703	2,000,000—9,000,000
3	$7.5\sqrt{f_c'}$	$8.2\sqrt{f_c'}$	23.3	2,424,121	2,000,000—9,000,000
4	$12\sqrt{f_c'}$	$11.6\sqrt{f_c'}$	43.2	519,799	200,000—1,000,000
5	$12\sqrt{f_c'}$	$11.1\sqrt{f_c'}$	42.0	318,958	200,000—1,000,000

Although it is clear that the test results were well within the range of the expected results, with such wide ranges of expected fatigue life, it is difficult to determine how well the test results compared with the data from previous tests. Figure 5-2 provides a much clearer comparison. In this figure the results from the four beam tests are plotted with the results of all available tests from the literature

123

reviewed, as well as the strand fatigue data compiled by Paulson, et al. (1983). From this figure, it is obvious that the beam fatigue test results compare very well with the previous results and fall well within the expected ranges of fatigue life.

From these results shown in Figure 5-2, it is apparent that the fatigue life of the prototype bridge would be expected to be less than 2,000,000 cycles if the applied loading corresponds to an index stress of $12\sqrt{f_c'}$. The mean life for this level of loading is approximately 500,000 cycles, which is below any normally expected design life. Therefore, the data considered in this thesis indicate that using a stress index of $12\sqrt{f_c'}$ for evaluation or design of prestressed concrete bridges would be unconservative. However, it is important to note that the calculations used to determine the stress index were based on measured material properties of the prototype bridge and test specimens, which are considerably higher than the originally specified material strengths.
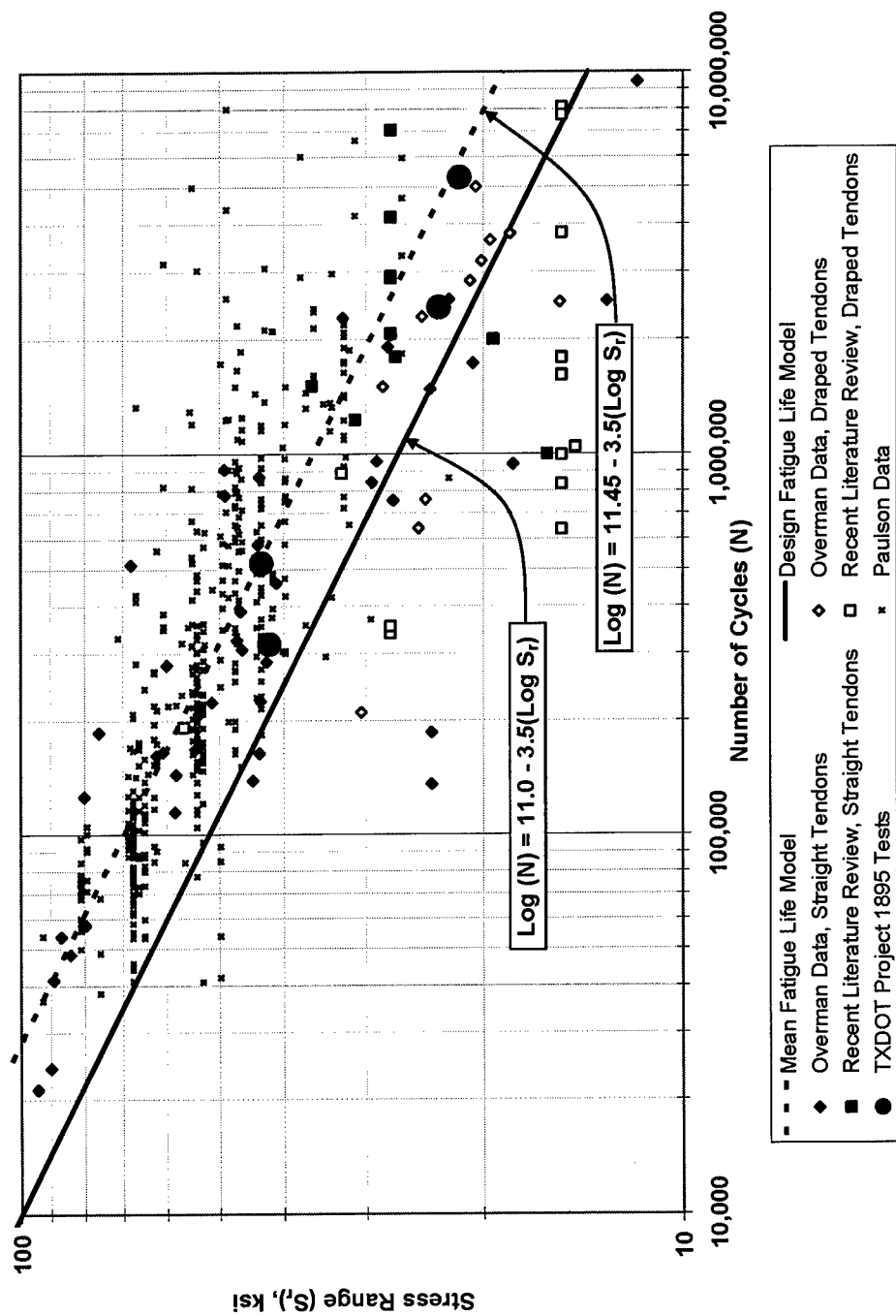
Figure 5-2 Comparison of All Available Beam Fatigue Data

125

CHAPTER 6

Conclusions and Recommendations

6.1 CONCLUSIONS

The results of the seven-wire strand and pretensioned concrete beam tests presented in this thesis cannot be used to disprove the fatigue models developed in previous investigations (Paulson, et al., 1983). The test results further support the theory that the fatigue life of a pretensioned concrete beam with straight single-strand tendons is primarily related to the stress range experienced by the strands.

The published literature does not include a single case of a strand fatigue failure in an uncracked prestressed concrete beam. It is not considered possible to design a prestressed concrete beam such that the stress range in the strand is sufficiently large to cause a fatigue failure without cracking the concrete first. With this in mind, it is rational to specify that the fatigue capacity of a pretensioned concrete beam is satisfactory if the extreme concrete tensile stress is limited such that no cracking can occur. Because the mean fatigue strength of concrete in compression, tension, and bending can be taken as 55 percent of the nominal strength values, the extreme fiber concrete tensile stress should be less than 55 percent of the modulus of rupture. For normal weight concrete subject to bending stresses, this would be 55 percent of $7.5\sqrt{f_c'}$, or $4.1\sqrt{f_c'}$. Because the 55 percent limit represents a mean value, it would then be conservative to keep the bottom fiber tensile stress less than $3\sqrt{f_c'}$ in order to ensure that the concrete did not crack when subjected to cyclic loads.

Once a beam section has cracked, there is no proven correlation between fatigue life of the strand and bottom fiber concrete stress calculated using an uncracked section analysis. Rather, the strand stress range should be calculated using cracked-section analyses that are easily programmed using spreadsheets or by using commercially available section analysis software.

The fatigue provisions of the AASHTO LRFD Bridge Specifications (2003) appear to be well founded. In this document, any beam with a calculated extreme fiber concrete tensile stress that exceeds $3\sqrt{f_c'}$ must be evaluated in greater detail and the stress range in the strand must be determined. For prestressing strand with a radius of curvature greater than 30 ft, the allowable stress range is 18.0 ksi. Based on the mean fatigue life model (Paulson et al., 1983) a stress range of 18.0 ksi corresponds to an expected fatigue life of over 11,000,000 cycles. Based on the design fatigue life model, this stress range corresponds to a design fatigue life of over 4,000,000 cycles.

Therefore, it is recommended that the fatigue criteria used to evaluate existing prestressed concrete girder bridges not be based on extreme fiber concrete tensile stresses. An approach similar to that in the AASHTO LRFD Bridge Specifications (2003) should be adopted.

6.2 RECOMMENDATIONS FOR FURTHER RESEARCH

Although a significant amount of research has been conducted to investigate the reduction of fatigue life due to metal-on-metal fretting (such as draped strands in prestressed beams or deviators in post-tensioned beams), the mechanisms within the concrete that influence the fatigue life of the strand have not been studied in detail. For a high percentage of the fatigue tests of pretensioned concrete beams with straight strands, the data appear to be well correlated with the data from in-air fatigue of strands. However, some beams

127

experienced significantly shorter fatigue lives than would be predicted using the fatigue models for strand in air (Paulson et al. 1983). It is likely that the interaction between the concrete and the strand is different than that of air and strand. This difference may be related to the friction between the concrete and the strand in the vicinity of the cracks where the strand debonds from the concrete.

In conducting the post-mortem investigations of the test beams, surface oxidation was found on the strands in the vicinity of cracks in the concrete. While temperature and humidity are not controlled in the Ferguson Structural Engineering Laboratory and the average relative humidity is around 70 percent, it seems unlikely that enough air could have circulated into the beams to cause the amount of corrosion observed. It is more likely that the oxidation was caused by fretting corrosion, indicating that the concrete can also cause fretting of the prestressing strand.

During the course of the beam testing for this project several aspects of the beam behavior appeared to depend on the response of the strand. Although an exhaustive search was done, no information was found in the literature to relate strain in the transverse direction to longitudinal strain for prestressing strand. Given the helical configuration of seven-wire strand, it was not assumed that the Poisson's ratio for Grade 270 steel would be applicable. Testing of seven-wire strand should be conducted to derive an empirical relationship between longitudinal and lateral strain in prestressing strand under uniaxial loading. This information will be useful for understanding the observed behavior of the strain gages attached to the surface of the concrete in the vicinity of a crack and to evaluate condition of the prestressing strands within a beam.

APPENDIX A

Test Data from Literature Review

This appendix provides fatigue data (stress range and number of cycles to failure) from reports reviewed for this paper. Data already listed by Paulson et al. (1983) and Overman (1984) are not listed.

Section A.1 presents prestressing strand fatigue data collected by VSL Corporation (1992) and provided to the University of Texas at Austin, Ferguson Structural Engineering Laboratory. Section A.2 presents pretensioned, prestressed beam fatigue testing data taken from two papers (Muller and Dux 1994, and Harajli and Naaman 1985).

A.1 PRESTRESSING STRAND IN-AIR FATIGUE TEST DATA

This section provides data collected and provided by VSL Corporation (1992). The data are presented from eight series of tests and only those results for which the wire fractured along the free length are reported.

Table A-1 Strand Fatigue Test Data Received from VSL Corporation (1992)

TEST SERIES 1		
STRAND #	RANGE (KSI)	NUMBER OF CYCLES
2	55.3	379980
6	55.3	275220
7	55.3	328680
8	55.3	316800
10	55.3	245520

129

12	55.3	322740
13	55.3	277200
14	55.3	495000
15	55.3	362340
16	55.3	312840
17	55.3	340560
18	55.3	563832

TEST SERIES 2

SAMPLE #	RANGE (KSI)	NUMBER OF CYCLES
13	55.3	87120
21	55.3	127800
23	55.3	132660
24	55.3	144540
26	55.3	83160
27	55.3	178200
29	55.3	164340
31	55.3	193040
32	55.3	213660
33	55.3	172260
34	55.3	192060
35	55.3	126720
36	55.3	150480
37	55.3	142560
38	55.3	152460
39	55.3	172260
40	55.3	154800
41	55.3	120780
42	55.3	128700
47	55.3	136620
49	55.3	106920
51	55.3	161676
52	55.3	148500
54	55.3	129024

55	55.3	142560
56	55.3	112860
57	55.3	132660
58	55.3	148500
59	55.3	120780
60	55.3	180180
61	55.3	112860
62	55.3	144540
63	55.3	112860
64	55.3	130680
66	55.3	152460
67	55.3	140580
68	55.3	124240
69	55.3	112860
72	55.3	124740
73	55.3	154440
74	55.3	126720
75	55.3	120780
76	55.3	156420
77	55.3	142560
79	55.3	114840
81	55.3	160380
82	55.3	132660
83	55.3	164340
84	55.3	104940
86	55.3	138600
88	55.3	122760
89	55.3	112860
90	55.3	128700
91	55.3	110880
92	55.3	154440
93	55.3	160380
94	55.3	152460
95	55.3	158400
96	55.3	120780
97	55.3	128700
101	55.3	114840
102	55.3	134640

103	55.3	158400
104	55.3	100880
105	55.3	106920
106	55.3	122760
107	55.3	134640
109	55.3	132660
110	55.3	122760
112	55.3	94860
113	55.3	120960
114	55.3	128700
116	55.3	69300
117	55.3	126252
119	55.3	123372
120	55.3	104940
121	55.3	142524
122	55.3	140580
123	55.3	138600
125	55.3	132660
127	55.3	160380
128	55.3	136620
139	55.3	126720
142	55.3	59400
165	55.3	90800
174	55.3	88200
189	55.3	96200
208	55.3	90000
210	55.3	79560
211	55.3	109800
212	55.3	99360
213	55.3	100800
214	55.3	86400
215	55.3	90000
218	55.3	75600
219	55.3	127800
220	55.3	151200
221	55.3	185400
222	55.3	138600
223	55.3	129600

224	55.3	194400
226	55.3	216000
227	55.3	187200
228	55.3	154800
229	55.3	136800
230	55.3	142200
231	55.3	172800
232	55.3	140400
233	55.3	192600
234	55.3	244800
235	55.3	280800
236	55.3	106200
237	55.3	111600
238	55.3	138600
239	55.3	115200
240	55.3	127800
241	55.3	122400
242	55.3	124200
243	55.3	120600
244	55.3	140400
245	55.3	131400
246	55.1	263000
247	55.1	282000
248	55.1	225000
250	55.1	438000
252	55.1	158000
253	55.1	212000
256	55.1	321000

TEST SERIES 3

SAMPLE #	RANGE (KSI)	NUMBER OF CYCLES
4	56.91	320000
7	55.49	1293000
8	54.07	303000
9	52.64	625000

133

10	51.22	443000
11	49.8	612000
12	46.95	1095000
17	45.53	225000
19	39.84	742000
21	38.41	311000
25	71.14	330000
27	68.29	170000
28	64.02	145000
30	59.76	219000
32	56.91	234000
33	52.64	317000
34	46.95	644000
35	44.11	1439000
39	48.37	380000
41	39.84	548000

TEST SERIES 4

SAMPLE #	RANGE (KSI)	NUMBER OF CYCLES
2	47.5	510000
3	47.5	315000
4	47.5	295000
7	47.5	343400
8	55	592000
9	55	1627300
10	55	1625000
11	50.6	7082000

TEST SERIES 5

SAMPLE #	RANGE (KSI)	NUMBER OF CYCLES
1	42.87	294000
2	42.87	150000

134

TEST SERIES 6		
SAMPLE #	RANGE (KSI)	NUMBER OF CYCLES
8	52.12	619400
16	52.12	352000
19	52.12	514200
59	52.12	624000
67	52.12	611600
69	52.12	453200
87	52.12	805200
91	52.12	696700
103	52.12	1036000

TEST SERIES 7		
SAMPLE #	RANGE (KSI)	NUMBER OF CYCLES
2	52.12	75600
20	52.12	59400
27	52.12	79560
28	52.12	99360
29	52.12	90000
30	52.12	90000
31	52.12	86400
55	52.12	88200
65	52.12	90800
84	52.12	838800
85	52.12	304200
87	52.12	365400
88	52.12	473400
89	52.12	354600
90	52.12	387000
91	52.12	396000

92	52.12	378000
93	52.12	327000
94	52.12	75600
95	52.12	142200
96	52.12	165600
103	52.12	441540
104	52.12	158380
105	52.12	396000
108	52.12	215920
110	52.12	199800
111	51.81	182850
114	51.81	79560
115	51.81	99360
116	51.81	90000
117	51.81	90000
	51.81	86400

TEST SERIES 8

SAMPLE #	RANGE (KSI)	NUMBER OF CYCLES
1	50.9	75600
2	50.9	142200
3	50.9	165600

A.2 PRESTRESSED CONCRETE BEAM FATIGUE TEST DATA

This section provides data from pretensioned prestressed concrete beam fatigue tests found in the literature. Table A-2 contains data from tests conducted by Muller and Dux (1994). Only data from tests with constant-amplitude loading histories are presented from their work. Table A-3 contains data from tests conducted by Harajli and Naaman (1985). Only data from fully-prestressed beams are presented from their work.

136

Table A-2 Beam Fatigue Test Data from Muller and Dux (1994)

Specimen	Strand Stress Range (ksi)	Number of Cycles	Strand Configuration
PS2	27.6	7,058,000	Straight
PS3	27.6	2,069,000	Straight
PS4	27.6	4,173,000	Straight
VP2	36.3	1,510,000	Straight
VP3	27.6	2,926,000	Straight
VP4	27.6	2,890,000	Straight
PT2	31.2	1,230,000	Straight
HD516-3	27.6	339,000	Draped
HD516-4	27.6	354,000	Draped
HD516-5	14.5	1,043,000	Draped
HD1025-1	32.6	890,000	Draped
HD1025-2	56.6	192,000	Draped
HD525-1	15.2	8,100,000	Draped
HD525-2	15.2	7,740,000	Draped
HD550-1	15.2	995,000	Draped
HD550-2	15.2	3,800,000	Draped
HD51400-1	15.2	835,000	Draped
HD51400-2	15.2	635,000	Draped
HD5B-1	15.2	1,610,000	Draped
HD5B-2	15.2	1,790,000	Draped

Table A-3 Beam Fatigue Test Data from Harajli and Naaman (1985)

Specimen	Strand Stress Range (ksi)	Number of Cycles	Strand Configuration
PD1	16.0	1,000,000	Straight
PD2	19.3	2,000,000	Straight
PD3	27.1	1,800,000	Straight

137

APPENDIX B

Strand Test Grip Details

B.1 BRIEF OVERVIEW

In reviewing results from strand fatigue tests performed by various researchers, it becomes evident that failure of the strand is often initiated at the grips, and the results of tests that fail in this manner are not representative of the response of strand in prestressed concrete members. A threaded aluminum block grip has been used with some success at the Ferguson Structural Engineering Laboratory to reduce the likelihood of grip failures, and was initially used for the tests described in this thesis. Unfortunately, all of the strands tested using these grips failed in fatigue at the initial contact between the grip and the strand.

An alternative grip was eventually developed. Lamb and Frank (1985) reported that in their strand tests, "None of the tests performed with the pre-deformed copper wedges produced failures within the anchorage region." With this in mind, copper wire was positioned between the wires of the strand and the inside surfaces of the aluminum block grips were machined smooth. With this grip design, successful fatigue tests were conducted with wire breaks located along the free length of the strand. The design has some distinct advantages over other methods. It is relatively inexpensive, because the aluminum block can be used repeatedly; only the copper wire needs to be replaced. It is also reasonably quick to set up, especially compared with systems where epoxies or other substances must be hardened around the strand.

This smooth aluminum block grip is described in detail in Section B.2. The threaded aluminum block grip, though unsuccessful in these tests, will be described in Section B.3, as a basis for comparison.

B.2 SMOOTH ALUMINUM BLOCK GRIP

B.2.1 Grip Description and Geometric Properties

The final version of the smooth aluminum block grip with the integral copper wire wrapped between the wires of the prestressing strand is shown in Figure B-1. Also shown are the ¼-in. diameter pegs used to align the two sides of each grip. The pegs were cut from ¼-in. diameter steel bolts. It is important that their length is less than the combined thickness of the two halves of the grip, so that the test machine head squeezes down on the aluminum grip unimpeded by the steel pegs. The pegs shown were approximately 1 ¾-in. long.
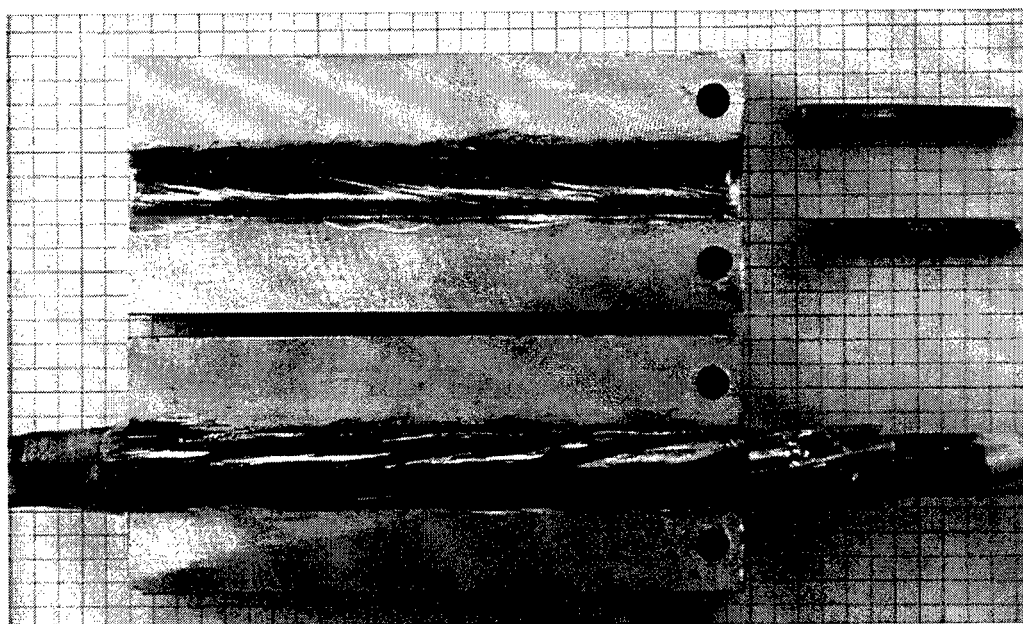

Figure B-1   Successful Smooth Aluminum Block Grip

139

The copper wire wrapped on the prestressing strand must be large enough to completely fill the interstitial region between the wires and the aluminum grip when the grip is squeezed in the machine head. For the ½-in. diameter, low relaxation strand used, 10–gage, single-strand copper wire was found to work successfully. Figure B-2 displays the 10-gage copper wire wrapped onto the end of a test specimen just prior to installation in the aluminum block grip. As shown in Figure B-3, this gage of wire appeared too large when initially installed, but produced satisfactory results. Smaller gage copper wire was used initially, but fatigue failures still occurred within the grips. Ordinary cellophane tape was used to hold the copper wires in place during installation. The 10-gage copper wire pieces were preformed by twisting each along the strand before all six were positioned on the strand.
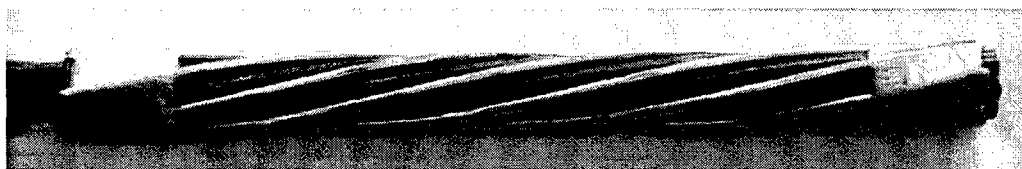

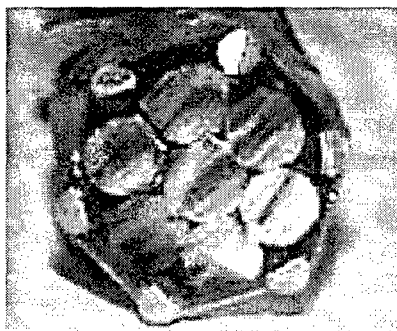*Figure B-2 Copper Wire Wrap, Ready for Installation*

Figure B-3 Copper Wire End View

The hydraulic gripping pressure of the testing machine is critical. The pressure must be set just high enough to prevent slipping. For the machine used, a hydraulic gripping pressure between 1800 and 2000 psi was found to be

140

successful. If the pressure is too high, the soft copper will be crushed to such an extent that the aluminum will be in contact with the steel. When the harder aluminum is pressed against the steel wires of the strand, it creates significant stress raisers in the contact region which induce premature fatigue failures.

Figures B-4 and B-5 show an end view and a top view of the grip drawn with dimensions. The outside dimensions of the block are not critical. As seen in Figure B-4, there must be some clearance between the center of the circle and the inner face of the grip, in this case 0.015 in. was used. This gap ensures that the interior faces of the two grip halves do not come into contact, which would cause the pressure to be transferred directly from one grip into the other.

The taper on the left end of the grip shown in Figure B-5 was formed in an attempt to provide a stress transition region into the grip. This transition region is intended to reduce the stress raisers in this region by developing full pressure over a finite length, rather than immediately at a point. It should be noted, however, that the use of this sort of transition taper did not improve the performance of the threaded grips. No smooth grip was ever attempted without the transition taper, so it is not known whether this is critical.
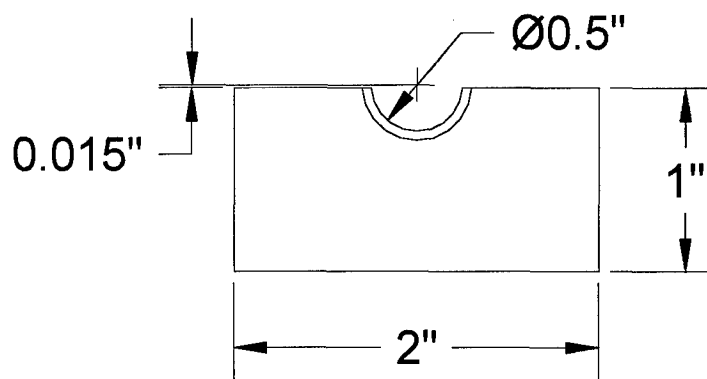

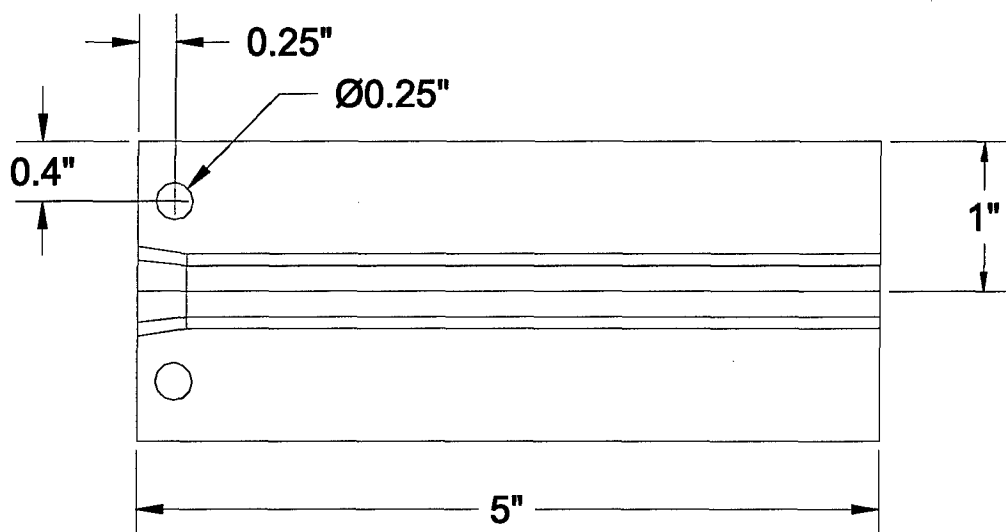*Figure B-4 End View with Dimensions*

141

Figure B-5 Top View with Dimensions

B.2.2 Important Points on Grip Production

This section is not intended to provide specific instructions on machining, because machining methods depend on the type of machine used and the skills of the machinist. Rather, the section is intended to provide helpful ideas and suggestions.

This smooth grip can be made from 1-in. by 2-in. aluminum stock. Lengths should be cut slightly longer than desired, to allow for machining to desired length. The faces of the grip should be machined to ensure the faces are parallel. This is especially true of the faces which are parallel with the strand along the length of the grip. The key consideration is that the circular groove must be parallel to the exterior faces of the grip to prevent accidental bending stresses in the strand during an intended straight tension test.

142

The term "smooth grip" refers to the surface of the circular groove into which the strand is inserted. By using a smooth surface, the groove can be cut into the face using a ½-in. diameter circular tipped cutting tool. The advantage is that a short cutting tool will provide a very accurate cut, ensuring that the groove is indeed parallel with the external faces. With the threaded grip, a hole must be drilled using a long drill bit. There is no way to ensure that the drill bit does not wobble, which can introduce imperfections in the parallel geometry.

The gap that is left between the two halves of the grip is provided by cutting the circular groove to the proper depth. Using the dimensions shown in Figure B-4, the circular tipped cutting tool was set to cut 0.235 in. below the top surface of the aluminum block, keeping the center of the hole 0.015 in. outside of the block as shown. This provides a theoretical 0.03 in. gap between the two halves of the grip when placed into the machine. The actual gap width varies depending on the gage of the copper wire used and the hydraulic pressure of the gripping heads. Figure B-6 displays the gap in a grip mounted into the load frame.

Figure B-6 Grip Loaded into Load Frame

The ¼-in. diameter alignment peg holes are drilled by machine in both halves of the grip simultaneously (with the halves held together) to ensure alignment of the holes. Prior to loading the aluminum grips into the load frame, the pegs will hold the two sides of the aluminum grips together better if slight imperfections are introduced into the pegs. This can be done by bending them very slightly. Insertion is then made more difficult, but is still easy with a hammer. The pins can also be easily removed with the use of a slender punch and a hammer. Bolts could be used, but this would require that the ends of the aluminum blocks are left out of the load frame's grip head jaws, which effectively decreases the grip's surface area on the strand.

The tapered transition region would best be made with a conical cutting tool, which was not available on this project. Consequently, a skilled technician formed the taper by hand using a round file.

144

B.3 THREADED ALUMINUM BLOCK GRIP

B.3.1 Grip Description and Geometric Properties

The smooth grip evolved from the threaded grip. As such, the block exterior dimensions and the placement and size of the alignment peg holes are identical to those shown in Figures B-4 and B-5. The difference is that the circular groove is threaded and no copper was used, as shown in Figure B-7. The threading was standard course thread cut using a ½-in. tap with a 13 thread per inch pitch.
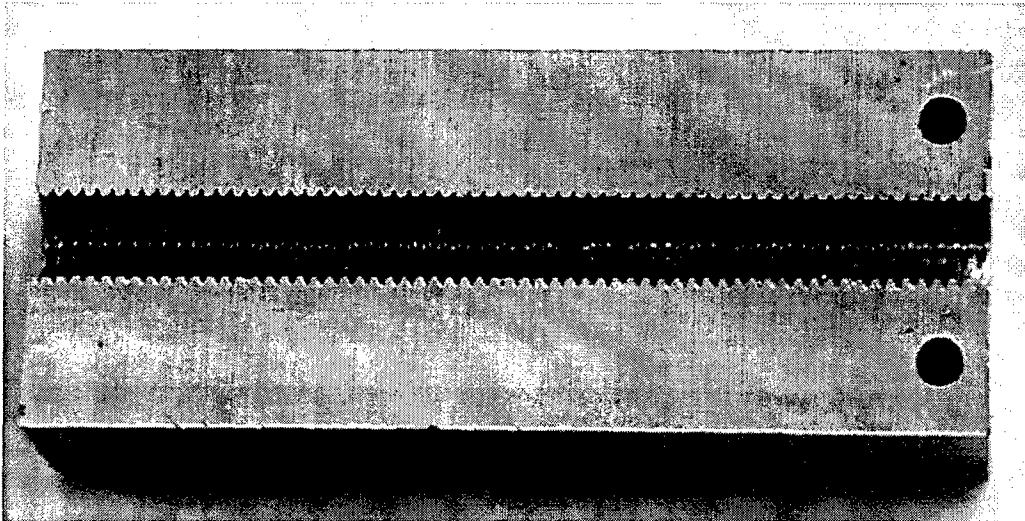

Figure B-7 Interior Face of an Unused Threaded Grip

The purpose of the threading was to increase the surface area in contact with the prestressing strand. As can be seen in Figure B-8, the wires of the prestressing strand were pressed into the threads, enabling some additional contact further around the circumference of the individual wires. All of the tests using this grip had failures at the first point of contact between the grip and the strand. A transition taper was tried to lessen the stress concentration at the face of the grip, but the strand still failed at the point of first contact between the strand

145

and the grip. The grip shown in Figure B-8 is an example of a grip with a tapered entry.
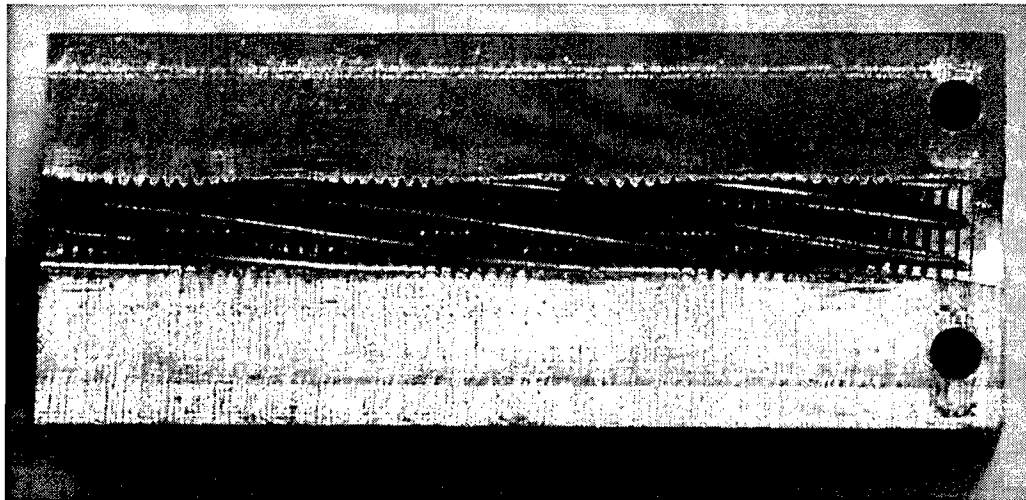

Figure B-8 Used Threaded Grip with Tapered Entry

Aside from the fact that no successful fatigue tests were run with this grip, its other major disadvantage is that the each pair of grips can only be used to test one strand. Multiple tests could be run but at the risk of misaligning the wires with the impressions left in the threads by the wires of previous strands. This would cause a reduction in the contact surface area between the grip and the strand.

It should be noted that the threaded grip did have limited success in testing 0.6-in. diameter strand during fatigue tests performed in the same machine just prior to this project's tests. Of the twelve 0.6-in. specimens tested, three failed in the grips (Eggers, 2003). The grips were of similar design, but used a 5/8-in. course threaded tap with an 11 thread per inch pitch.

B.3.2 Important Points on Grip Production

For the threaded grip, 2-in. by 2-in. aluminum stock was used. The stock was cut into 5-in. lengths. The ends were then machined to be square with the

146

sides of the blocks. Then a hole was drilled down the center of the block on its longitudinal axis. The hole was drilled with a 27/64-in. drill bit, which is the prescribed hole size for the tap used. The threads were then tapped into the hole using a course threaded ½-in. tap with a 13 thread per inch pitch.

The alignment peg holes were drilled into the sides of the blocks. The grip was then placed in a saw and cut down the center of the block, along the longitudinal axis of the grip. The size of the gap left between the two halves of this type of grip depends upon the thickness of the saw blade.

APPENDIX C

Extensometer Details

C.1 BACKGROUND

The overall goal of the strand testing was to ensure that the strand that was used to construct the beam specimens satisfied all provisions of ASTM A 416. While a specific requirement for modulus of elasticity is not explicitly stated therein, the modulus of elasticity was important in calculating expected stresses in the beams.

An "apparent" modulus of elasticity can be obtained by dividing change in load by the change in average strain along the local axis of the strand wires. The strain measured by the strain gages is less than the average strain along the longitudinal axis of the strand, so apparent modulus is higher than the strand modulus. To get an accurate measurement of the strand modulus of elasticity, an extensometer should be used.

No extensometers were available at Ferguson Structural Engineering Laboratory, so an extensometer was designed and constructed as part of this project. Small variations in the value of the modulus of elasticity have minimal effect on beam stress calculations, so the extensometer was not classified using the provisions in ASTM Practice E 83. However, the details of the extensometer are included here should the reader desire to verify its classification.

C.2 OVERALL DESCRIPTION

As can be seen in Figure C-1, the extensometer consists of 3 aluminum blocks, two steel rods, and two linear variable differential transformers (LVDTs).

148

For simplicity, the aluminum blocks will be identified by location: top, middle, or bottom.
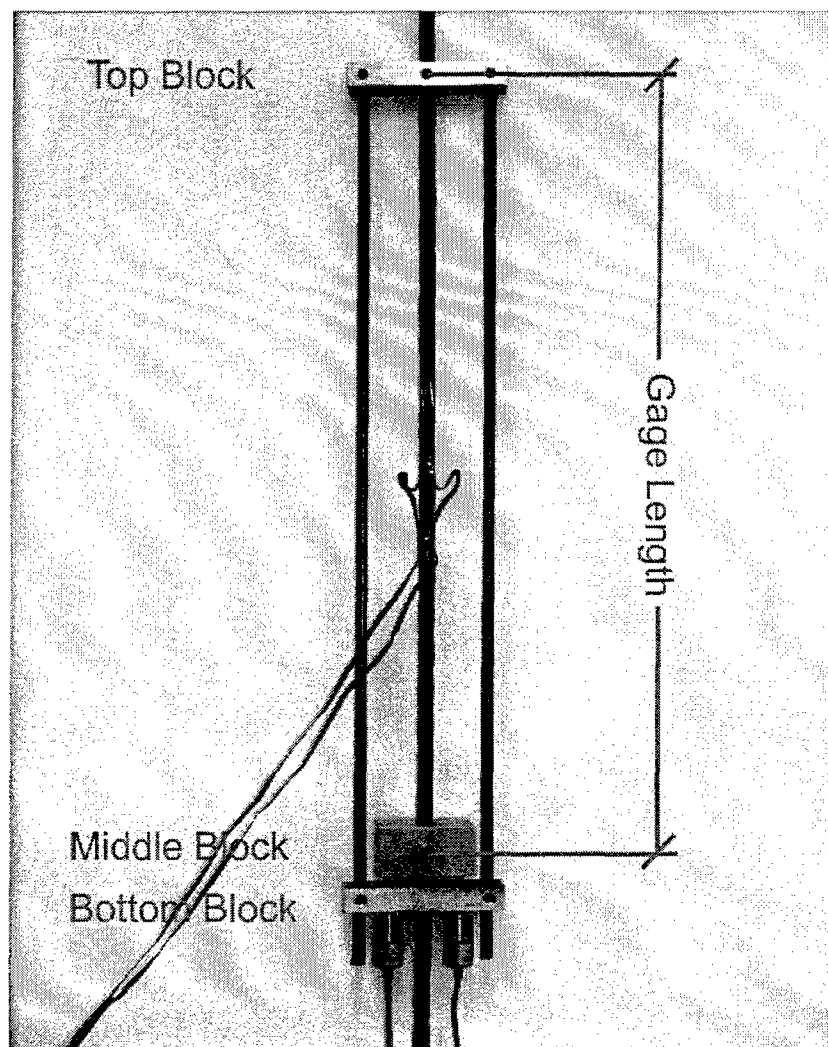

Figure C-1 Full View of Extensometer

The middle vertical member shown in Figure C-1 is the prestressing strand. The extensometer is used to measure the longitudinal displacement of the strand over the gage length. The gage length is the distance between the setscrews in the top and middle blocks. The distance between the top and bottom

149

blocks is held constant by the two, round steel rods. As can more easily be seen in Figure C-2, the bottom block holds the two LVDTs.

When tension is applied to the strand, the middle block moves relative to the top and bottom blocks, and the LVDTs record the relative movement between the middle and bottom blocks. In order to minimize errors introduced by accidental bending of the strand or rotation of the blocks, two transformers (equidistant from the strand) are used and their measurements are averaged.
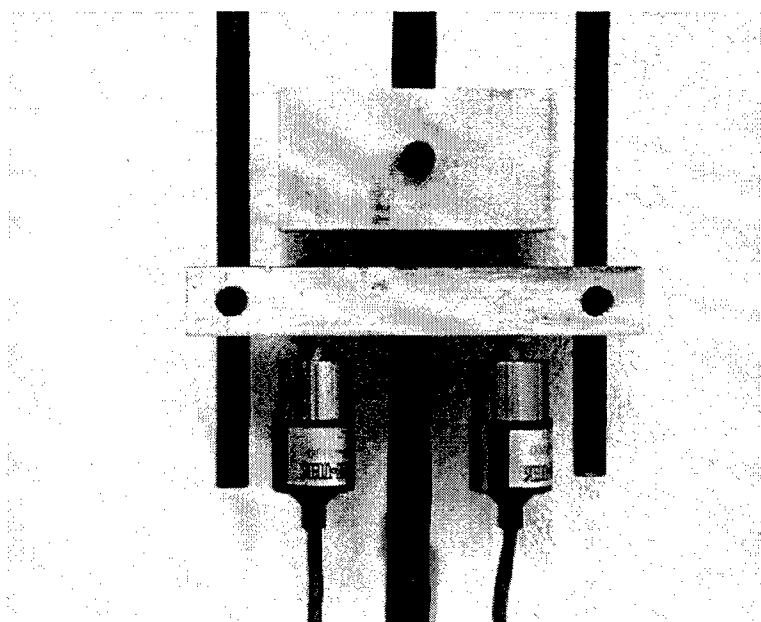

Figure C-2 Closer View of Bottom Blocks and Displacement Transformers

There are two extensometer requirements in ASTM A 370 and A 416. One is for measuring the 1% elongation for determining yield strength, the other is for measuring total elongation at rupture. The requirements for the yield strength elongation should be more applicable to the modulus of elasticity tests, since elastic deformations are measured in both cases. Because no specific gage length was required for this test, the 24-in. gage length required in the total elongation test was used.

150

The accuracy of the extensometer is dependent on the LVDTs. For this test, TRANS-TEK Series 350 General Purpose DC Gaging LVDTs, model number 0350-0000 were used. They had a working range of ±0.050 in and an overall mechanical travel of 0.16 in. They had a non-linearity rated at less than 0.50% full scale over the total working range. The maximum tip force for a single gage is 57 grams. This tip force is the force that the steel rods, the aluminum blocks and setscrews must overcome, and is obviously insignificant with regard to extensometer deformation.

The overall concept of the extensometer is not complicated. The most difficult part of making the extensometer was machining the aluminum blocks. While there are certainly an infinite number of different possible dimensions, the dimensions are shown in the following section for reference. A convenient feature of this extensometer is that it has an adjustable gage length. If a longer gage length is needed, then longer 3/8-in. steel rods can be used. The gage length is only limited by the useful stroke length of the LVDTs. If too short of a gage length is used, the accuracy obviously decreases. The ideal gage length is one that uses nearly the full stroke length of the LVDTs during the test.

C.3 ALUMINUM BLOCK DIMENSIONS

C.3.1 Top Aluminum Block Dimensions

The top aluminum block has a hole for the strand to pass through, two holes for the steel rods, and three threaded setscrew holes. Since the top block grips the strand, the hole for the strand is machined as closely as possible to the size of the outside diameter of the strand in order to minimize rotational movement. Figures C-3 and C-4 show the top and front views of the top block.
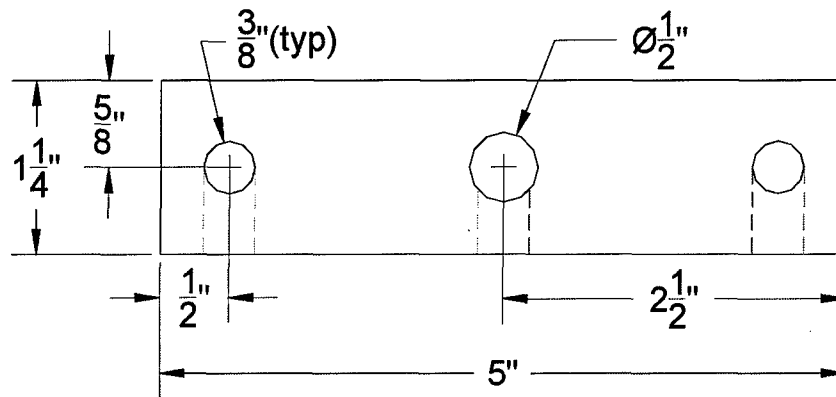
151

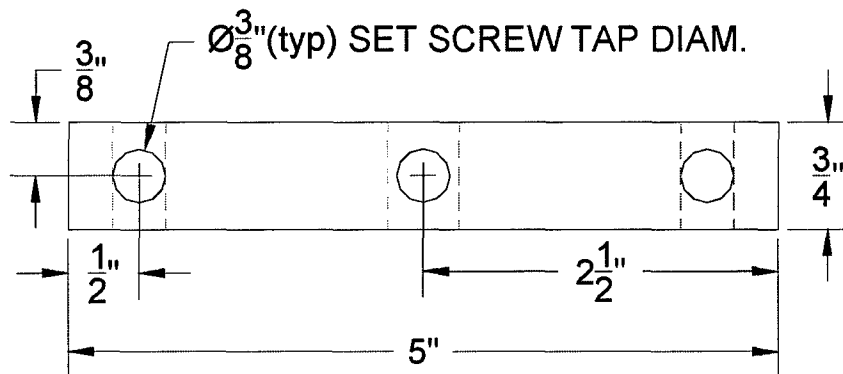*Figure C-3 Top View of Top Aluminum Block*

Figure C-4 Front View of Top Aluminum Block

C.3.2 Middle Aluminum Block Dimensions

The middle aluminum block has a hole for the strand to pass through and one threaded setscrew hole. In order to minimize rotational movement, the hole for the strand is machined as closely as possible to the size of the outside diameter of the strand. Additionally, because it does not have the stabilizing support of the steel rods, the block was made thicker than the top and bottom blocks. Figures C-5 and C-6 show the top and front views of the middle block.
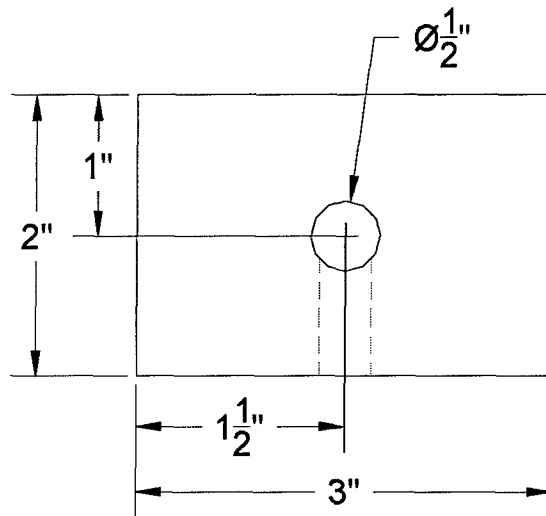
152

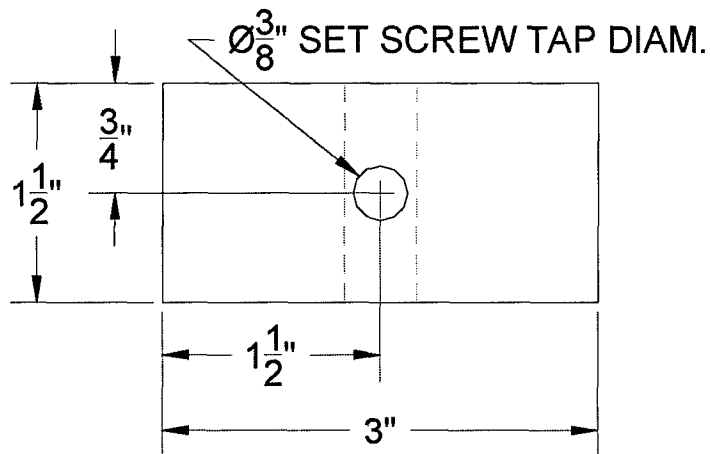*Figure C-5 Top View of Middle Aluminum Block*

Figure C-6 Font View of Middle Aluminum Block

C.3.3 Bottom Aluminum Block Dimensions

The top aluminum block has a hole for the strand to pass through, two holes for the steel rods, two holes for the LVDTs and two threaded setscrew holes. Since the bottom block does not grip the strand, the hole for the strand is

153

machined slightly larger than the strand to allow free movement of the strand through the block. The holes for the LVDTs required countersinking because of the available thread length on the transducers. The LVDTs used have lock nuts for positioning. Figures C-7 and C-8 show the top and front views of the bottom block.
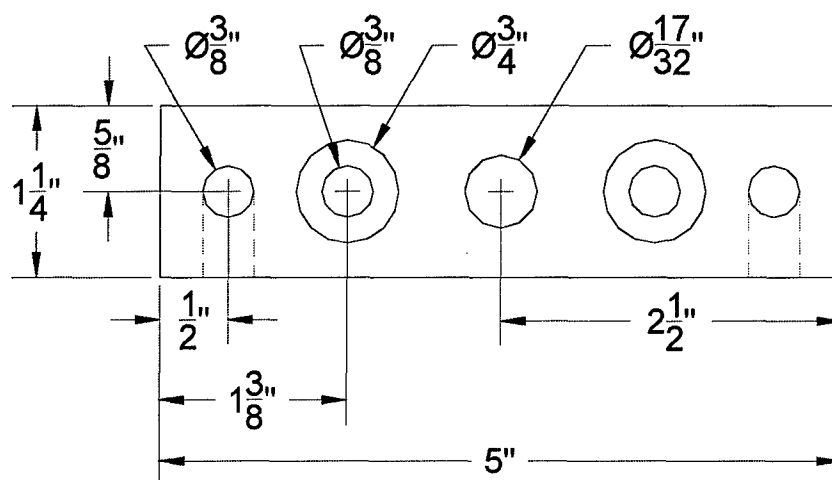

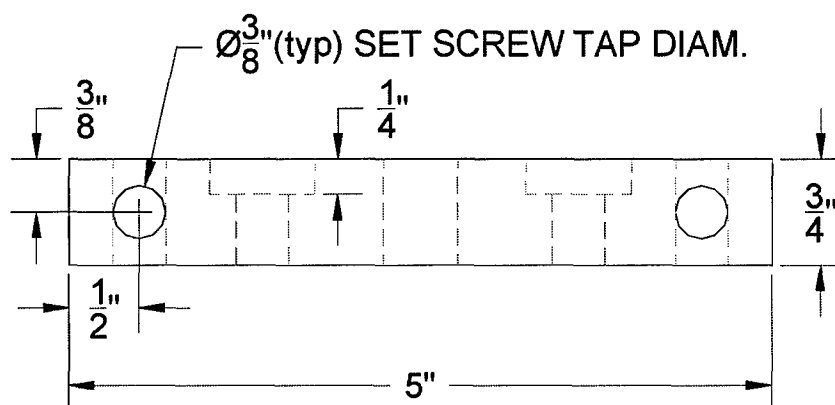*Figure C-7 Top View of Bottom Aluminum Block*

Figure C-8 Front View of Bottom Aluminum Block

References

AASHTO LRFD Bridge Design Specifications (2003). American Association of State Highway and Transportation Officials, Washington, D.C.

AASHTO Standard Specifications for Highway Bridges (2002). American Association of State Highway and Transportation Officials, Washington, D.C.

ACI Committee 215 (1997). "Considerations for Design of Concrete Structures Subjected to Fatigue Loading." ACI Manual of Concrete Practice.

ASTM A 370 (2002). "Standard Test Methods and Definitions for Mechanical Testing of Steel Products." American Society for Testing and Materials, West Conshohocken, PA.

ASTM A 416 (1999). "Standard Specification for Steel Strand, Uncoated Seven-Wire for Prestressed Concrete." American Society for Testing and Materials, West Conshohocken, PA.

ASTM A 931 (2002). "Standard Test Method for Tension Testing of Wire Ropes and Strand." American Society for Testing and Materials, West Conshohocken, PA.

ASTM C 39/C 39M (2001). "Standard Test Method for Compressive Strength of Cylinder Concrete Specimens." American Society for Testing and Materials, West Conshohocken, PA.

ASTM C 469 (2002). "Standard Test Method for Static Modulus of Elasticity and Poisson's Ratio of Concrete in Compression." American Society for Testing and Materials, West Conshohocken, PA.

ASTM Practice E 83 (2003). "Standard Practice for Verification and Classification of Extensometer System." American Society for Testing and Materials, West Conshohocken, PA.

Bílý, M. (1993). Cyclic Deformation and Fatigue of Metals. Elsevier Science Publishers, Amsterdam, The Netherlands.

Brooks, C.R., and Choudhury, A. (2002). Failure Analysis of Engineering Materials. The McGraw-Hill Company, Inc., New York, NY.

Collins, M.P. and Mitchell, D. (1997). Prestressed Concrete Structures. Response Publications, Toronto, Canada.

Eggers, J.C. (2003). "Cable Stay Fatigue Analysis for the Fred Hartman Bridge." M.S. Thesis, Department of Civil Engineering, The University of Texas at Austin.

Hagenberger, M.J. (2003). "Determining the Appropriate Concrete Tensile Stress Limit for Load Rating Prestressed Concrete Bridges." PhD Dissertation to be submitted, Department of Civil Engineering, The University of Texas at Austin.

Harajli, M.H., and Naaman, A.E. (1985). "Static and Fatigue Tests on Partially Prestressed Beams." Journal of Structural Engineering, Vol. 111, No. 7, July, 1985, pp. 1602-1618.

Klesnil, M. and Lukáš, P. (1992). Fatigue of Metallic Materials, 2nd Edition. Elsevier Science Publishing Company, Inc., New York, NY.

Lamb, J., and Frank, K. (1985). "Development of a Simple Fatigue Resistant Stay Cable Anchorage." Research Report 384-1F, Center for Transportation Research, Bureau of Engineering Research, The University of Texas at Austin, Austin, TX, November, 1985.

Muller, J.F., and Dux, P.F. (1994). "Fatigue of Prestressed Concrete Beams with Inclined Strands." Journal of Structural Engineering, Vol. 120, No. 4, April, 1994, pp. 1122-1139.

Naaman, A.E., and Founas, M. (1991). "Partially Prestressed Beams under Random-Amplitude Fatigue Loading." Journal of Structural Engineering, Vol. 117, No. 12, December, 1991, pp. 3742-3761.

Overman, T.R. (1984). "Flexural Fatigue Behavior of Pretensioned Concrete Girders." M.S. Thesis, Department of Civil Engineering, The University of Texas at Austin.

Paulson, C., Frank, K., and Breen, J. (1983). "A Fatigue Study of Prestressing Strand." Research Report 300-1, Center for Transportation Research, Bureau of Engineering Research, The University of Texas at Austin, Austin, TX, April, 1983.

PCI (1992). PCI Design Handbook, Precast and Prestressed Concrete, 4th Edition. Precast/Prestressed Concrete Institute, U.S.A.

Polák, J. (1991). Cyclic Plasticity and Low Cycle Fatigue Life of Metals. Elsevier Science Publishing Company, Inc., New York, NY.

Rao, C., and Frantz, G.C. (1996). "Fatigue Tests of 27-Year-Old Prestressed Concrete Bridge Box Beams." PCI Journal, Vol. 41, No. 5, September-October, 1996, pp. 74-83.

Roller, J.J., Russell, H.G., Bruce, R.N., and Martin, B.T. (1995). "Long-Term Performance of Prestressed, Pretensioned High Strength Concrete Bridge Girders." PCI Journal, Vol. 40, No. 6, November-December, 1995, pp. 48-59.

Russell, B.W., and Burns, N.H. (1993). "Static and Fatigue Behavior of Pretensioned Composite Bridge Girders Made with High Strength Concrete." PCI Journal, Vol. 38, No. 3, May-June, 1993, pp. 116-128.

Shahawi, M.E., and Batchelor, B.D. (1986). "Fatigue of Partially Prestressed Concrete." Journal of Structural Engineering, Vol. 112, No. 3, March, 1986, pp. 524-537.

VSL Corporation personal communication with Dr. John E. Breen, March, 1992.

Wollmann, G.P., Yates, D.L., Breen, J.E., and Kreger, M.E. (1996). "Fretting Fatigue in Post-Tensioned Concrete Beams." ACI Structural Journal, Vol. 93, No. 2, March-April, 1996, pp. 172-179.

Vita

Bryan Earl Heller was born on February 25, 1968, in Carson City, Nevada, to C.A. Jack Heller and Janet B. Heller. Bryan graduated Cum Laude from Brigham Young University in April, 1992, with a Bachelor of Science degree in Civil Engineering. He then went to the Naval Officer Candidate School in Newport, Rhode Island, and was commissioned as an officer in the U.S. Navy in September, 1992. After rigorous training in nuclear engineering, Bryan served for 3 ½ years aboard the USS GEORGIA, SSBN 729, qualifying as a nuclear engineering officer and earning the gold dolphins of a Submarine Warfare Officer. He then transferred to the Navy's Civil Engineer Corps, and moved to Virginia Beach, Virginia, where he became registered as a licensed Professional Engineer. Most recently, he qualified as a Seabee Combat Warfare Officer in Naval Mobile Construction Battalion FOUR. Bryan came to the University of Texas at Austin in August, 2002, and then began his graduate research work at the Ferguson Structural Engineering Laboratory under the supervision of Dr. Sharon L. Wood. Bryan graduated with a Master of Science in Civil Engineering in August 2003.

Permanent Address: 712 Highland Street
Carson City, NV 89703
United States of America

This thesis was typed by the author.